NASA/TM-20205000060

Advanced Modular Power System Fully Populated Electronics Enclosure Thermal Testing

Anthony Colozza
HX5 Sierra, LLC, Brook Park, Ohio

Brian Burson, Karin Bozak, and Brent Gardner
Glenn Research Center, Cleveland, Ohio

August 2020

NASA STI Program . . . in Profile

Since its founding, NASA has been dedicated to the advancement of aeronautics and space science. The NASA Scientific and Technical Information (STI) Program plays a key part in helping NASA maintain this important role.

The NASA STI Program operates under the auspices of the Agency Chief Information Officer. It collects, organizes, provides for archiving, and disseminates NASA's STI. The NASA STI Program provides access to the NASA Technical Report Server—Registered (NTRS Reg) and NASA Technical Report Server—Public (NTRS) thus providing one of the largest collections of aeronautical and space science STI in the world. Results are published in both non-NASA channels and by NASA in the NASA STI Report Series, which includes the following report types:

- TECHNICAL PUBLICATION. Reports of completed research or a major significant phase of research that present the results of NASA programs and include extensive data or theoretical analysis. Includes compilations of significant scientific and technical data and information deemed to be of continuing reference value. NASA counter-part of peer-reviewed formal professional papers, but has less stringent limitations on manuscript length and extent of graphic presentations.

- TECHNICAL MEMORANDUM. Scientific and technical findings that are preliminary or of specialized interest, e.g., "quick-release" reports, working papers, and bibliographies that contain minimal annotation. Does not contain extensive analysis.

- CONTRACTOR REPORT. Scientific and technical findings by NASA-sponsored contractors and grantees.

- CONFERENCE PUBLICATION. Collected papers from scientific and technical conferences, symposia, seminars, or other meetings sponsored or co-sponsored by NASA.

- SPECIAL PUBLICATION. Scientific, technical, or historical information from NASA programs, projects, and missions, often concerned with subjects having substantial public interest.

- TECHNICAL TRANSLATION. English-language translations of foreign scientific and technical material pertinent to NASA's mission.

For more information about the NASA STI program, see the following:

- Access the NASA STI program home page at http://www.sti.nasa.gov

- E-mail your question to help@sti.nasa.gov

- Fax your question to the NASA STI Information Desk at 757-864-6500

- Telephone the NASA STI Information Desk at 757-864-9658

- Write to:
  NASA STI Program
  Mail Stop 148
  NASA Langley Research Center
  Hampton, VA 23681-2199

NASA/TM-20205000060

Advanced Modular Power System Fully Populated Electronics Enclosure Thermal Testing

Anthony Colozza
HX5 Sierra, LLC, Brook Park, Ohio

Brian Burson, Karin Bozak, and Brent Gardner
Glenn Research Center, Cleveland, Ohio

National Aeronautics and
Space Administration

Glenn Research Center
Cleveland, Ohio 44135

August 2020

Level of Review: This material has been technically reviewed by technical management.

Available from

NASA STI Program
Mail Stop 148
NASA Langley Research Center
Hampton, VA 23681-2199

National Technical Information Service
5285 Port Royal Road
Springfield, VA 22161
703-605-6000

This report is available in electronic form at http://www.sti.nasa.gov/ and http://ntrs.nasa.gov/

Contents

Advanced Modular Power System Fully Populated Electronics Enclosure Thermal Testing

Anthony Colozza
HX5 Sierra, LLC
Brook Park, Ohio 44142

Brian Burson*, Karin Bozak, and Brent Gardner
National Aeronautics and Space Administration
Glenn Research Center
Cleveland, Ohio 44135

Summary

A thermal test of an enclosure housing the Advanced Modular Power System (AMPS) electronics cards was performed. The enclosure was fully populated with 17 nonfunctioning AMPS electronics cards. Heaters were applied to the cards to simulate their operation. A cold plate was installed on the top of the case. The case was then insulated to simulate its installation within an electronics rack with the face and rear of the enclosure left open. The cold plate was connected to a chiller that provided cooling water at a fixed input temperature to the cold plate. Flow rates from the chiller of 0.0, 1.4, and 1.8 L/min were tested. The test was operated at each flow rate over a range of heater power levels until the steady-state temperature of the electronics cards was reached. Heater power levels from 2.5 to 45 W/card were tested. The data collected was used to determine the steady-state operating temperature of the cards, the temperature distribution between the cards, the time to reach steady-state temperature, the change in steady-state temperature with change in heater power, the temperature distribution between the cards at the steady-state condition, and the heat lost to the surrounds by the enclosure. One of the main goals of the testing was to determine how much waste heat the cards could generate and still maintain a touch temperature at or below 40 °C. Based on this requirement, for the three cooling rates tested, the maximum card waste heat that could be generated by each individual card was 3.9, 16.3, and 17.6 W, respectively. An analysis was also set up to provide an analytical model to estimate the card temperature under different cold plate flow rates and card heater power levels. The results of the analysis were compared to that of the experiment testing the range of flow rates and power levels.

1.0 Introduction

The objective of the Advanced Modular Power System (AMPS) power-conditioning card designs is to be modular and interchangeable, enabling them to be utilized in different locations and for conditioning output power for different types of loads. The AMPS architecture for spacecraft applications is intended to be a robust, cost-saving approach to power system conditioning and control that provides inherent redundancy and reliability. The current AMPS architecture consists of seven module types. These can be used interchangeably to provide the various functions for power control and conditioning. This overall approach is illustrated in Figure 1.

*Summer Intern in Lewis' Educational and Research Collaborative Internship Program (LERCIP), undergraduate at Ohio State University.

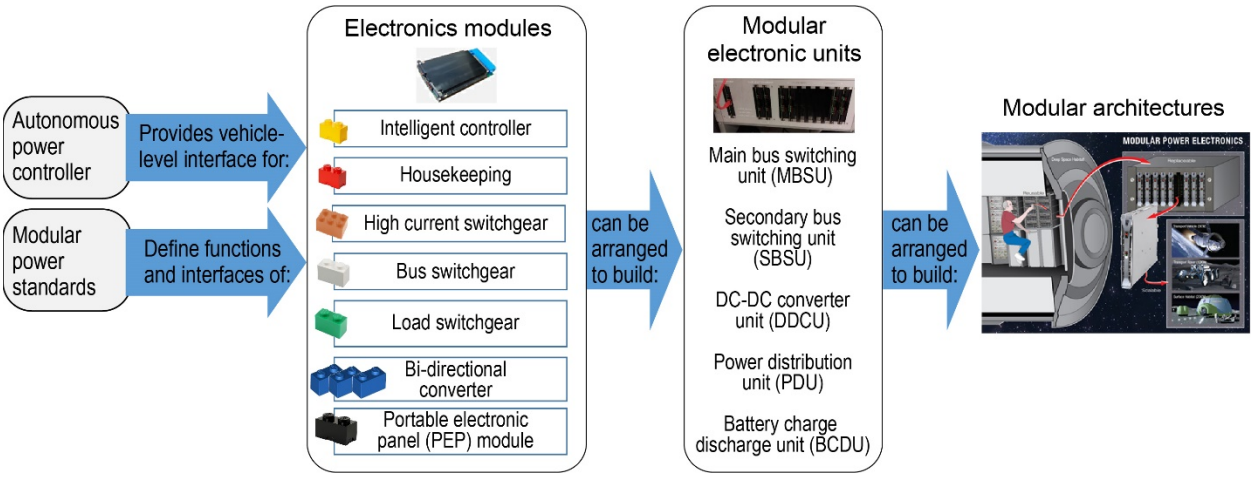

Figure 1.—Advanced Modular Power System modules and power system architecture approach. Direct current (DC).

TABLE I.—ADVANCED MODULAR POWER SYSTEM (AMPS) POWER-CONDITIONING CARD FUNCTION AND SPECIFICATIONS

Card type	Application	Card size by slot requirement
Controller module (CTLM)	Provides the spacecraft to internal network adapter, translates commands and telemetry, and monitors the module status	3U × 1 slot
Housekeeping power module (HKPM)	Generates Housekeeping power bus (5 VDC) from 120-VDC source	3U × 1 slot
Load switchgear module (LSGM)	Four-channel unidirectional switch with configurable current limiting and resettable trip Provide 4 – 4 A independent switches that can be paralleled together to increase the current switching capability (4, 8, 12, 16 A, etc.) Each channel can switch up to 4 A from 1 to 150 VDC	3U × 1 slot
Bus switchgear module (BSGM)	Bidirectional bus switch (supply and return) with configurable resettable trip levels Can switch up to 40 A at 120 VDC	3U × 1 slot
Bidirectional converter module (BDCM)	Bidirectional direct current (DC)/DC converter with configurable current and voltage setpoints Configurable and resettable trip levels Primary at 120 VDC at 40 A Secondary set to either 120 VDC at 40 A or 28 VDC at 160 A	3U × 3 slots
Portable equipment power module (PEPM)	Variable output, isolating DC/DC converter (3 to 28 VDC at 5.3 A) Load cable or user programmable output with remote voltage sense	3U × 1 slot
High current switchgear module (HCSM)	Bidirectional supply side switch with configurable and resettable trip levels Can switch up to 200 A at 120 VDC	3U × 3 slots

Each type of electronics module provides a specific function and has a specific power handling capability. The current card format is a 3U height card that utilizes one to three slots within the enclosure. The various types of AMPS cards and their functions are given in Table I.

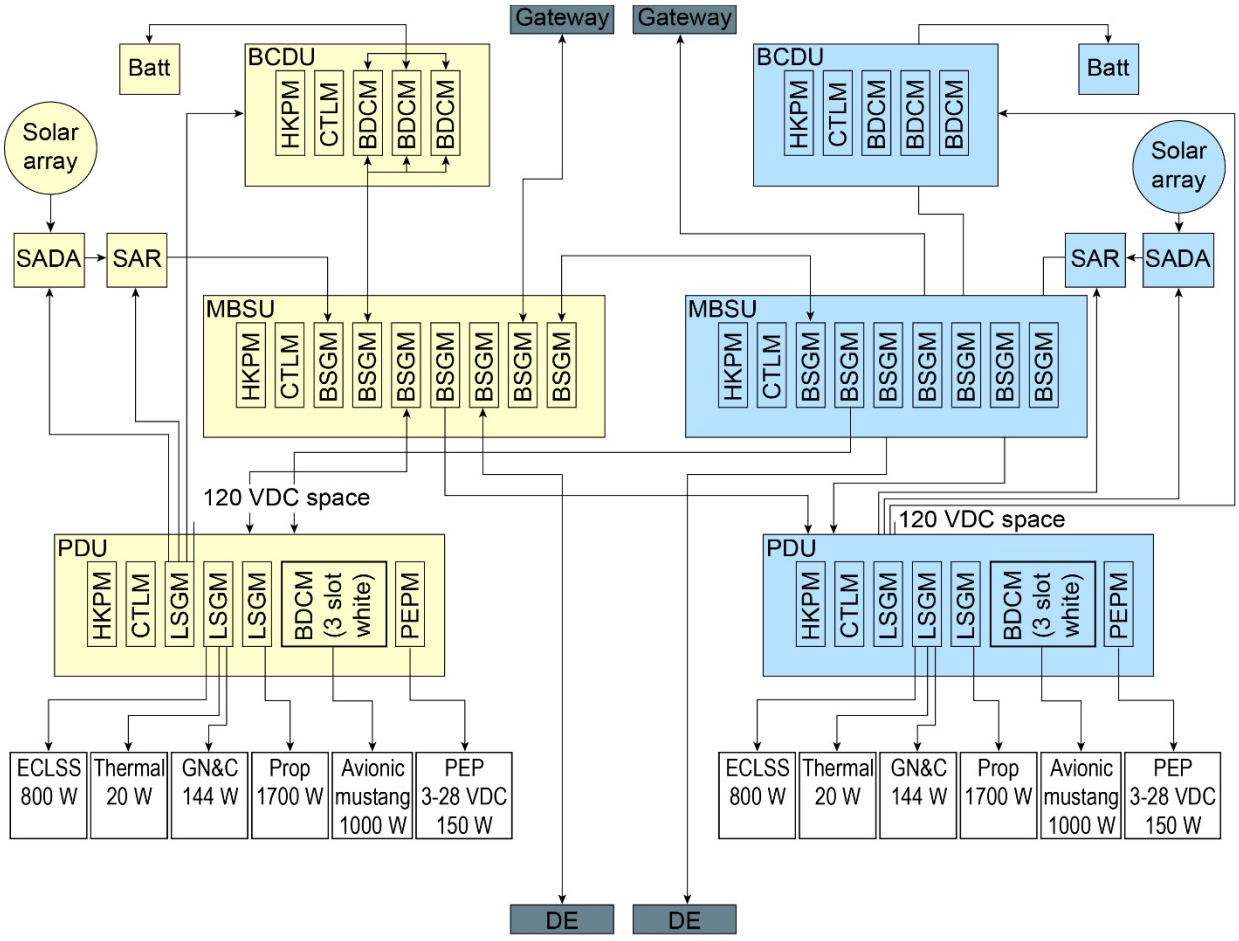

Figure 2.—Example Advanced Modular Power System card layout for Lunar Ascent Vehicle application. Battery (Batt). Battery charge discharge unit (BCDU). Bidirectional converter module (BDCM). Bus switchgear module (BSGM). Controller module (CTLM). Decent element (DE). Environmental control and life support system (ECLSS). Guidance, navigation, and control (GN&C). Housekeeping power module (HKPM). Load switchgear module (LSGM). Main bus switching unit (MBSU). Power distribution unit (PDU). Portable equipment panel (PEP). Portable equipment power module (PEPM). Propulsion (Prop). Solar array drive assembly (SADA). Solar array regulator (SAR).

The number and type of cards used in a given enclosure can vary depending on the application. An example AMPS-based power system layout is shown in Figure 2. This figure shows the possible AMPS power condition cards that would be utilized and their arrangement for a possible Lander Ascent Element electrical power system architecture. It also demonstrates how the various AMPS cards can be combined. For this architecture, each of the subsystems (environmental control and life support system (ECLSS); thermal; guidance, navigation, and control (GN&C); propulsion; and avionics) will receive a single 120-VDC powered input (except for avionics which will receive a 28-VDC input to show the different capabilities of the AMPS cards). Those subsystems will perform the control and switching to their lower level components. The AMPS cards could also perform these switching functions just by increasing the number of power distribution unit (PDU) cards.

The power processing and load requirements from the cards housed in each of the enclosures can vary considerably depending on their function. Example load power requirements for avionics, ECLSS, thermal control, propulsion, and GN&C are shown in Figure 3 along with the AMPS card breakdown and estimated power dissipation needed to perform these functions in Table II.

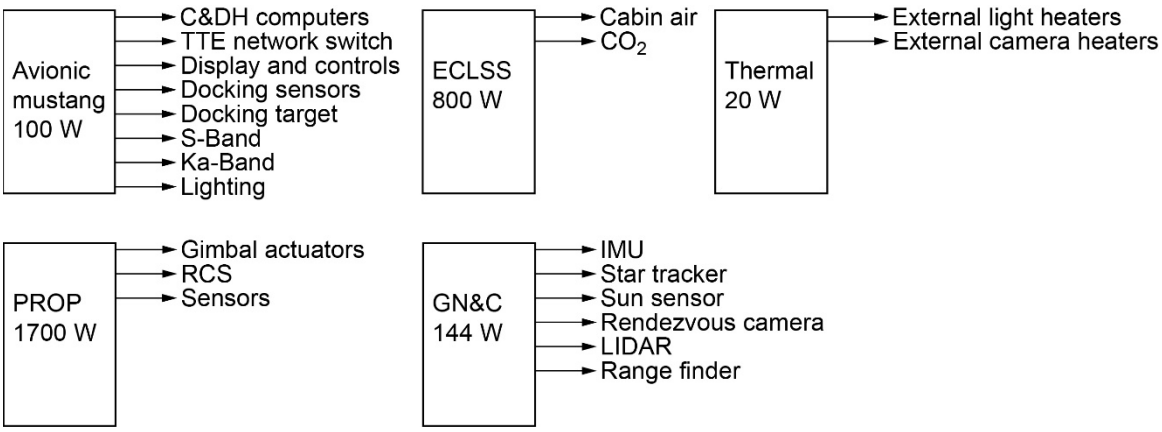

Figure 3.—Advanced Modular Power System card breakdown. Command and data handling (C&DH). Environmental control and life support system (ECLSS). Guidance, navigation, and control (GN&C). Inertial measurement unit (IMU). Light detecting and ranging (LIDAR). Propulsion (Prop). Reaction control system (RCS). Time-triggered Ethernet (TTE).

TABLE II.—ADVANCED MODULAR POWER SYSTEM (AMPS) CARD BREAKDOWN AND ESTIMATED POWER DISSIPATION

EPS cards[a]	Number of slots	Power channel A	Power channel B	Mass per channel, kg	Total mass, kg	Volume, m W×L×H	Power dissipation, W
BCDU							
HKPM	1	1	1	1.25	2.5	0.0254×0.305×0.146	0.75
CTLM	1	1	1	1.25	2.5	0.0254×0.305×0.146	3
BDCM	1	1	1	1.25	2.5	0.0254×0.305×0.146	20
BDCM	1	1	1	1.25	2.5	0.0254×0.305×0.146	20
BDCM	1	1	1	1.25	2.5	0.0254×0.305×0.146	20
Total	5	--	--	6.25	12.5	0.127×0.305×0.146	63.75
MBSU							
HKPM	1	1	1	1.25	2.5	0.0254×0.305×0.146	1.35
CTLM	1	1	1	1.25	2.5	0.0254×0.305×0.146	3
BSGM	1	1	1	1.25	2.5	0.0254×0.305×0.146	4.06
BSGM	1	1	1	1.25	2.5	0.0254×0.305×0.146	6.13
BSGM	1	1	1	1.25	2.5	0.0254×0.305×0.146	8.05
BSGM	1	1	1	1.25	2.5	0.0254×0.305×0.146	8.05
BSGM	1	1	1	1.25	2.5	0.0254×0.305×0.146	0
BSGM	1	1	1	1.25	2.5	0.0254×0.305×0.146	6.13
BSGM	1	1	1	1.25	2.5	0.0254×0.305×0.146	8.05
Total	9	--	--	11.25	22.5	0.2286×0.305×0.146	44.82
PDU							
HKPM	1	1	1	1.25	2.5	0.0254×0.305×0.146	1.05
CTLM	1	1	1	1.25	2.5	0.0254×0.305×0.146	3
LSGM	1	1	1	1.25	2.5	0.0254×0.305×0.146	3.07
LSGM	1	1	1	1.25	2.5	0.0254×0.305×0.146	3.32
LSGM	1	1	1	1.25	2.5	0.0254×0.305×0.146	4.00
BDCM	3	1	1	3.75	7.5	0.0762×0.305×0.146	20
PEPM	1	1	1	1.25	2.5	0.0254×0.305×0.146	10.5
Total	9	--	--	11.25	22.5	0.2286×0.305×0.146	44.95
Overall total				28.75	57.5	0.5842×0.305×0.146	-------

[a]Bidirectional converter module (BDCM). Battery charge discharge unit (BCDU). Bus switchgear module (BSGM). Controller module (CTLM). Electrical power system (EPS). Housekeeping power module (HKPM). Load switchgear module (LSGM). Main bus switching unit (MBSU). Power distribution unit (PDU). Portable equipment power module (PEPM).

Since there is a considerable amount of variation possible in the type and power load of the AMPS cards housed in a given enclosure, the thermal control of the enclosure has to be designed to meet the worst-case operating heat load. To determine the coolant requirements needed to meet the heat load generated within an enclosure, a series of tests were performed. These tests were a follow-on to the initial enclosure thermal testing for the AMPS electronics cards (Ref. 1). This follow-on testing was performed to evaluate the cooling requirements for a fully populated enclosure over a range of heat loads generated by the AMPS cards within the enclosure. This card enclosure has 17 slots with a backplane that provides the input and output power interface, as well as communications to the cards. The cards slide into the enclosure and plug into the backplane.

The enclosures and their connections are regarded as part of the spacecraft structure and provide the electrical connections between the cards and the loads, as well as the thermal control for the cards. The final configuration will be dependent on the spacecraft design. However, for this evaluation the cold plates used to remove the heat from the electronics enclosure are located on the top of the case. This location represents the most likely configuration for the cooling system within the spacecraft. It also provides an accessible cooling configuration for the AMPS testbed that will be used to evaluate the card operation under a variety of loading conditions.

If, however, the enclosures are designed and installed as part of the spacecraft, then it may be possible that an integral cooling loop can be designed into the enclosures. This approach would provide the best heat removal capability especially if the coolant loop can be integrated into the support rails that the cards are pressed against to hold them in place.

2.0 Test Setup

As with the previous tests described in Reference 1, representative AMPS cards were installed within their individual cases with an electric heater to simulate the operation of the card.

During card operation, heat is generated from the electrical components and chips located on the printed circuit board. These heat sources are distributed over the board surface. Heat can be moved from these components to the enclosure through thermal planes located within the board or through the external card case, which is contacting the surface of the chips or other components. Heat is then conducted to the case support rails and locking mechanism.

Since the cards were not operational during the testing, a heater was installed on the card case to produce a controllable heat load on the card. This enabled the heat generated to be distributed within the enclosure and controlled the evaluation of how the card temperature varied with different heat loads and coolant flow rates and temperatures. To measure the card temperature, a type-K thermocouple was installed on the center of the card case. The heater and thermocouple placement are shown in Figure 4.

The AMPS card enclosure can hold 17 cards and was fully populated for the thermal testing. The card installation into the enclosure is shown in Figure 5. Once placed into a slot, the cards are locked into place using an nVent Schroff Birtcher™ Wedge-Loc® card retainer that expands using a sliding joint that expands outward as a screw is tightened. This compresses the card against the rails providing good thermal contact between the card and the rails.

A set of flexible strip heaters were used to simulate the operation of the cards and provide the desired waste heat to be removed by the cold plate. The heaters had a measured resistance of 135 Ω each, were wired in parallel, and powered with a Hewlett Packard 6030A power supply, as illustrated in Figure 6. The heaters wired into the terminal strip are also shown in Figure 7. The main leads from the power supply were connected to the terminal strip to distribute the power to the heaters. The output power of the supply to all of the heaters was varied to provide an input power per card from 2.5 to 45 W.

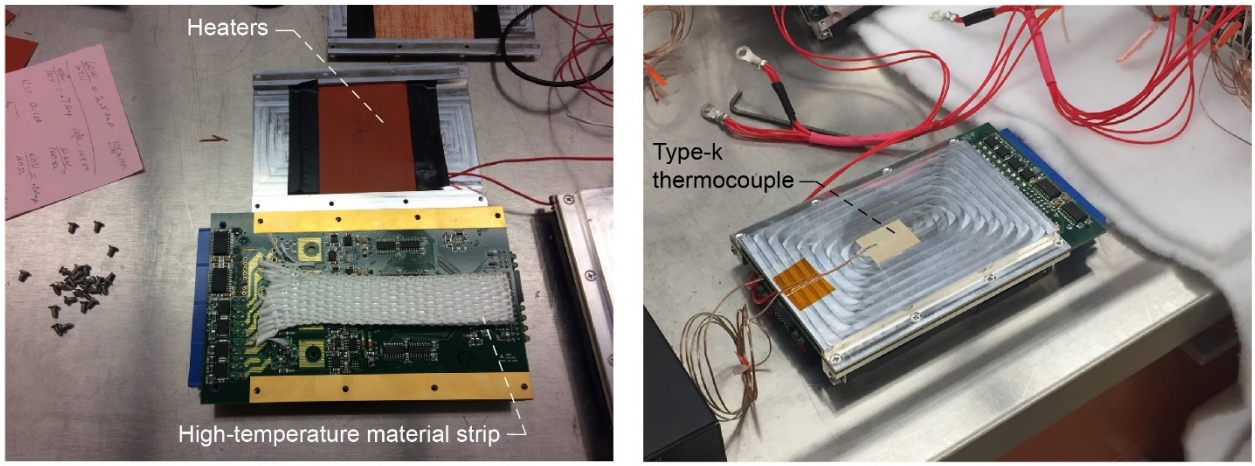

(a) (b)

Figure 4.—Advanced Modular Power System card heater and thermocouple placement for thermal testing. (a) Heater mounted on inside card thermal plane. High temperature material strip used for secure contact between heater and thermal plane. (b) Type-K thermocouple mounted on center of card case where heater was installed.

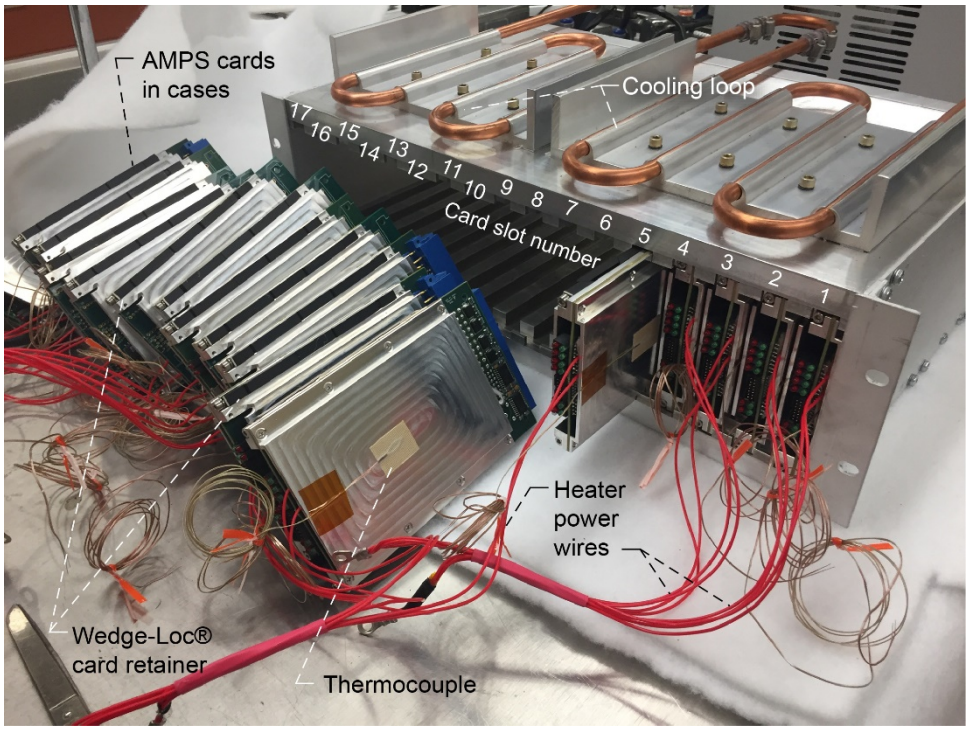

Figure 5.—Advanced Modular Power System (AMPS) cards being installed into enclosure.

(a)

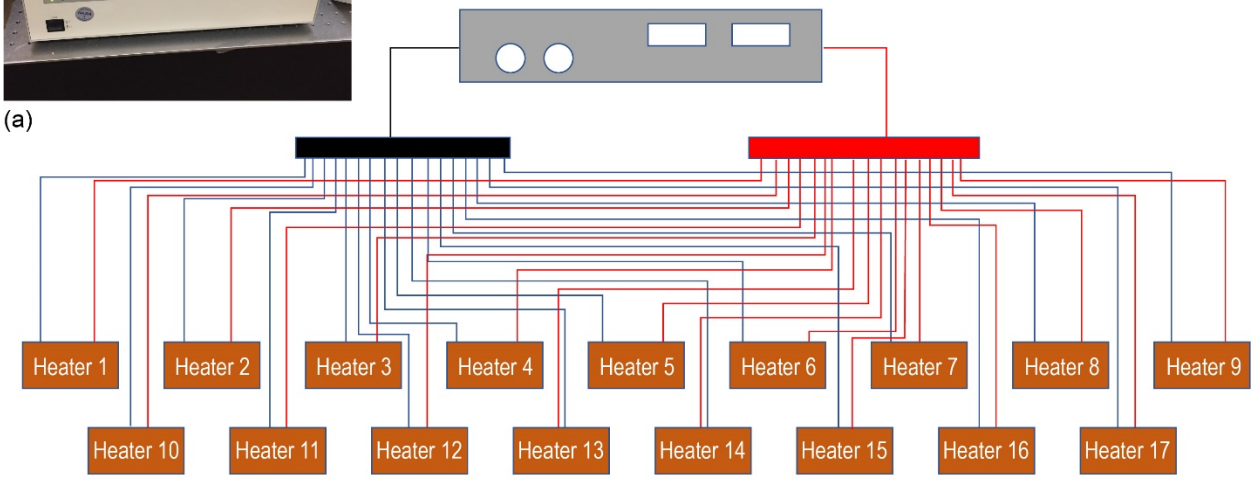

(b)

Figure 6.—Heater layout. (a) Hewlett Packard 6030A power supply. Output: 0 to 200 VDC, 0 to 17 A, and 1,000 W maximum. (b) Power wire layout. Heater resistance: 135 Ω.

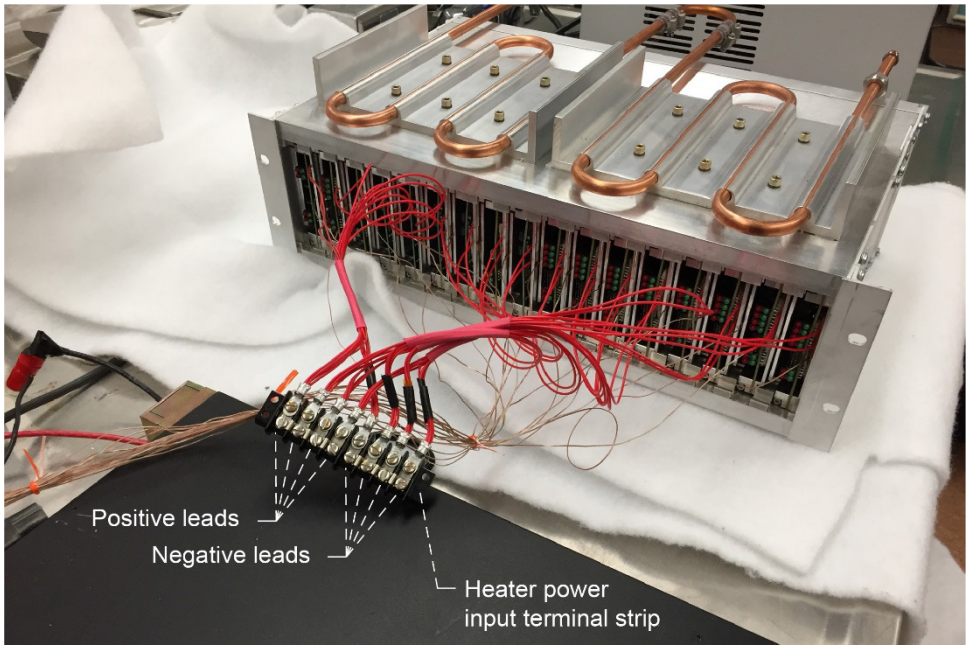

Figure 7.—Heaters wired to terminal strip.

A coolant loop was installed on the top of the enclosure to remove the heat generated from the AMPS cards. This orientation and cold plate are similar to what is being used in the AMPS testbed. It is also representative of how heat would be extracted from the AMPS cards once installed in a spacecraft. As mentioned previously, for spacecraft integration, the cooling loop could be further integrated into the case but the heat transfer path from the cards to the cooling is expected to be similar.

The coolant loop consisted of two aluminum cold plates bolted to the top of the enclosure with six screws each. A Laird Technologies, Inc., TFlex™ SF800 series thermal pad with a thermal conductivity of 7.8 W/mK was placed between the cold plate and enclosure top surface to reduce the contact resistance and improve heat flow to the coolant. The aluminum cold plates utilize a serpentine copper tube press fit to the plate through which the coolant flows. The copper tube makes four passes over the top surface of the cold plate. The two cold plates were connected in series. Flex lines were used to connect the cold plate tubes to the chiller. The coolant flow entered the left side of the first cold plate from the chiller and exited the right side of the second cold plate back to the chiller. The cold plates are shown mounted to the top of the case in Figure 8.

A PolyScience circulating bath chiller model 9102A11B was used to maintain the coolant flow at the desired setpoint temperature of 20 °C. During the testing, a fixed flow rate was used. The flow was set using a visual Blue-White Industries, Ltd. F–550 flowmeter, as shown in Figure 9, prior to the start of a test. The flow rate was checked periodically during the test to ensure that it was consistent throughout the test. The maximum flow rate achievable by the recirculating bath with the test setup was 1.8 L/min (0.48 gal/min).

To measure the water temperature into and out of the chiller, an Omega Engineering, Inc., model TC–K–NPT–G–72 inline type-K thermocouple probe was used on both the inlet and outlet water lines from the chiller as shown in Figure 10.

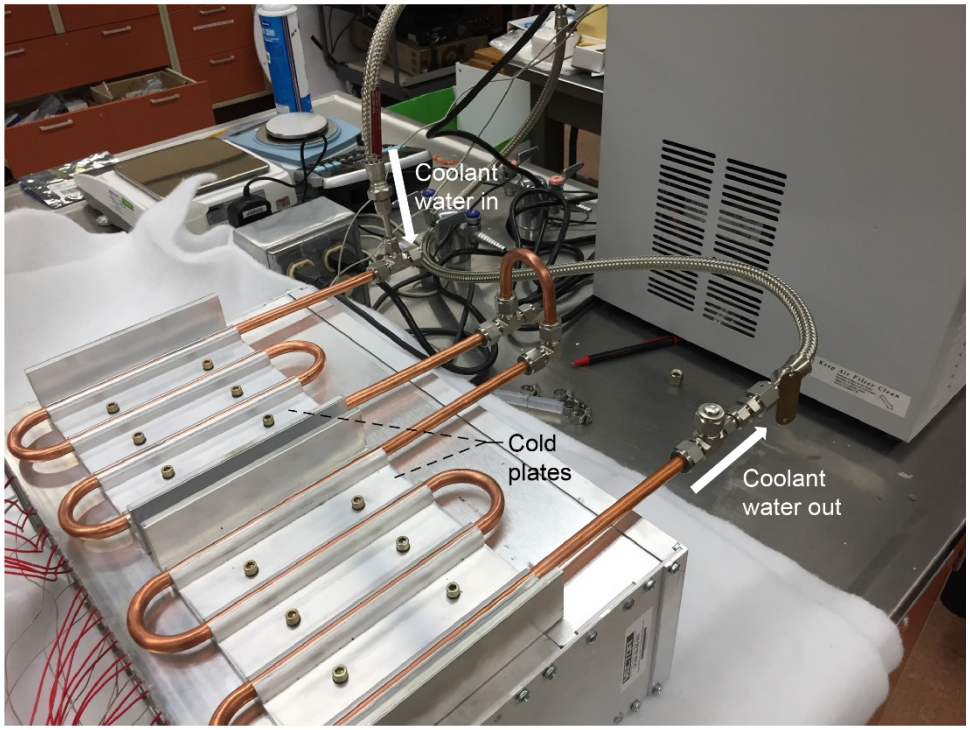

Figure 8.—Cold plate and fluid connections.

Figure 9.—Coolant system. (a) Flowmeter. (b) Recirculating bath.

Figure 10.—Coolant inlet and outlet water temperature sensors.

To reduce the convective heat transfer from the case, as well as conduction into the test table, a polyester insulation was used to wrap the electronics case for testing, as shown in Figure 11. The front and rear of the case was left open to enable natural convection from these surfaces. This represents the arrangement that would be present within the rack. It should be noted that the cold plates shown on top of the insulation were used as weights to hold the insulation in place and not used for cooling. An additional thermocouple was located on top of the insulation. This was used to measure the insulation temperature, as well as the ambient room temperature.

A total of 20 thermocouples were used to monitor temperatures during the testing. One thermocouple was located on each of the card cases, two were used to record the coolant water inlet and outlet temperature and one was used to monitor the insulation temperature. Data from these thermocouples was recorded with a GRAPHTEC Corporation GL820 data logger. The thermocouple channel input and corresponding location is given in Table III. The data logger was set to sample points from each thermocouple once every second. Data collection for each test was started prior to the power supply being turned on and continued until a steady-state temperature profile was achieved. The test setup is shown in Figure 12. This figure shows the chiller, fully populated enclosure, and data logger. In the figure, the insulation is removed from the top of the enclosure to show the cooling plates. During testing, the enclosure was fully insulated as shown in Figure 11.

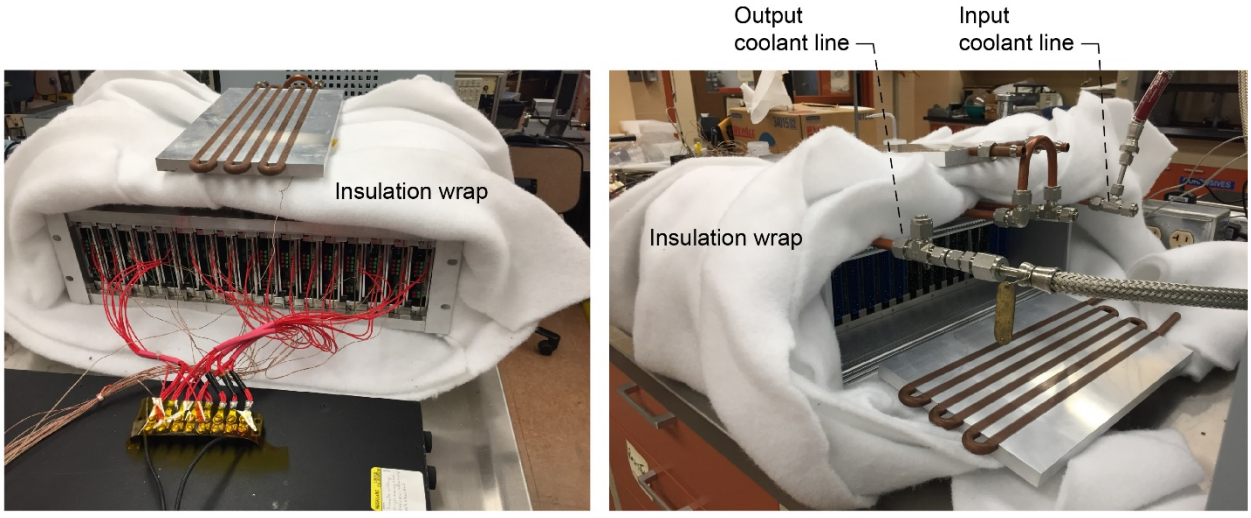

Figure 11.—Electronics case wrapped with insulation. (a) Front view. (b) Back view.

TABLE III.—DATA LOGGER THERMOCOUPLE (TC) CHANNEL ASSIGNMENT

Channel	Location	TC type	Channel	Location	TC type
1	Card 1	K	11	Card 11	K
2	Card 2	K	12	Card 12	K
3	Card 3	K	13	Card 13	K
4	Card 4	K	14	Card 14	K
5	Card 5	K	15	Card 15	K
6	Card 6	K	16	Card 16	K
7	Card 7	K	17	Card 17	K
8	Card 8	K	18	Coolant inlet	K
9	Card 9	K	19	Coolant exit	K
10	Card 10	K	20	Insulation surface	K

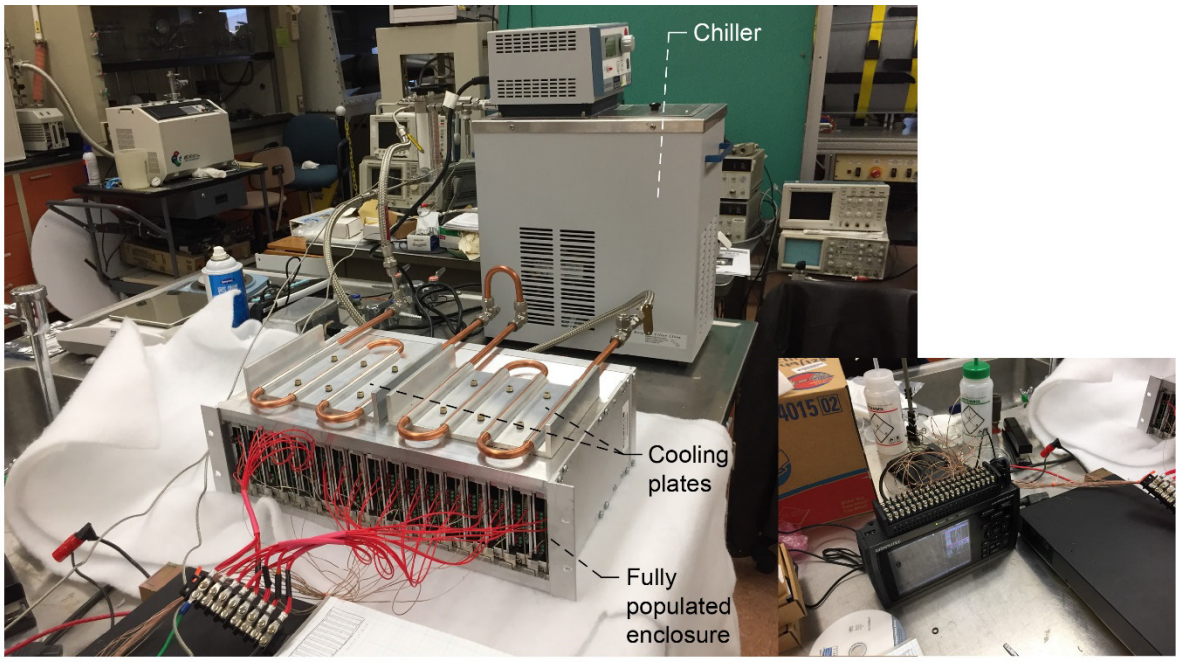

Figure 12.—Fully populated Advanced Modular Power System card enclosure thermal cooling test setup. (a) Full setup. (b) Data logger with thermocouples connected.

3.0 Analysis

An analytical model was set up to estimate the power-conditioning card temperature with the cold plates mounted to the top of the chassis to compare with the experimental results. The purpose of the analytical model is to provide the ability to make estimates of the card temperature (T_b) when operating under conditions that were not encountered during the experimental testing.

The heat flow from the card to the cold plate is illustrated in Figure 13. The chip temperature is given by the sum of the thermal resistances between the chip surface and the heat sink (R_{tot}), the waste heat generated by the board (P), and the coolant water temperature (T_c) as given by Equation (1).

$$T_b = T_c + R_{tot} P \tag{1}$$

The total thermal resistance in K/W is a sum of the individual resistances associated with the heat path shown in Figure 13 and represented by Equation (2). Each component will be further explained in subsequent equations.

$$R_{tot} = R_{c-p} + R_p + R_{p-r} + R_r + R_{c-cp} + R_{cp} + R_{cp-t} + R_c \tag{2}$$

Heat initially moves from the electronics components to the external conductive thermal plane. For the testing and analysis, the cards do not contain an internal thermal plane. The external thermal plane conducts the heat to the rails and case, which in turn transports the heat to the cold plate located on top of the case. Because each rail, except the rails associated with the ends of the case, are in contact with two cards, it was assumed that heat would flow from each card to two rails (one upper and one lower) and a portion of the case equivalent to the spacing between the cards. This minimizes the conduction area for each card to the cold plate representing a worst-case situation where all the cards are operational, producing the same amount of heat, and each is conducting its heat through a small portion of the case to the cold plate.

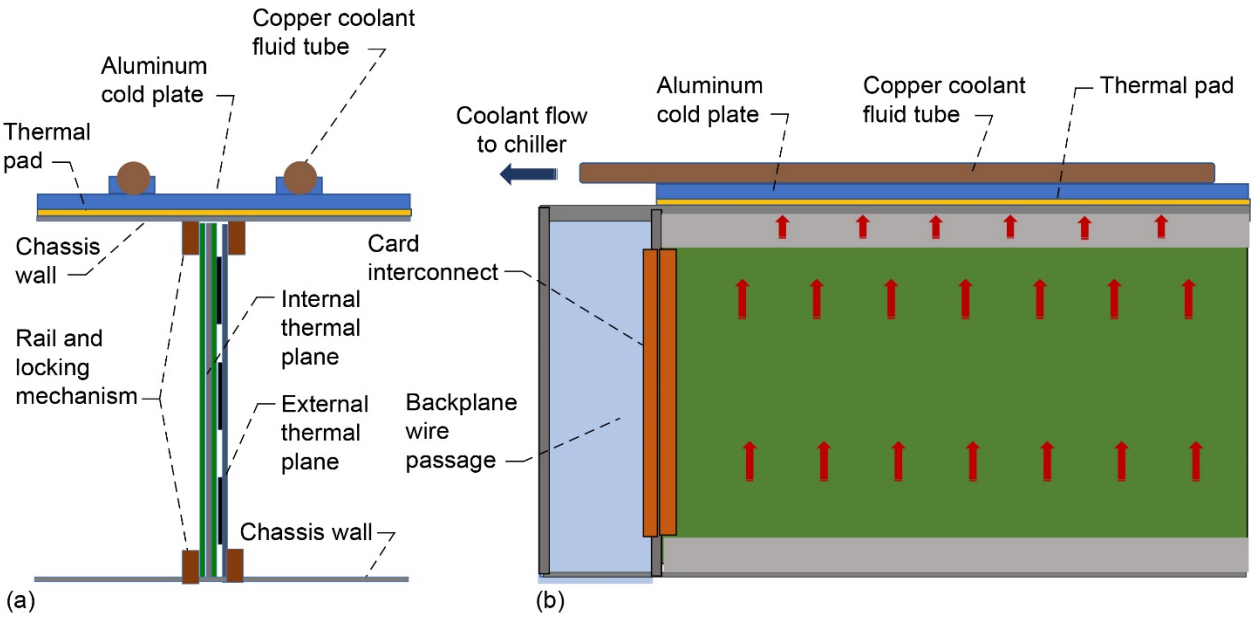

Figure 13.—Heat flow illustration from electronics to cold plate. (a) Front view. (b) Side view.

The thermal resistance for the heat flow from the electronics components to the conductive plane (R_{c-p}) in contact with their upper surface is given by Equation (3), which is based on the contact conductance between the electronics components and the external conductive plane [$R_{c(c-p)}$] and the surface area of the electronics chips (A_c).

$$R_{c-p} = \frac{R_{c(c-p)}}{A_c} \tag{3}$$

The thermal resistance for the heat conducted from the external thermal plane to the upper and lower rails (R_p) is based on the average distance between the heat source to the support rails (d_p), the thickness (t_p), length (L_p), and conductivity (k_p) of the thermal plane, given by Equation (4).

$$R_p = \frac{d_p}{t_p k_p L_p} \tag{4}$$

The thermal resistance associated with the contact between the thermal plane and the support rail (R_{p-r}) is given by Equation (5), which is based on the contact conductance between the thermal plane and the external support rails [$R_{c(p-r)}$] and the contact surface area between the two (A_r).

$$R_{p-r} = \frac{R_{c(p-r)}}{A_r} \tag{5}$$

The thermal resistance for the heat conducted through the rails and case (R_r) to the thermal pad beneath the cold plate is given by Equation (6). It is based on the thickness of the rail (t_r) and case (t_c), the conductivity (k_r) of the thermal plane, and the cross-sectional area (A_{rcs}) of the rails and portion of the case associated with the heat transfer from one card as given by Equation (7), where w_c is the width of the rail and case segment.

$$R_r = \frac{t_r + t_c}{2A_{rcs}k_r} \tag{6}$$

$$A_{rcs} = w_c L_p \tag{7}$$

The contact resistance between the cold plate and the top of the case (R_{c-cp}) is given by Equation (8), which is based on the contact conductance between the case and the cold plate [$R_{c(c-cp)}$] through the thermal pad. The cross-sectional area for this interface is the same as that given by Equation (7).

$$R_{c-cp} = \frac{R_{c(c-cp)}}{A_{rcs}} \tag{8}$$

The heat then flows from the cold plates to the coolant tube and into the coolant. The thermal resistance of the heat flow through and along the cold plate (R_{cp}) is given by Equation (9). This is based on the average distance along the cold plate to the coolant tube (d_{cp}), the cold plate thickness (t_{cp}), the thermal conductivity of the cold plate (k_{cp}), and the length of the cold plate (L_{cp}).

$$R_{cp} = \frac{d_{cp}}{t_{cp}k_{cp}L_{cp}} \tag{9}$$

The copper tubes are press fit onto the aluminum cold plate. The estimated contact resistance between the tubes and the cold plate (R_{cp-t}) is given by Equation (10). This resistance is based on the cooling tube length (L_t) and diameter (d_t) and the contact conductance between the cold plate and the tubes [$R_{c(cp-t)}$].

$$R_{cp-t} = \frac{4R_{c(cp-t)}}{\pi d_t L_t} \tag{10}$$

The final thermal resistance to be calculated is for the heat transfer from the coolant tube to the fluid (R_c). This thermal resistance is given by Equation (11) and is based on the convective coefficient (h_c) of the coolant flow through the tube.

$$R_c = \frac{2}{\pi d_t L_t h_c} \tag{11}$$

The h_c is given by Equation (12), which is based on the Nusselt number for flow through a tube (Nu_d) and the cooling fluid thermal conductivity (k_f).

$$h_c = \frac{\mathrm{Nu}_d k_f}{d_t} \tag{12}$$

The Nu_d is based on properties of the coolant fluid and the Reynolds number of the flow through the tube (Re_d). The Re_d is given by Equation (13). The Re_d is dependent on the coolant fluid properties of density (ρ_c) and dynamic viscosity (μ_c) and the flow rate (U_c) of the fluid through the tube.

$$\mathrm{Re}_d = \frac{U_c d_t \rho_c}{\mu_c} \tag{13}$$

The dynamic viscosity and density of water as a function of temperature are given by Equations (14) and (15), respectively.

$$\mu_c = \frac{\left(4.4954 \times 10^{13}\right) T_c^{-5.7342}}{T_c} \qquad \frac{\mathrm{N \cdot s}}{\mathrm{m}^2} \tag{14}$$

$$\rho_c = -404.87 + 14.121 T_c - 0.050664 T_c^2 + 7.7909 \times 10^{-5} T_c^3 - 4.6343 \times 10^{-8} T_c^4 \qquad \frac{\mathrm{kg}}{\mathrm{m}^3} \tag{15}$$

The flow velocity is determined from the volume flow rate (F_c) of the coolant from the chiller (in L/min) as given by Equation (16).

$$U_c = \frac{F_c}{15{,}000 \pi d_t^2} \qquad \frac{\mathrm{m}}{\mathrm{s}} \tag{16}$$

The Nu_d is dependent on the state of the flow, whether laminar or turbulent. Which in turn is dependent on the flow Re_d. For laminar flow, the Nu_d is a constant, as given by Equation (17) (Ref. 2). Once the flow becomes turbulent, the Nu_d is given by Equation (18) (Ref. 2).

$$\mathrm{Nu}_d = 4.36 \quad \text{for } \mathrm{Re}_d \le 2{,}300 \tag{17}$$

$$\mathrm{Nu}_d = \frac{\left(\frac{f}{8}\right)\left(\mathrm{Re}_d - 1{,}000\right)\mathrm{Pr}}{1 + 12.7\left(\frac{f}{8}\right)^{1/2}\left(\mathrm{Pr}^{2/3} - 1\right)} \qquad \text{for } 2{,}300 < \mathrm{Re}_d > 5 \times 10^6 \tag{18}$$

The friction factor (f) and Prandtl number (Pr), which are used to calculate the Nu_d are given by Equations (19) and (20), respectively (Ref. 2).

$$f = \left\{0.79\left[\ln\left(\mathrm{Re}_d\right) - 1.64\right]\right\}^{-2} \tag{19}$$

$$\mathrm{Pr} = \frac{c_p \mu_c}{k_f} \tag{20}$$

The cooling fluid specific heat c_p and k_f used to determine the Pr are given by Equations (21) and (22), respectively, for water as a function of its temperature.

$$c_p = 27{,}089 - 234.67 T_c + 0.8971 T_c^2 - 0.0015242 T_c^3 + 9.7841 \times 10^{-7} T_c^4 \tag{21}$$

$$k_f = 0.70611 - 0.0054621 T_c + 3.2801 \times 10^{-5} T_c^2 - 6.3266 \times 10^{-6} T_c^3 + 3.7935 \times 10^{-11} T_c^4 \tag{22}$$

The analysis previously outlined was used to estimate the steady-state operating temperature of an AMPS card operating within the enclosure over a range of thermal power levels that would be encountered during operation. The associated variables used in calculating the board temperature are summarized in Table IV.

Using the analysis outlined previously, the electronics board operating temperature was calculated over a range of operating powers for two flow rates, 1.8 and 1.4 L/min. These results are shown in Figure 14. The maximum desired operating temperature was given as 40 °C. The maximum power levels to maintain the board at 40 °C for each flow rate are listed in Table V.

The analysis showed that to maintain the card below the desired operating temperature of 40 °C, the card waste-heat power level has to be near or less than 17 W depending on the chiller flow rate. The chiller flow rate; however, did not have a significant effect on the operating temperature of the cards. The 22 percent reduction in flow rate from 1.8 to 1.4 L/min had only a 2.3 percent reduction in the allowable waste heat produced by the card at this power level.

TABLE IV.—VARIABLE VALUES USED FOR FOUR CASES EXAMINED

A_c (electronics components contact area to the thermal plane), cm^2	82.6
A_r (contact area between the thermal plane and the support rail), cm^2	39.6
d_{cp} (average distance along the cold plate to the coolant line), cm	1.0
d_p (distance from the center of the thermal plane to the support rail), cm	2.5
d_t (cooling tube diameter), mm	5
k_{cp} (thermal conductivity of the aluminum cold plate), W/mK	205
k_p (thermal conductivity of the aluminum thermal plane), W/mK	205
k_r (thermal conductivity of the aluminum support rail and case), W/mK	205
L_{cp} (cold plate length), cm	20.3
L_p (thermal plane length), cm	16.5
L_t (cooling tube length), cm	20.3
$R_{c(c-p)}$ (contact conductance between the electronic components and thermal plane), m^2K/W	0.0009
$R_{c(p-r)}$ (contact conductance between the thermal plane and support rails)[a], m^2K/W	0.00095
$R_{c(c-cp)}$ (contact conductance between the support rails and case to the cold plate through the thermal pad)[a], m^2K/W	0.001
t_p (thermal plane thickness), mm	3.0
t_c (case thickness), mm	15.6
t_{cp} (cold plate thickness), mm	5
t_r (support rail thickness), mm	8.5
T_c (coolant water inlet temperature), °C	20
w_c (case section width), mm	25.5
w_r (support rail width), mm	12.4

[a]Reference 1.

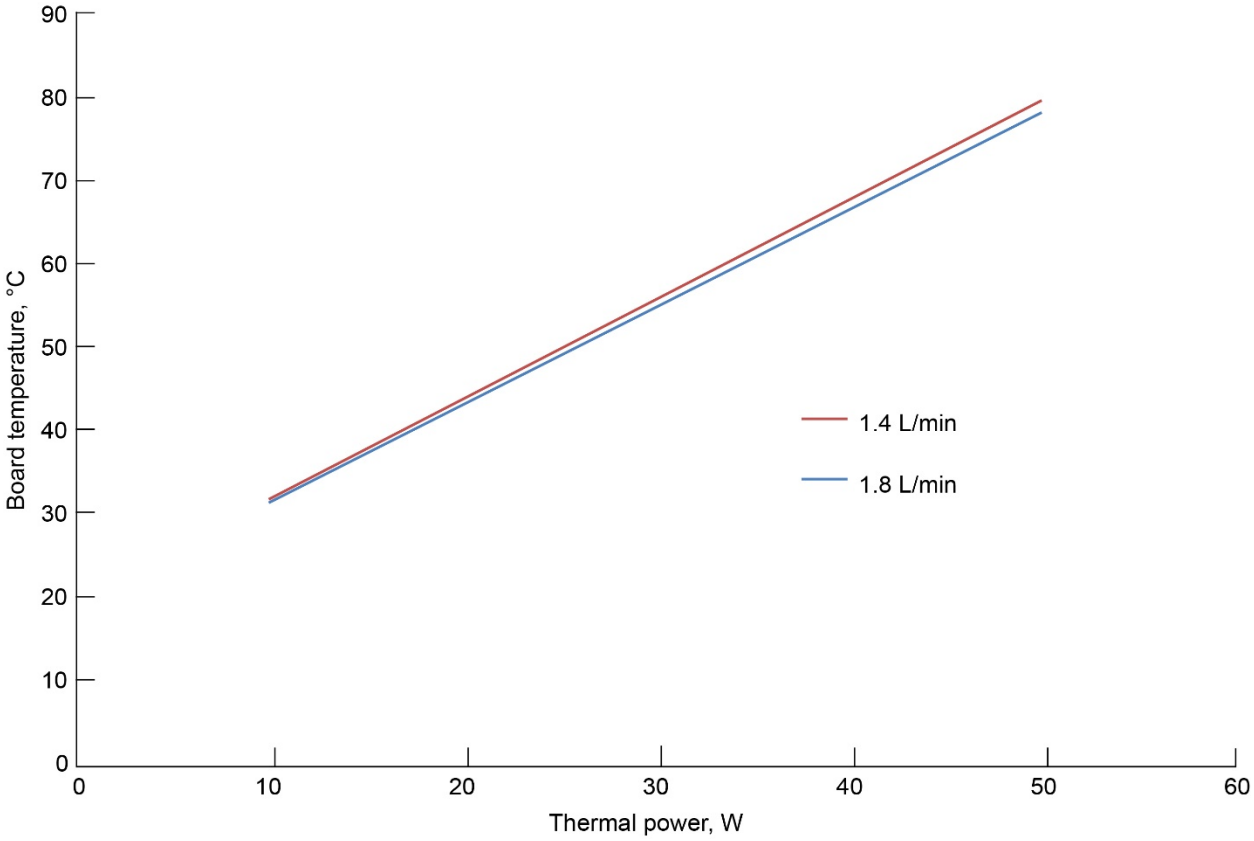

Figure 14.—Calculated board operating temperature versus waste heat for two chiller flow rates.

TABLE V.—ANALYSIS OF MAXIMUM POWER LEVEL FOR BOARD TO REMAIN AT OR BELOW 40 °C

Flow rate, L/min	Max power, W
1.4	16.7
1.8	17.1

4.0 Experimental Test Results

To validate the thermal model as well as provide additional insight into the effects of the cold plate interface to the electronics enclosure on the AMPS card electronics temperature, an experiment was performed. The experiment, described in Section 2.0, was used to simulate the heat generated from a fully populated enclosure containing 17 AMPS electronics cards and determine their operating temperature.

The card test data for each flow rate and heater power-level combination is given in the Appendix, Figure 30 to Figure 70. It should be noted that for all heater power levels tested there was an error in the temperature output of card 16 for the 1.8 L/min flow rate tests and card 17 for the 1.4 L/min flow rate tests. The temperature for these cards was reading significantly higher than the other cards during the corresponding series of tests. In both instances, this was due to an error in the thermocouple output. The data from these cards was not included in any of the averages shown in the following results.

The steady-state operating temperature of the cards, as well as the temperature distribution between the cards, was determined from the data collected. The experiment was performed for two coolant flow rates of 1.4 and 1.8 L/min, as well as a no cooling case (0.0 L/min) in which the chiller was turned off and there was no coolant flow through the cold plate. The average card temperatures for these three operating conditions are shown in Figure 15. This figure represents the average steady-state card temperature of the 17 cards within the enclosure during the test at the specified heater power level.

Similar to the analysis results, the change in card temperature with a change in flow rate was fairly small. For example, changing the flow rate from 1.8 to 1.4 L/min (22 percent decrease) resulted in an increase in the card temperature of 1.7 °C (4.3 percent increase) at an operating card power of 17.5 W. The increase in card temperature with increasing power was similar for both the 1.8 and 1.4 L/min cases. However, for the no cooling case, this rate significantly increased. The card power levels needed to reach the 40 °C maximum temperature are given in Table VI for the three cases.

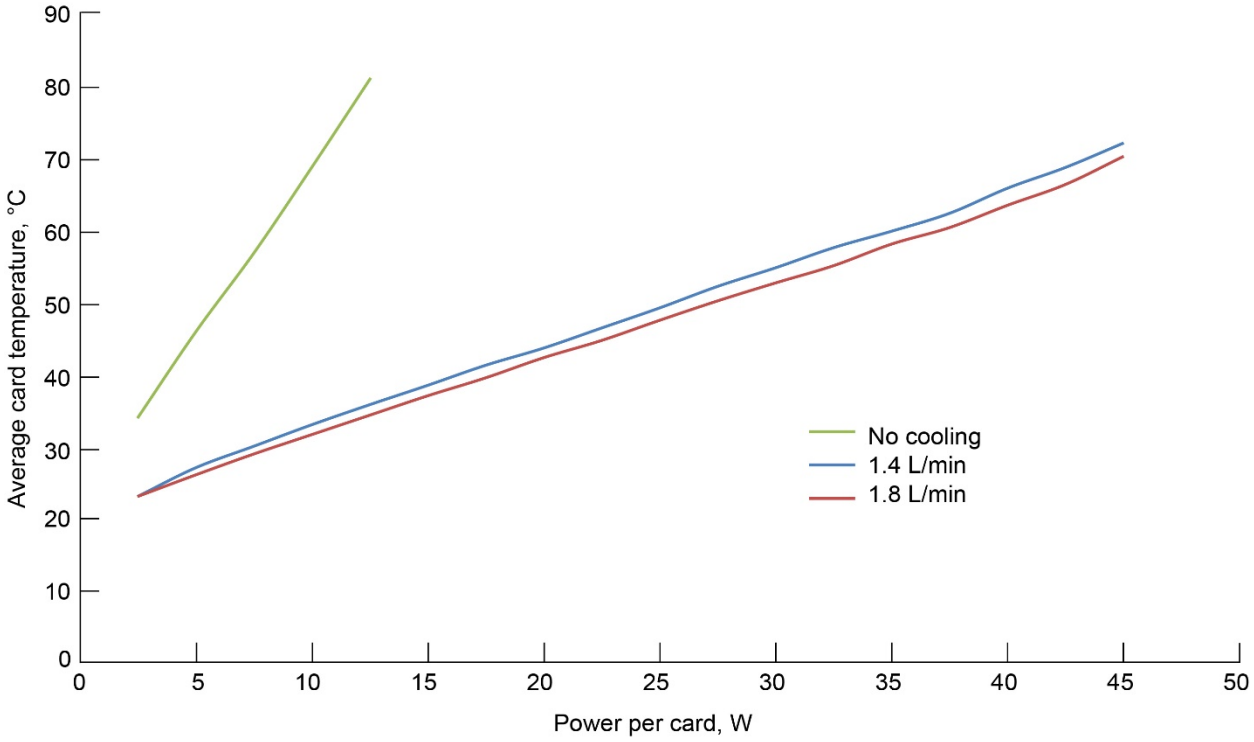

Figure 15.—Average steady-state card temperature versus heater input power.

TABLE VI.—EXPERIMENTAL RESULTS OF MAXIMUM POWER LEVEL FOR BOARD TO REMAIN AT OR BELOW 40 °C

Flow rate, L/min	Max power, W
0	3.9
1.4	16.3
1.8	17.6

Plotting the data shown in Table VI, a curve fit can be made to estimate the maximum power per card needed to remain at or below the 40 °C-touch temperature limit. This curve fit is shown in Figure 16 for the three flow rates tested. A polynomial curve fit was used to estimate what the maximum waste heat per card would be following the trend set by the three test data points. Based on the data, the maximum waste heat per card allowable would be approximately 18 W with a required coolant flow rate of just over 2 L/min. Flow rates above this would not enable appreciably higher waste heat levels for the electronics cards.

The rate of change in card temperature with changes in input power is shown in Figure 17. This figure shows that the rate for both cases with cooling flow are fairly similar and constant at approximately 1.1 °C change in card temperature for 1 W change in power over the majority of the power range tested. The rate does begin to increase at power levels above 35 W/card and at low power levels of less than 5 W/card. The no cooling case had a much higher rate of change of temperature with input power. It averaged approximately 4.7 °C change in temperature per 1 W change in input power. However, this rate varied considerably over the power range tested. The heat transfer from the noncooled case is due to natural convection to the surroundings from the case front and rear. Natural convection can be significantly affected by any air currents in the room or any change in the room temperature. Therefore, the variation in the temperature rise with input power for this case is likely due to the variation in the natural convection rate from the varying conditions within the room.

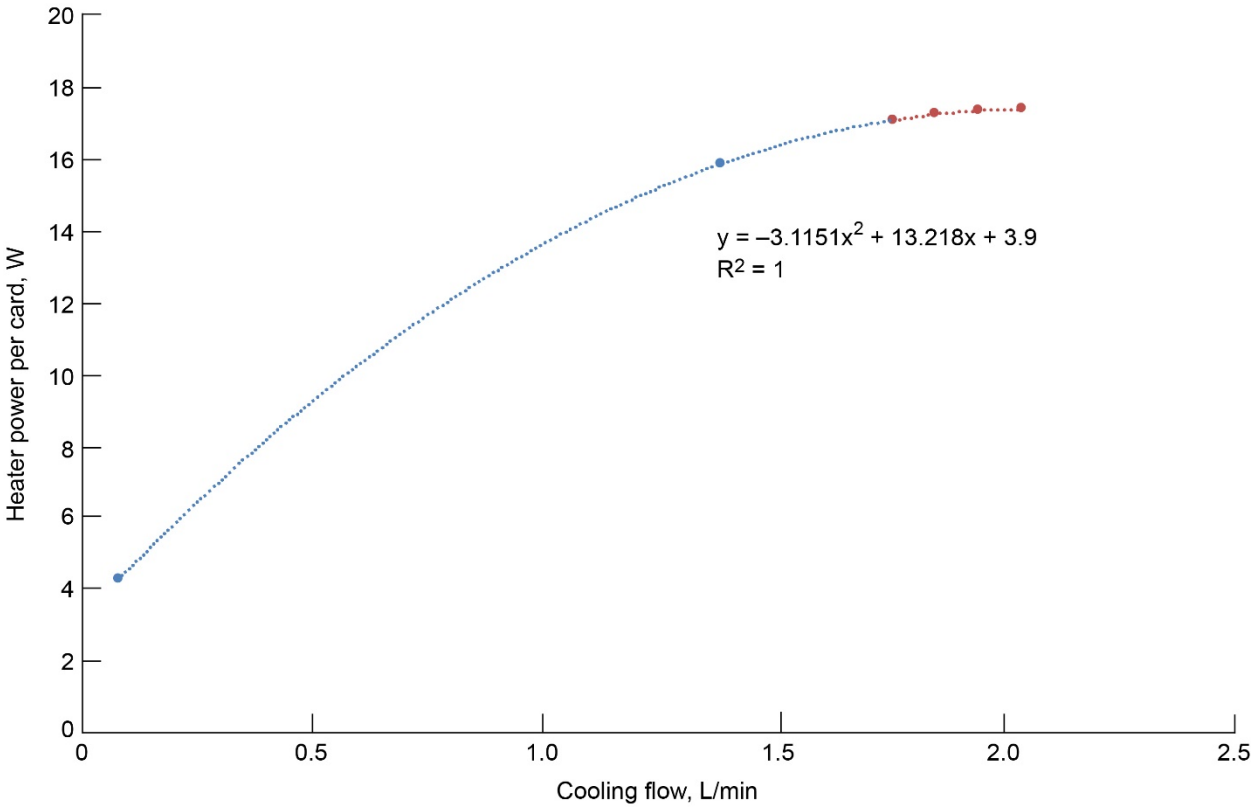

Figure 16.—Maximum waste heat power per card over range of flow rates.

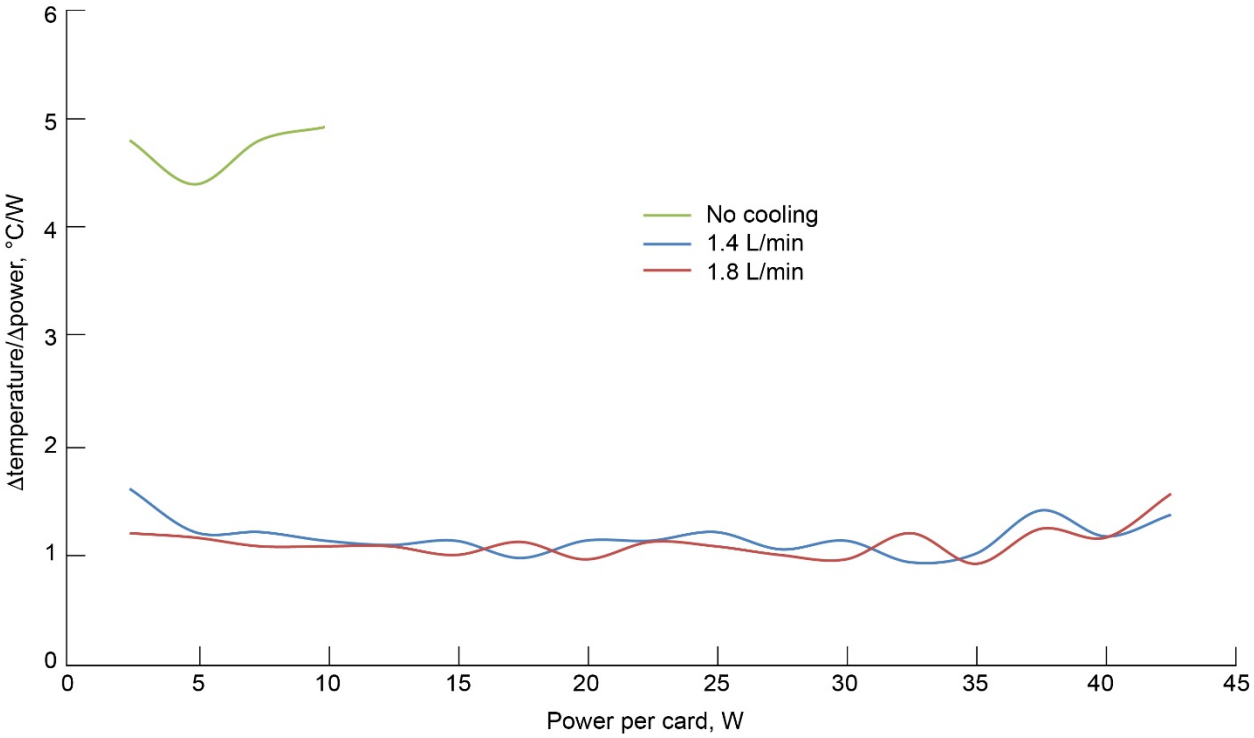

Figure 17.—Change in temperature with power as function of input power to card.

TABLE VII.—SUMMARY OF TIME TO ACHIEVE STEADY-STATE OPERATING TEMPERATURE

Flow rate, L/min	Heater power range, W/card	Time to steady-state range, min
0.0	2.5 to 12.5	160 to 202
1.4	2.5 to 45	57 to 70
1.8	5 to 45	51 to 60

The approximate time to reach steady state for each power level and flow rate was also determined. This is shown in Figure 18. For the cases with cooling flow, there was a slow increase in the time to reach steady state with increasing heater power level. The average time to reach steady state decreases with increasing coolant flow, as shown in Figure 19. The longer duration needed to reach steady state with lower flow rates is what would be expected. As shown in Figure 15, the steady-state operating temperature increases with decreasing flow rate. Therefore, because of the thermal mass of the components within the system (enclosure, cards, etc.), it should take longer to heat the system up to a higher steady-state temperature. The results shown in Figure 18 are summarized in Table VII. The estimated times to reach steady state are based on the curve fit of the data.

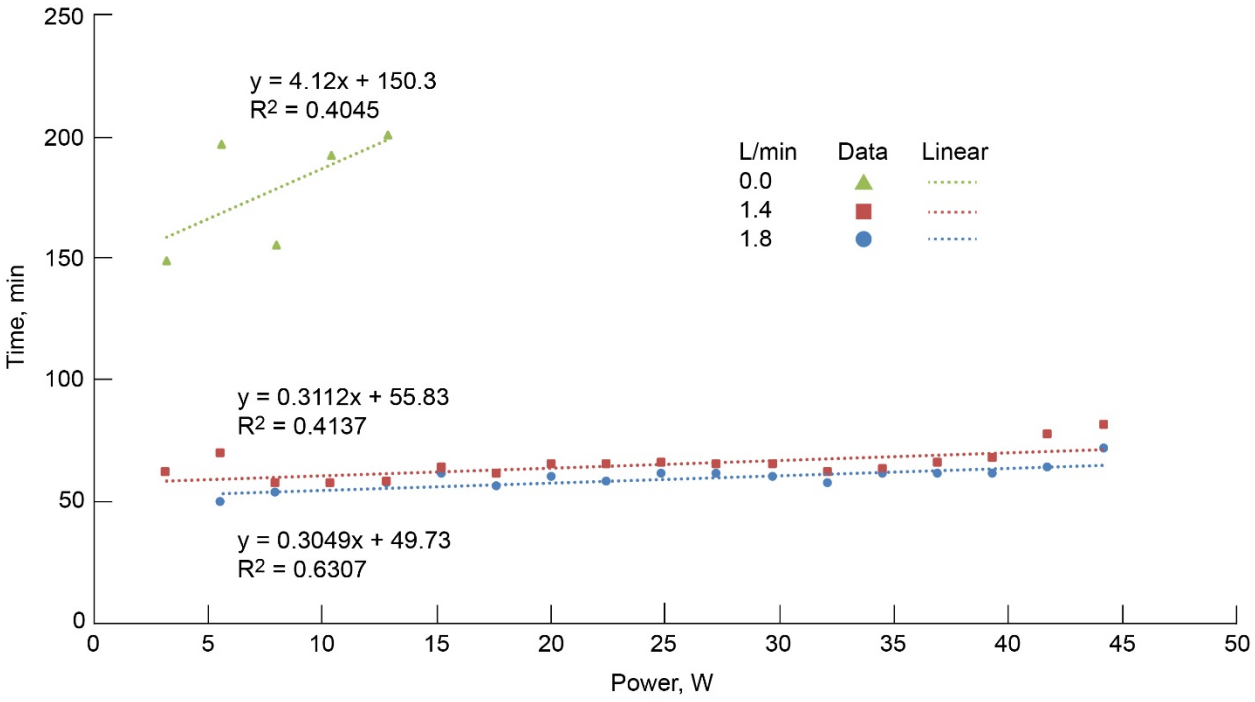

Figure 18.—Time to reach steady state as function of card heater power.

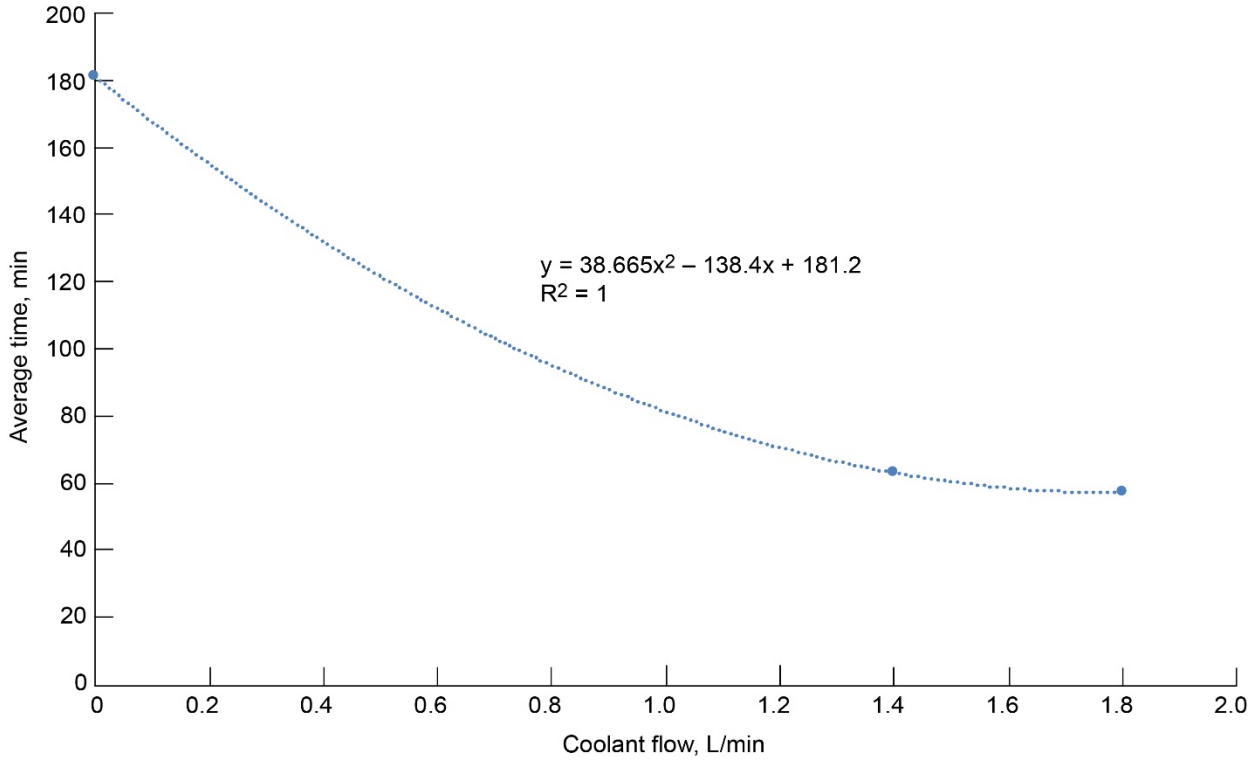

Figure 19.—Average time to reach steady state as function of coolant flow rate.

The variation in card temperature within the enclosure was also determined through the testing. Figure 20 shows the maximum card temperature achieved for the cards within the enclosure over the range of power levels tested with a coolant flow rate of 1.8 L/min. It also shows that the variation in card temperature increased with increasing heater power level. The card temperature distribution, also at 1.8 L/min coolant flow, is shown in Figure 21 for three power levels (45, 25, and 5 W/card). The maximum variation in card temperature of 6.3 °C occurs at the highest tested power level of 45 W/card.

The temperature distribution shown in Figure 21 demonstrates that at low power levels, such as the 5 W/card shown, the temperature variation between the cards is small and the temperature distribution between the cards is uniform. As the power level per card increases, the temperature variation between the cards also increases. This is likely due to variations in thermal contact resistance between the cards and the case rails. This variation can be caused by differences in the bolt torque of each Wedge-Loc® used to secure the card within the case or due to variations in the surface finish of the case rails and/or cards. This is also evident in the data shown in Figure 20, where a particular card will run cooler or hotter than other cards over the full range of heater powers tested. For example, card 6 was the coolest of all the cards tested over all heater power levels, whereas card 17 was the warmest. For cards near the end of the case, such as card 17, additional factors can come into play, such as a longer heat path to the cold plate.

The temperature distribution for the cards within the enclosure at the 1.4 L/min cooling flow rate are shown in Figure 22 and Figure 23. These results are similar to those seen with the higher flow rate of 1.8 L/min shown in Figure 20 and Figure 21. The variation in card temperature increased with increasing power level. At the highest power level tested of 45 W/card, the maximum temperature variation between the cards was 5.8 °C. This is similar to what was seen with the higher coolant flow case shown in Figure 20. The temperature distribution of the cards shown in Figure 23 is similar to that of Figure 21. At low heater power levels, there is little variation, and as the power level increases, the variation between the cards also increases. This variation follows the same pattern of individual card temperatures for both cooling flow cases. As surmised previously, this is likely due to variations in contact resistance between the cards and the case rail. Since the same pattern emerged for both flow rate cases, this tends to support this conjecture.

The card temperature for the last case with no cooling flow is shown in Figure 24 and Figure 25. The temperatures follow a similar pattern as with the previous cases that utilized a cooling flow. As the heater power level increased, the variation in card temperature also increases. However, this variation was slightly less than that seen with the cooling flow cases. The maximum variation between the card temperatures for the highest power level tested of 12.5 W/card was 4 °C. The distribution in card temperature also followed a similar pattern. For the lower heater power levels, the card temperatures were uniform. As the heater power level was increased, the variation also increased. However, for the case where there was no cooling, the variation in the card temperature differed somewhat from the active cooling cases. This change in the temperature variation between the cards is due to the difference in heat transfer between the cooling and noncooling cases. The noncooling case relies solely on natural convection to remove heat from the cards, whereas the cooling cases use conduction to the cooling plate and then convection into the cooling fluid. Although, some patterns in the distribution were similar, which can be attributed to variations in the thermocouple accuracy.

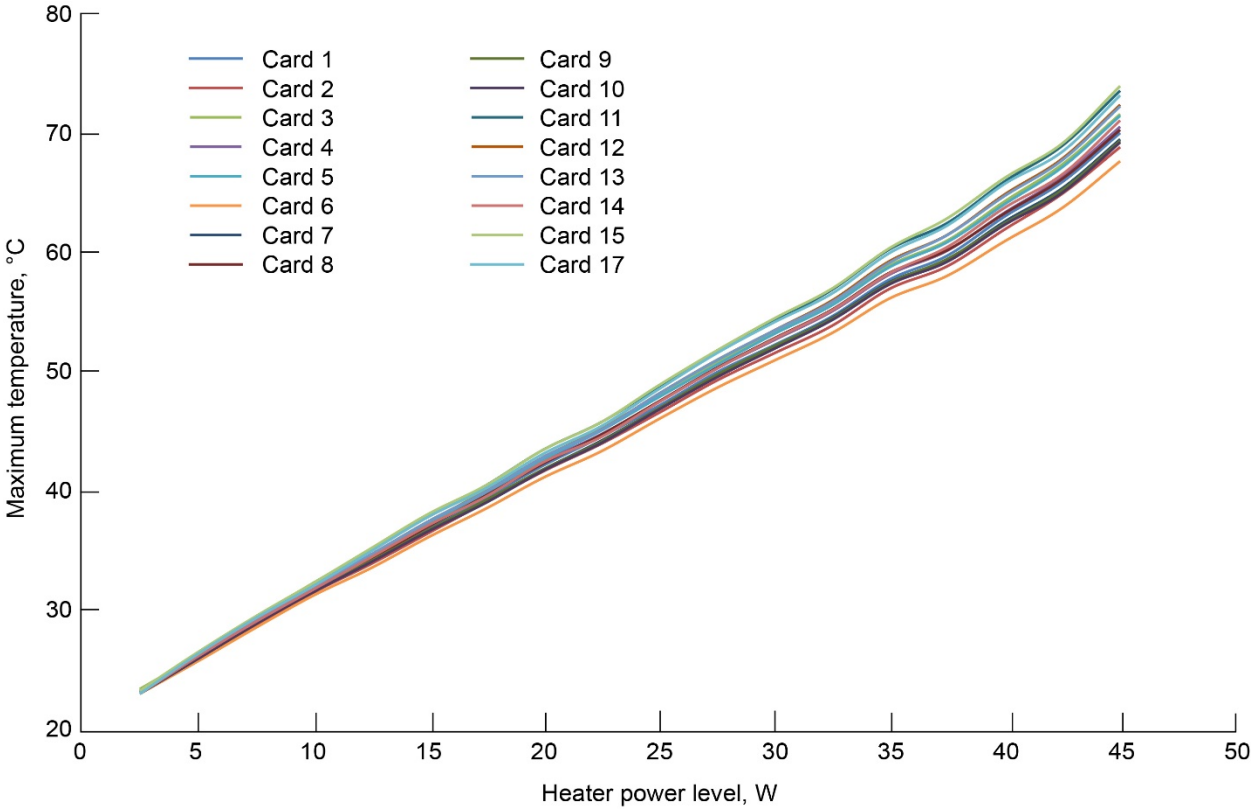

Figure 20.—Maximum individual card temperature over range of power levels tested for cooling flow rate of 1.8 L/min.

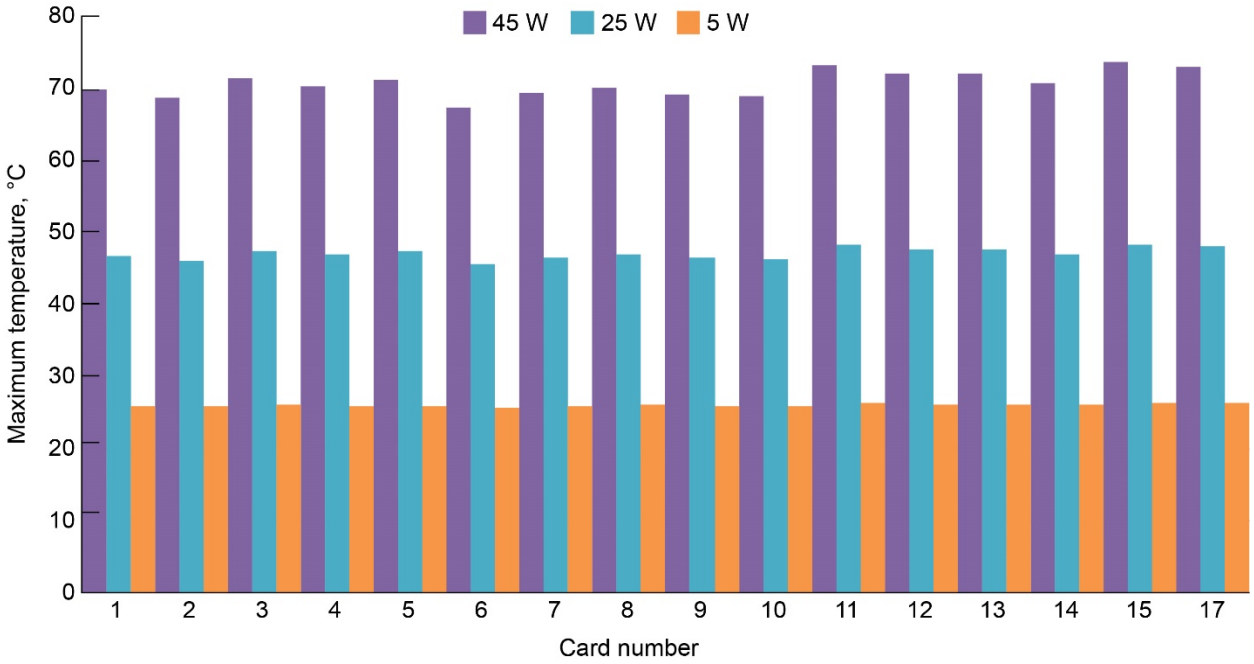

Figure 21.—Maximum card temperature distribution for three tested heater power levels for cooling flow rate of 1.8 L/min.

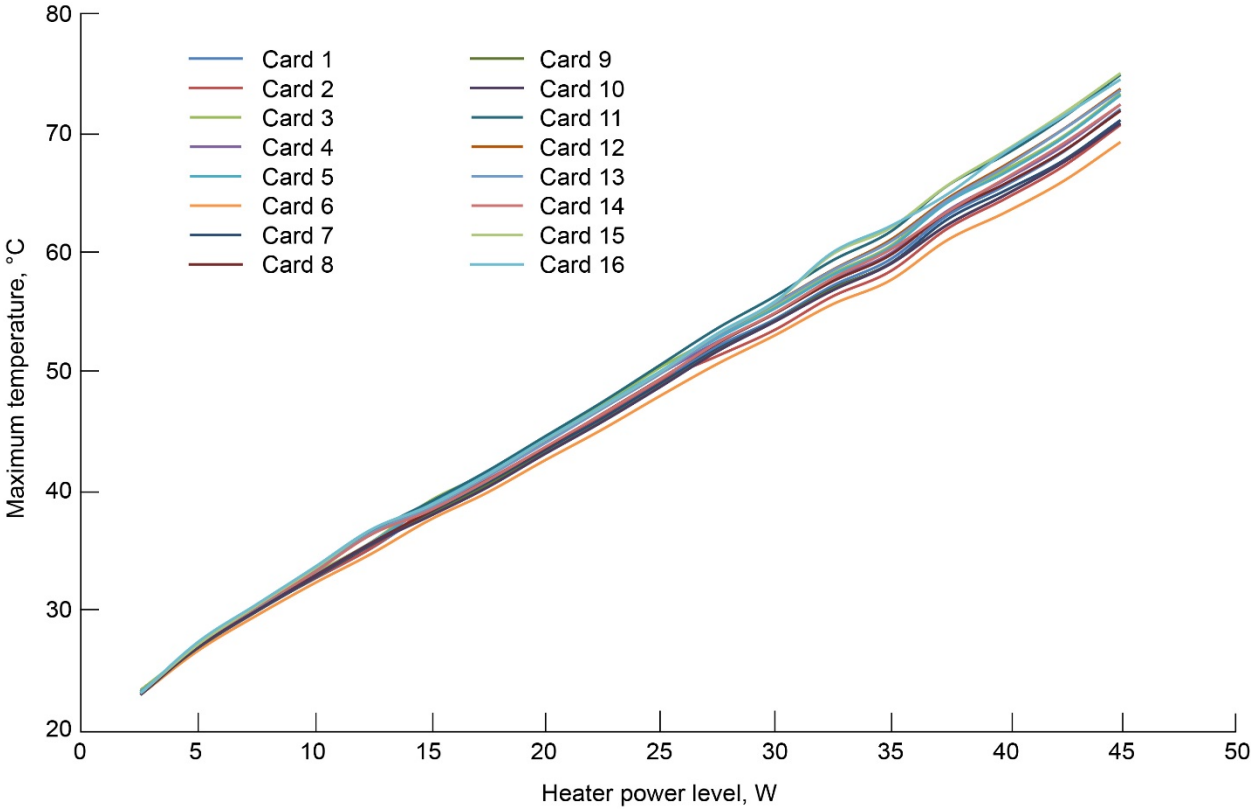

Figure 22.—Maximum individual card temperature over range of power levels tested for cooling flow rate of 1.4 L/min.

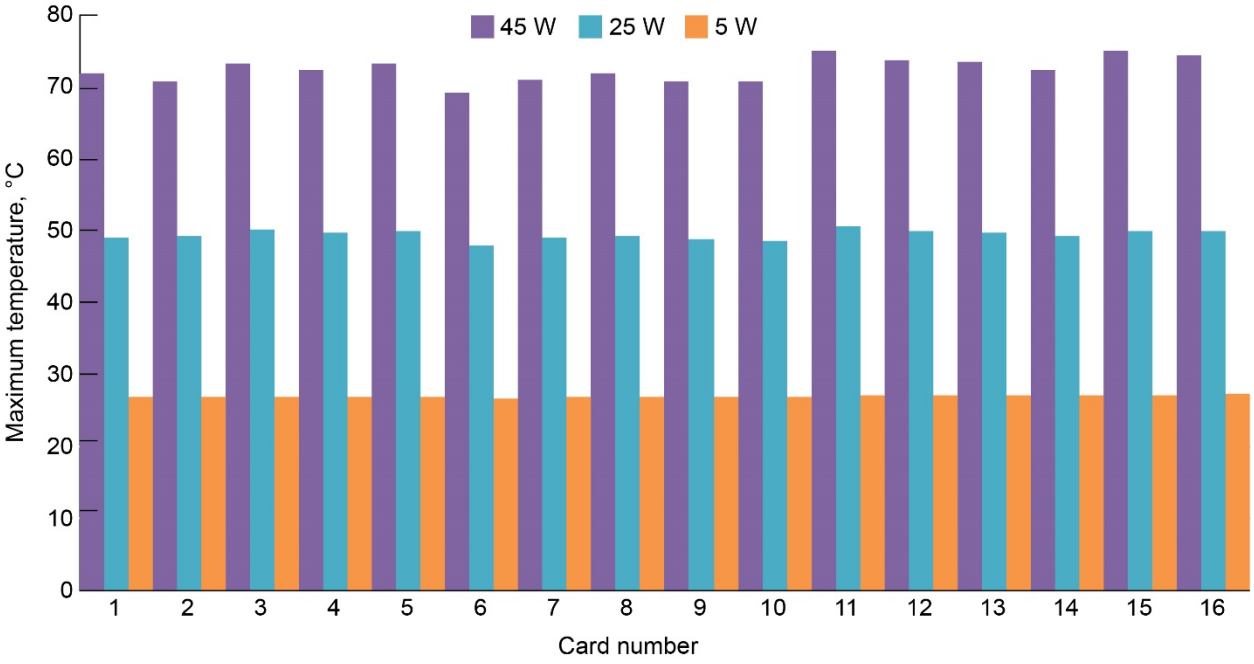

Figure 23.—Maximum card temperature distribution for three tested heater power levels for cooling flow rate of 1.4 L/min.

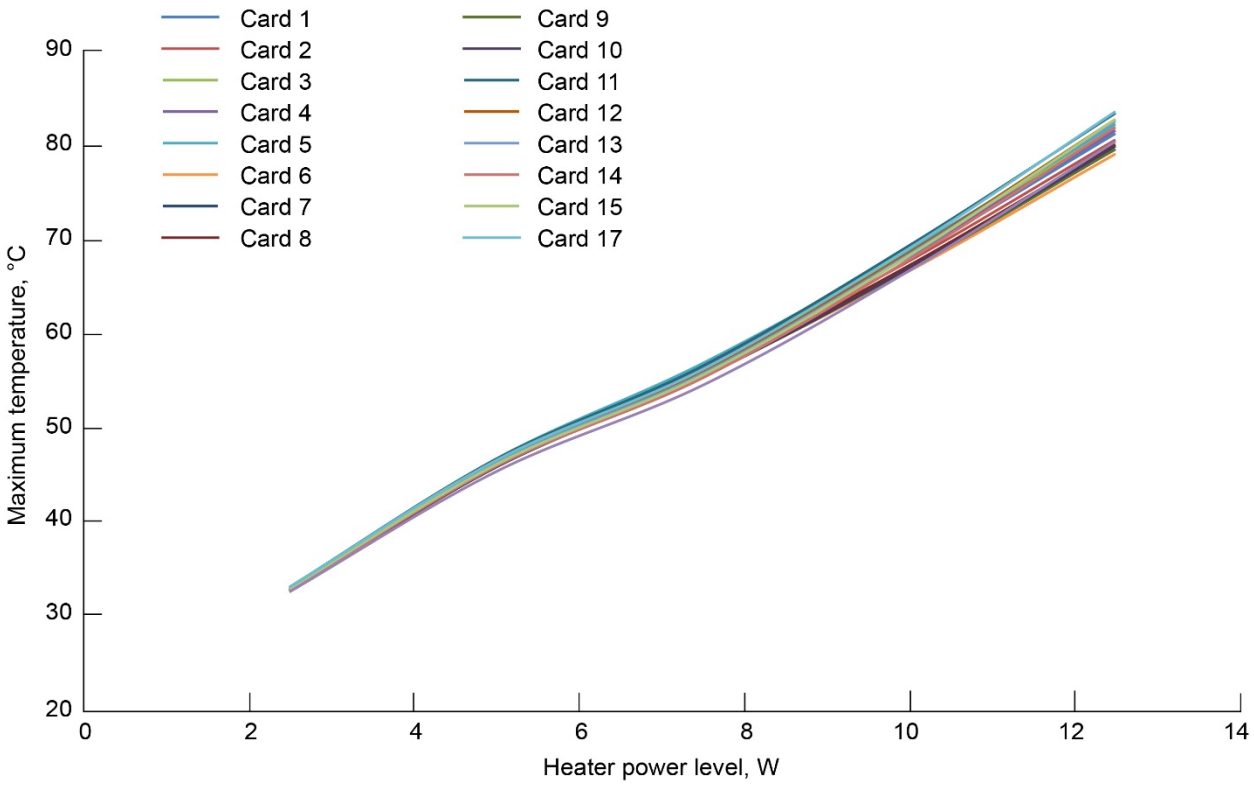

Figure 24.—Maximum individual card temperature over range of power levels tested with no cooling flow.

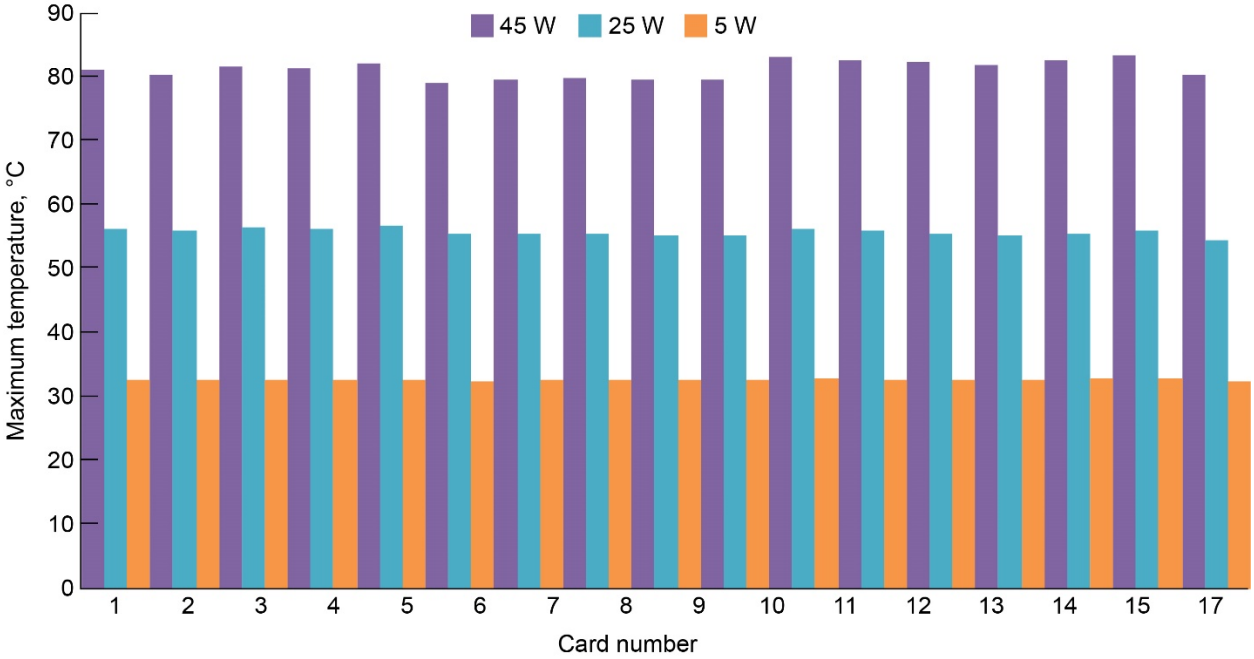

Figure 25.—Maximum card temperature distribution for three tested heater power levels with no cooling flow.

The coolant temperature into and out of the cold plate, as well as the insulation surface temperature, are also shown on the data plots given in the Appendix. For most of the cases, the cold plate coolant inlet temperature was constant throughout the test. The cold plate coolant exit temperature would increase and reach a steady-state operating condition at some point after the test begins, as shown in Figure 26. For this case, with 27.5 W of heater power per card and a coolant flow rate of 1.8 L/min at approximately 300 min into the test, the temperature difference between the coolant inlet and outlet from the cold plate becomes constant at approximately 3 °C for the remainder of the test. For heater power levels above 35 W/card, the inlet temperature to the cold plate begins to rise during the test. This is due to reaching the limits of the chiller's ability to remove the added heat to the water. The chiller is rated at a maximum 500 W of cooling capacity at 20 °C. This rise in the chiller output water temperature is shown in Figure 26 for a heater power of 45 W/card. At approximately 30 min into the test, the cold plate coolant inlet temperature begins to rise. This occurs when the system reaches the steady-state temperature difference between the cold plate inlet and exit coolant temperatures or approximately 4.9 °C. This temperature difference is maintained throughout the test as the inlet coolant temperature rises.

Figure 26 and Figure 27 also show the coolant and insulation temperatures. The insulation surface temperature for the 27.5 W/card case increases by approximately 1.5 °C from the start of the test to where steady-state conditions are reached, whereas for the 45 W/card case, it increases by approximately 4 °C. This rise in the insulation temperature indicates that some of the heat generated is entering the surroundings instead of the cold plate.

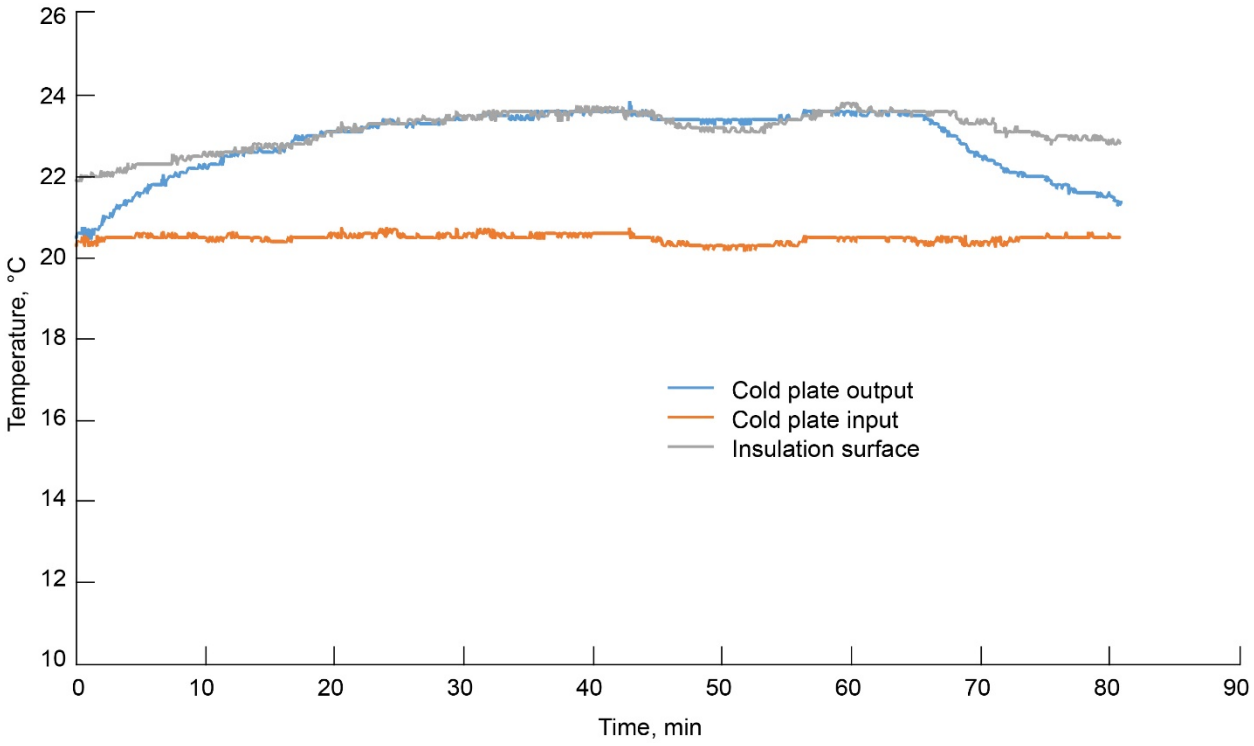

Figure 26.—Coolant and insulation temperatures for heater power of 27.5 W/card and coolant flow rate of 1.8 L/min.

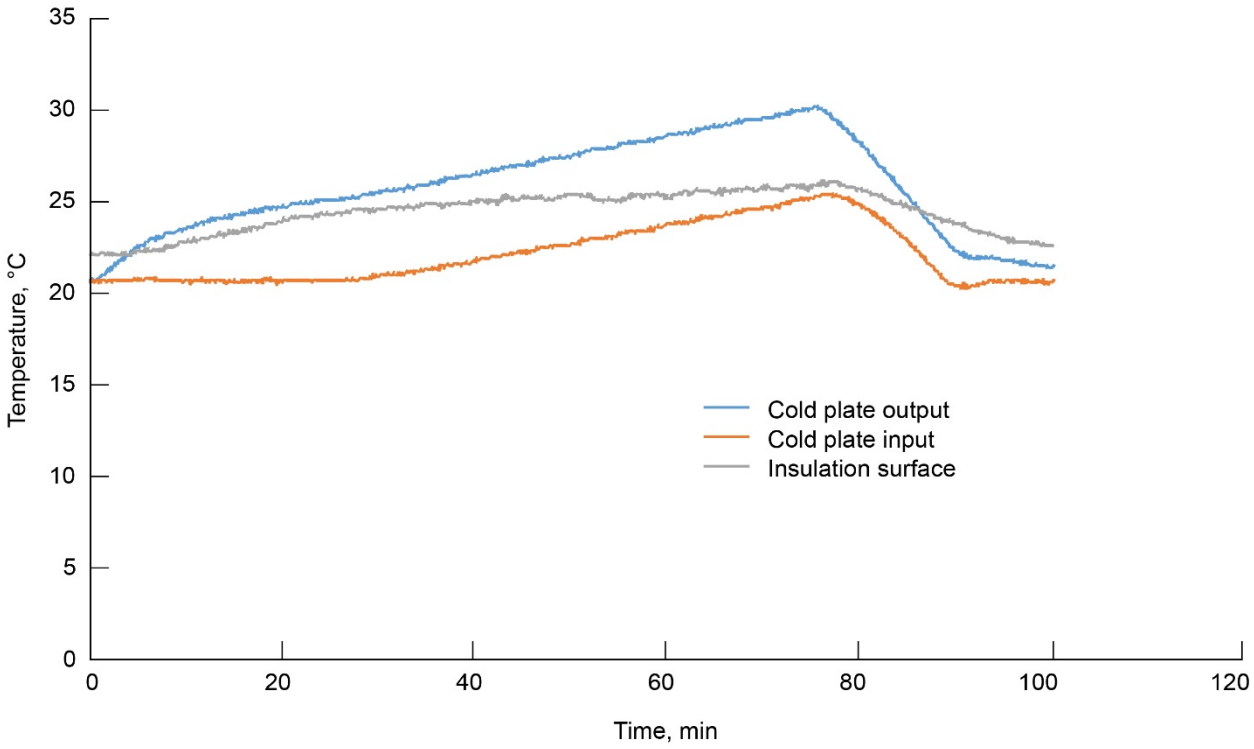

Figure 27.—Coolant and insulation temperatures for heater power of 45 W/card and coolant flow rate of 1.8 L/min.

Using the measured change in the water temperature from the inlet and outlet of the cold plate, an estimate of the heat loss to the surroundings can be made. The heat absorbed by the water in the cold plate (Q) is given by Equation (23), which is dependent on the measured output temperature of the coolant water from the cold plate (T_{co}), the specific heat of water (c_p, assumed a constant at 4,188 J/°C·kg), and the mass flow of the coolant through the cold plate ($\dot{m}$ in kg/m^3).

$$Q = c_p \dot{m} \left(T_{co} - T_c \right) \tag{23}$$

The $\dot{m}$ given by Equation (24) is dependent on the density (ρ_c) of the coolant based on its average temperature as it flows through the cold plate (T_{cavg}).

$$\dot{m} = \rho_c \frac{F_c}{60 \cdot 1{,}000} \tag{24}$$

$$\rho_c = 1{,}002.2 - 0.12325 T_{cavg} - 0.0031937 T_{cavg}^2 \tag{25}$$

The calculated heat loss to the surroundings for both flow cases is shown in Figure 28. The results are similar in both cases with approximately 20 percent of total heat generated being lost to the surroundings. This heat loss to the surroundings is for an insulated enclosure with an open front and back panel, which is an accurate representation of an installed enclosure in a rack.

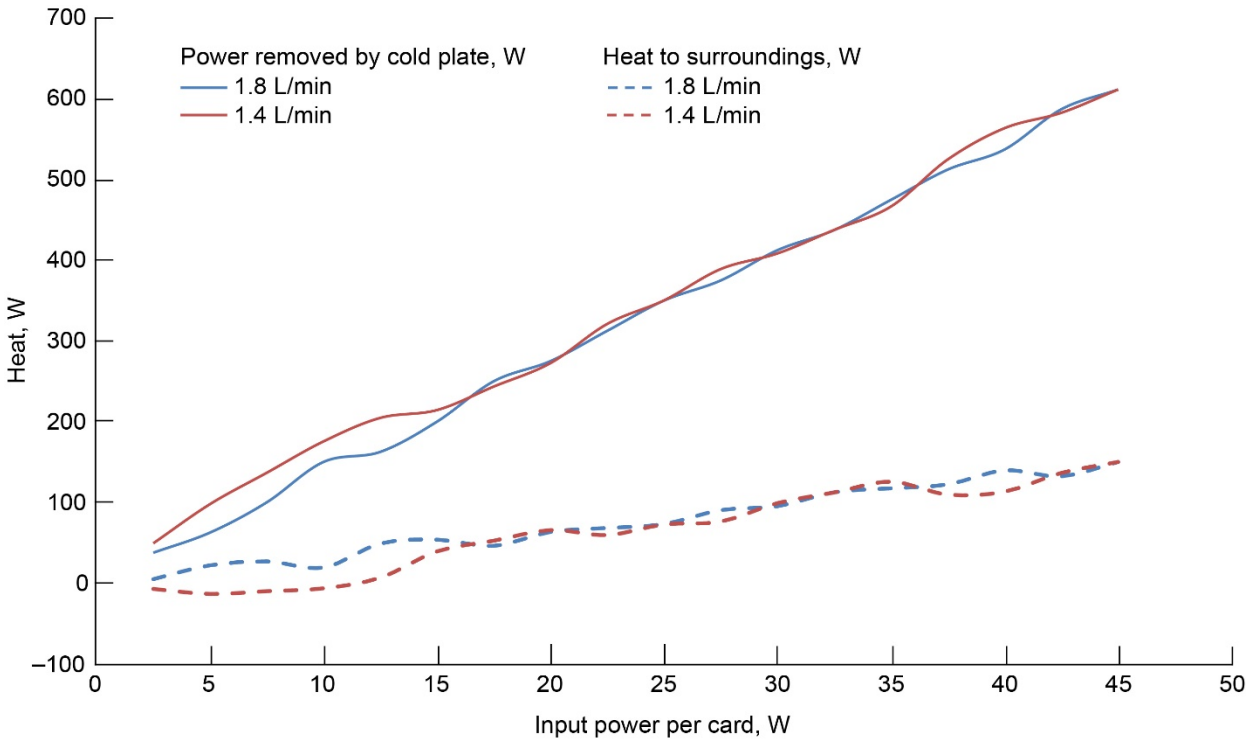

Figure 28.—Heat removed by cold plate and lost to surroundings for range of card heater power.

It should be noted that the heat lost to the surroundings was calculated as negative for the lower power levels with the 1.4 L/min coolant flow case. This is likely due to inaccurately setting the coolant flow from the chiller to the desired 1.4 L/min level for those cases. Small changes in the coolant flow will have a significant effect on the calculated heat absorbed by the coolant water, which in turn will affect the calculated heat loss to the surroundings.

The heat loss shown in Figure 28 also collaborates the rise in cold plate inlet coolant temperature seen after the heater power level is at 35 W/card. At the 35 W/card level, there is a total of 595 W of heat being put into the enclosure. The chillers maximum heat removal capacity is 500 W. However, Figure 28 shows that the heat loss to the surroundings at 35 W/card is just over 100 W. Therefore, subtracting that loss from the total heat input puts the heat removed by the chiller at around 500 W, which is its maximum capacity. Therefore, for this test setup any heater power level above that will cause a rise in the cold plate inlet coolant temperature above the 20 degree setpoint.

5.0 Comparison Between Analysis and Experimental Results

A comparison between the card temperatures predicted by the analysis, outlined in Section 3.0 and the results given in Section 4.0, is shown in Figure 29.

The results between the analysis and the experiment were similar. At lower power levels, the difference between them was on the order of a few percent. As the power level per card increased, the difference between the predicted and tested card temperatures increased. This variation ranged from 0 to 7 percent for the 1.8 L/min test data and 3.5 to 9.6 percent for the 1.4 L/min test data.

The reason for the variation is likely due to the heat lost to the surroundings. This heat loss reduces the heat load on the cold plate. This additional heat loss mechanism would be temperature dependent, and therefore, would increase as the case and card temperature increases. This is consistent with the deviation pattern seen between the analysis and experimental results.

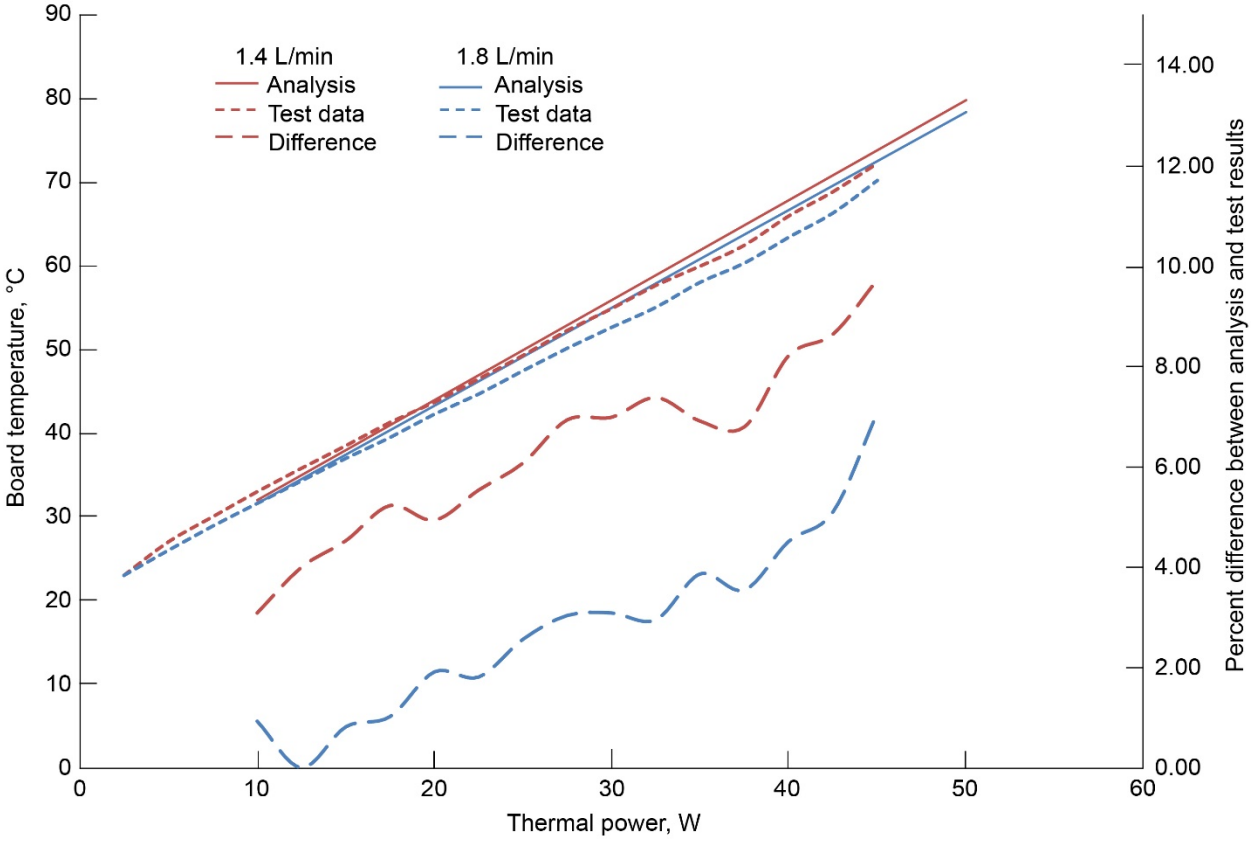

Figure 29.—Comparison of analysis and test results for average card temperature over range of heater power levels.

6.0 Conclusion

The Advanced Modular Power System card steady-state temperature results for operating a fully populated rack over a range of power levels are shown in Figure 15. Three cases were examined with different coolant flow rates, 0.0, 1.4, and 1.8 L/min. This cooling arrangement of having the cold plate located on top of the case produced a maximum waste heat per card of 3.9, 16.3, and 17.6 W, respectively, based on the coolant flow rate to maintain the card temperature below the desired touch temperature of 40 °C. Extrapolating the data shows that the maximum waste heat per card allowable would be approximately 18 W, and that flow rates above approximately 2 L/min will not have an appreciable effect in increasing the allowable waste heat per card.

With coolant flow to the cold plate, the change in steady-state card temperature with increasing heater power was just over 1 °C/W. For the case with no cooling flow, this value was approximately 4.7 °C/W. This difference in the change in card temperature with heater power between the cases with coolant flow and the case without was due to the difference in the heat transfer mechanism of removing the waste heat between those cases. The case without cooling had to rely on natural convection for heat removal, whereas the ones with cooling flow utilized forced convection to the cooling water, which is much more effective in removing the waste heat than natural convection.

The time needed to reach steady state also differed between the cases with cooling flow and the case without. As the heater power increased, the time for the card temperature to reach steady state also increased. For the cases with cooling flow, this time was on the order of 1 h, whereas for the case without cooling, it was on the order of 3 h.

The distribution in steady-state card temperature was also shown for the cooling rates and heater power levels tested. For all cases, as the heater power level increased, the variation in card temperature also increased. The maximum variation in the card temperature at steady-state conditions with the highest heater power level tested for each flow rate case of 1.8, 1.4, and 0.0 L/min was 6.3, 5.8, and 4 °C, respectively.

The difference in inlet and outlet coolant temperature from the cold plate was used to estimate the amount of heat that was lost to the surroundings due to natural convection during the testing. The analysis of the data showed that both cases with coolant flow were similar in the heat lost to the surroundings. This heat loss increased with increasing heater power level. The results showed that approximately 20 percent of the heater power was lost to the surroundings through natural convection.

An analysis was also set up to provide an analytical estimate of the card temperature based on the coolant flow rate and heater power level. The difference between the predicted steady-state card temperatures derived from the analysis to that experimentally determined increased as the heater power increased. The analysis predicted higher card temperatures than that determined from the experiment. For the 1.8 L/min flow rate, the difference between the analysis and experiment was 0 percent at low heater power levels to 7 percent at the highest heater power level tested. Similarly, for the 1.4 L/min case, the difference between the analysis and experiment varied between 3.5 to 9.6 percent. It is believed that the increasing variation in card temperature between the analysis and experiment was due to the heat loss to the surroundings, which was not accounted for in the analysis.

Appendix—Test Data

Figure 30 to Figure 70 contain test data from varying heater powers from 2.5 to 45 W at coolant flow rates of 1.8 and 1.4 L/min and 2.5 to 12.5 W at 0.0 L/min coolant flow rate.

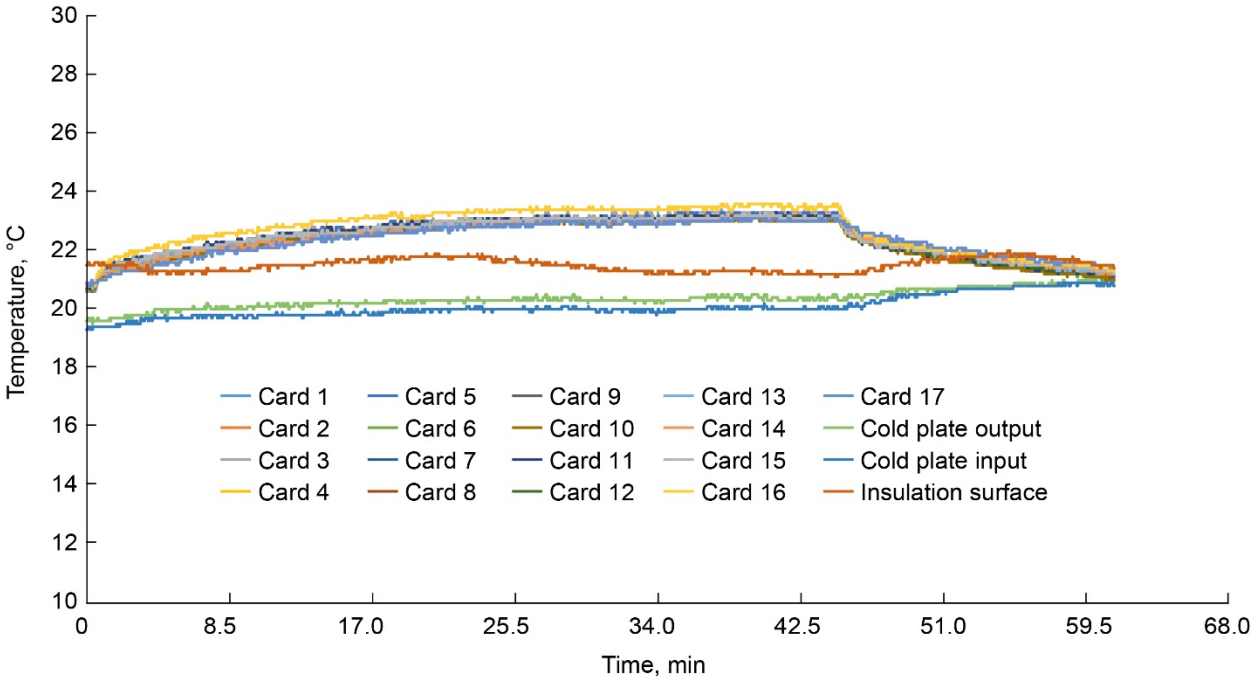

Figure 30.—Card temperature for 2.5 W heater power per card at 1.8 L/min cooling flow rate.

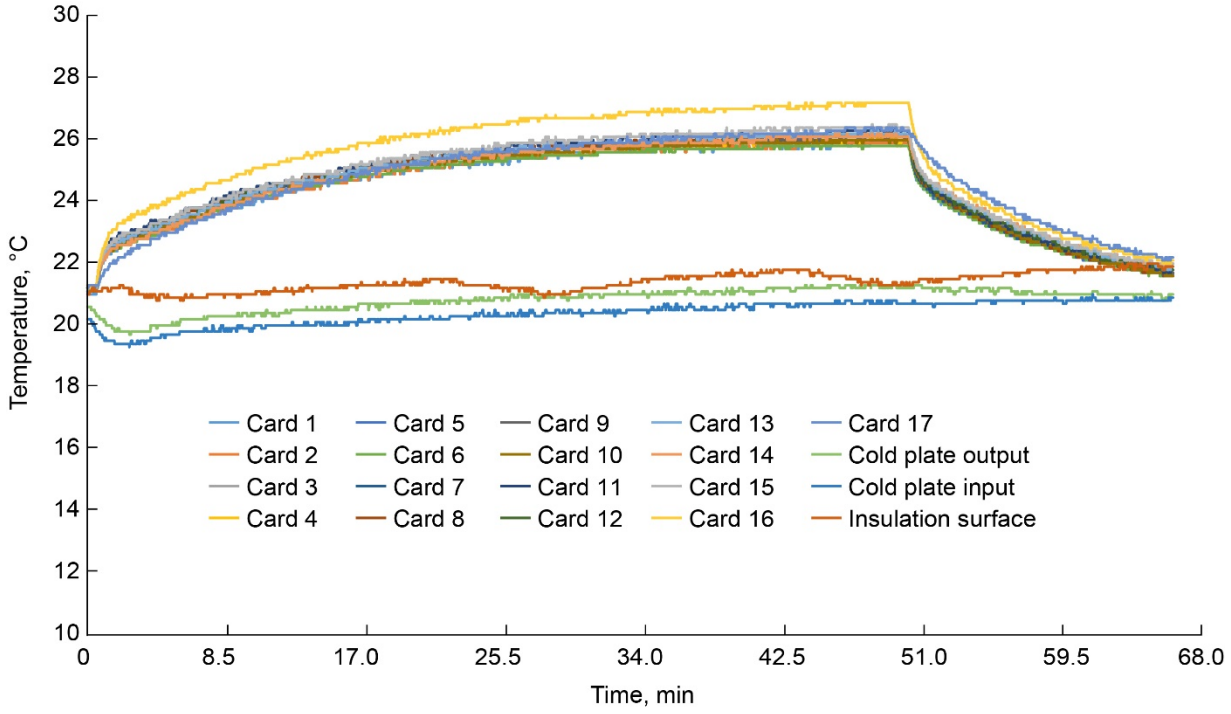

Figure 31.—Card temperature for 5.0 W heater power per card at 1.8 L/min cooling flow rate.

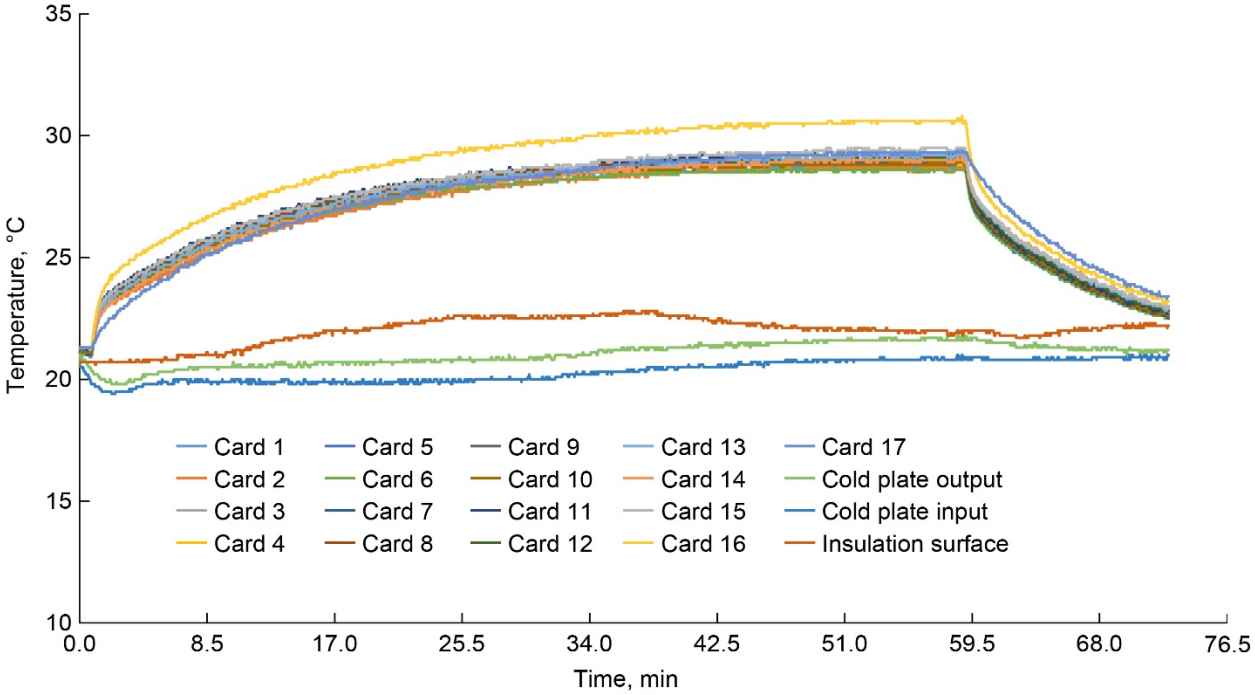

Figure 32.—Card temperature for 7.5 W heater power per card at 1.8 L/min cooling flow rate.

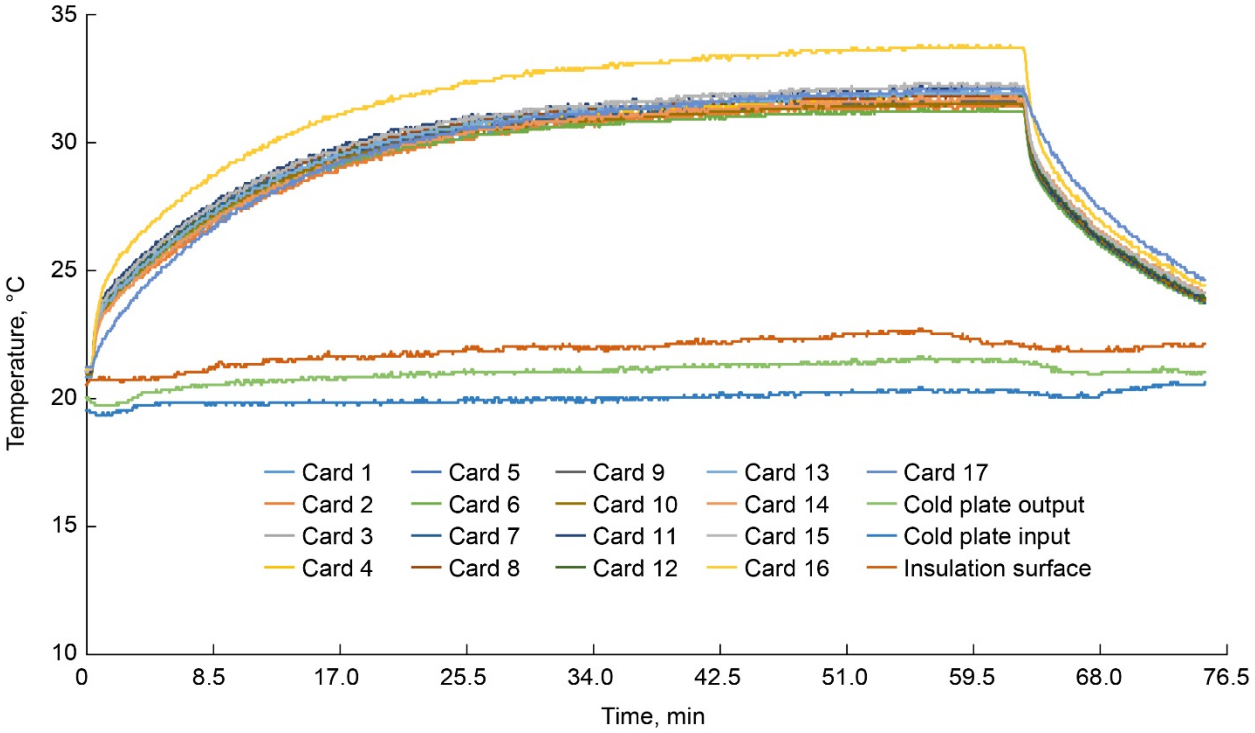

Figure 33.—Card temperature for 10.0 W heater power per card at 1.8 L/min cooling flow rate.

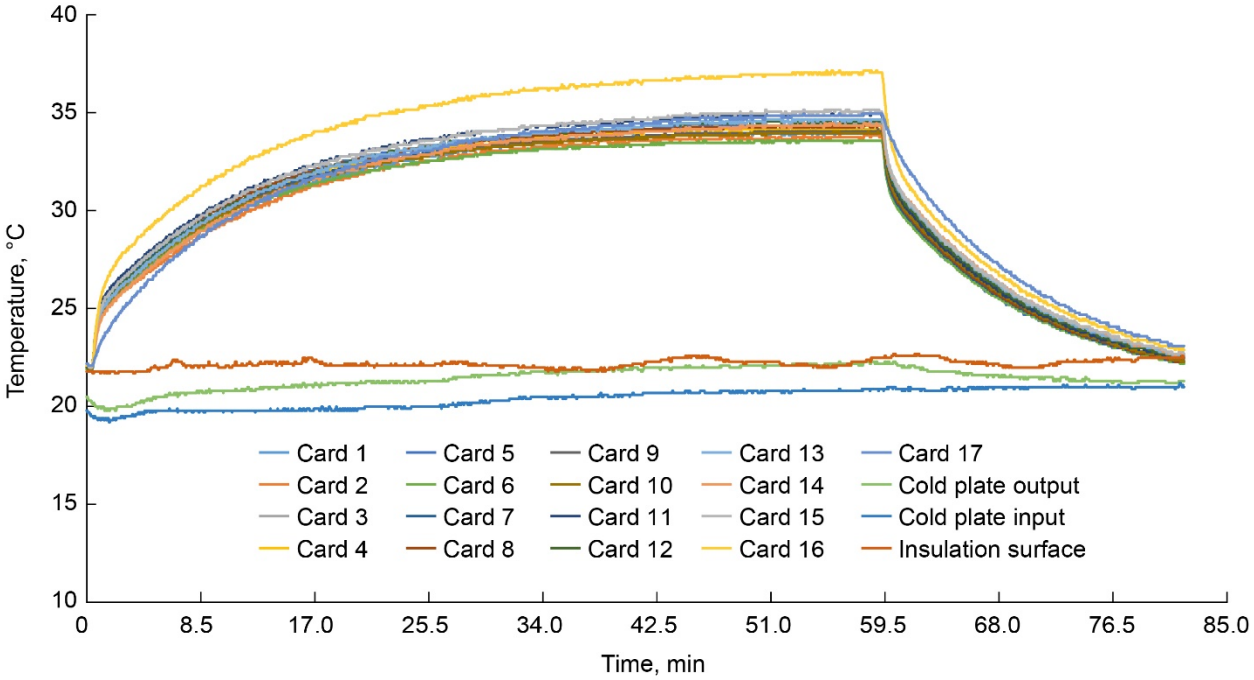

Figure 34.—Card temperature for 12.5 W heater power per card at 1.8 L/min cooling flow rate.

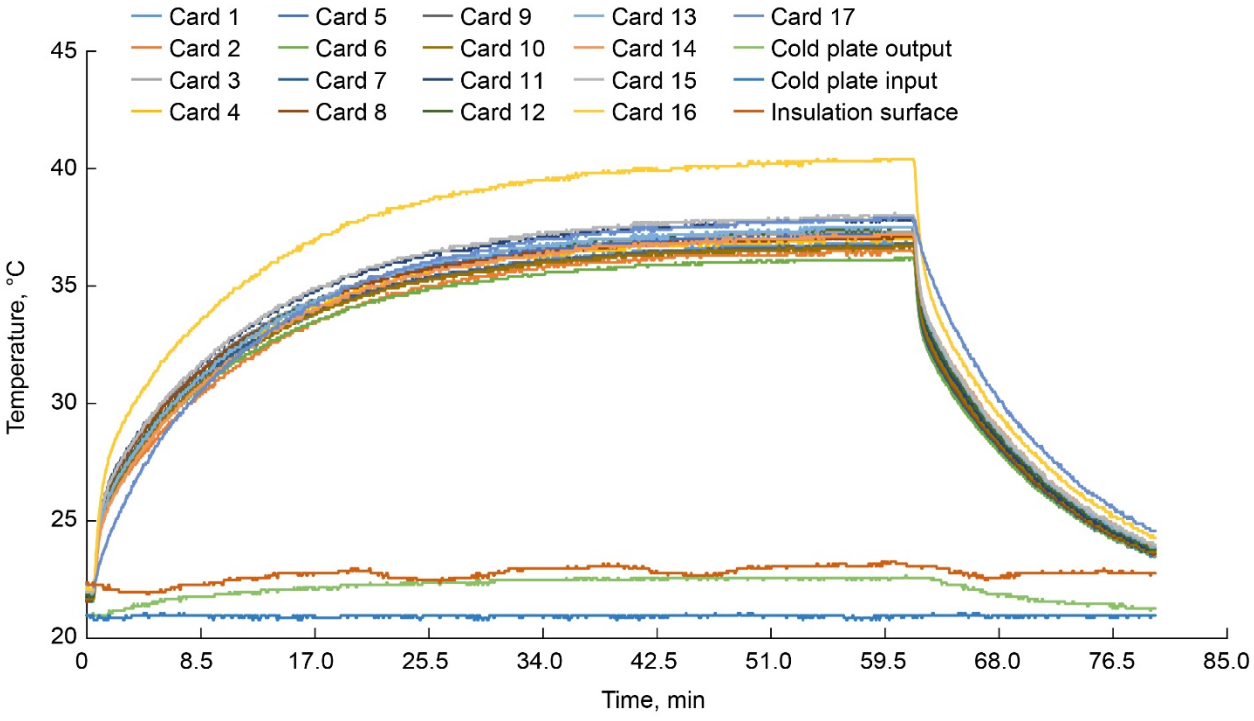

Figure 35.—Card temperature for 15.0 W heater power per card at 1.8 L/min cooling flow rate.

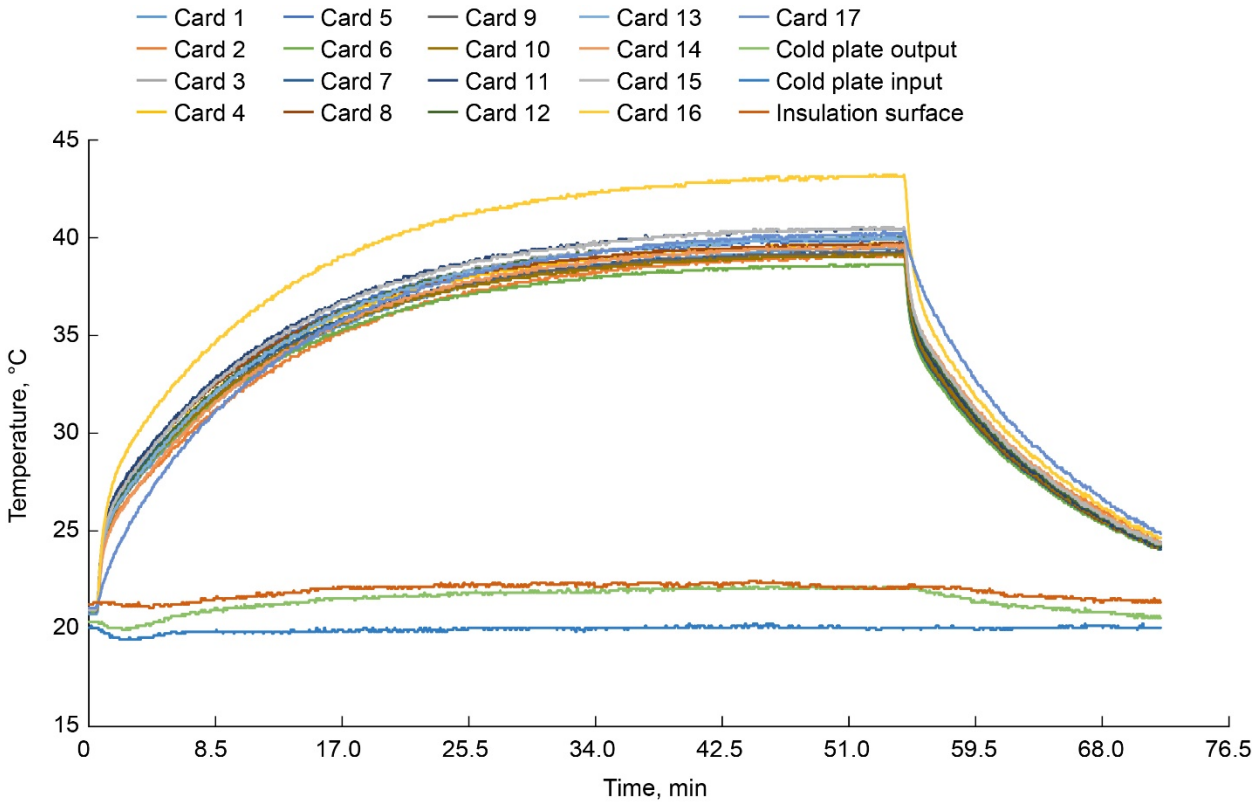

Figure 36.—Card temperature for 17.5 W heater power per card at 1.8 L/min cooling flow rate.

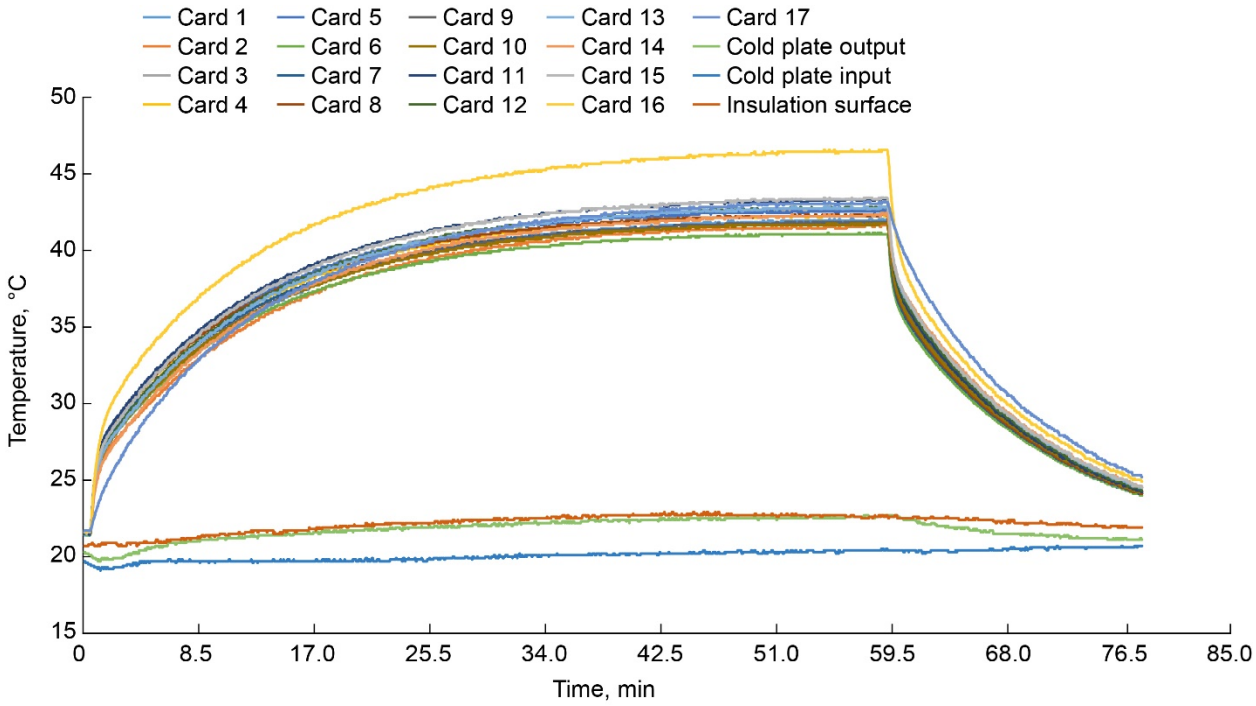

Figure 37.—Card temperature for 20.0 W heater power per card at 1.8 L/min cooling flow rate.

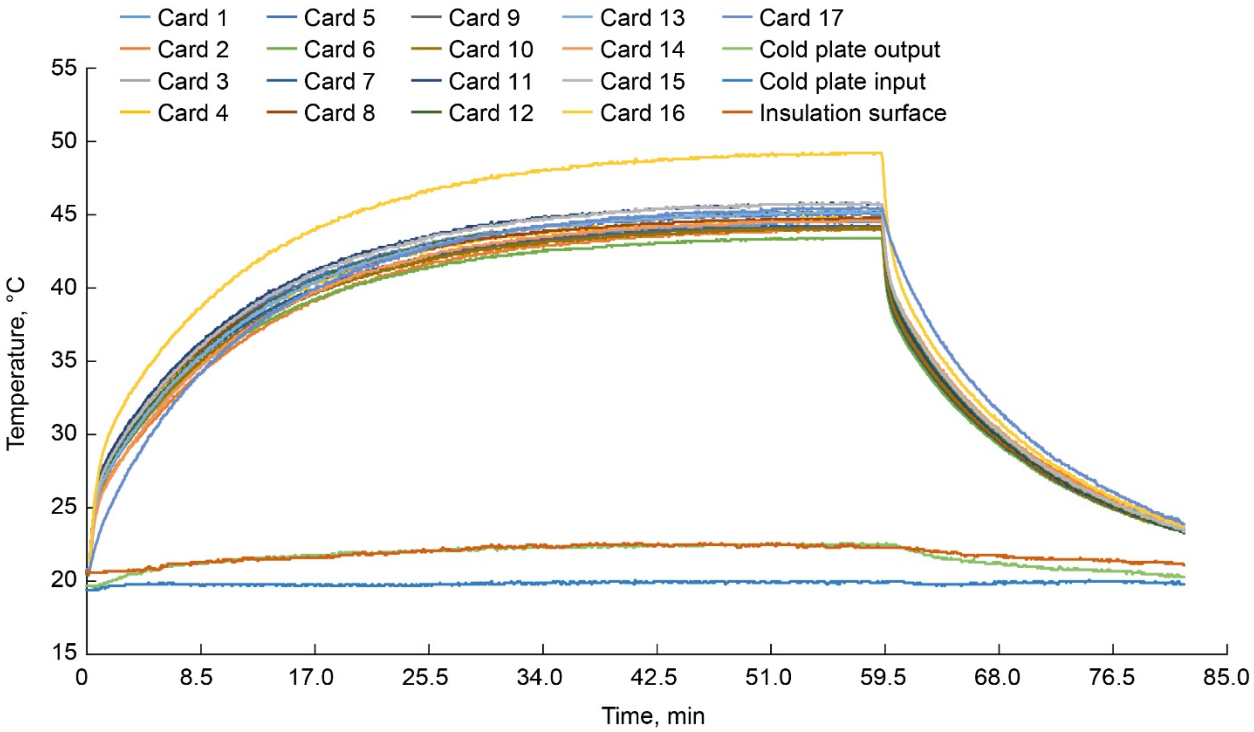

Figure 38.—Card temperature for 22.5 W heater power per card at 1.8 L/min cooling flow rate.

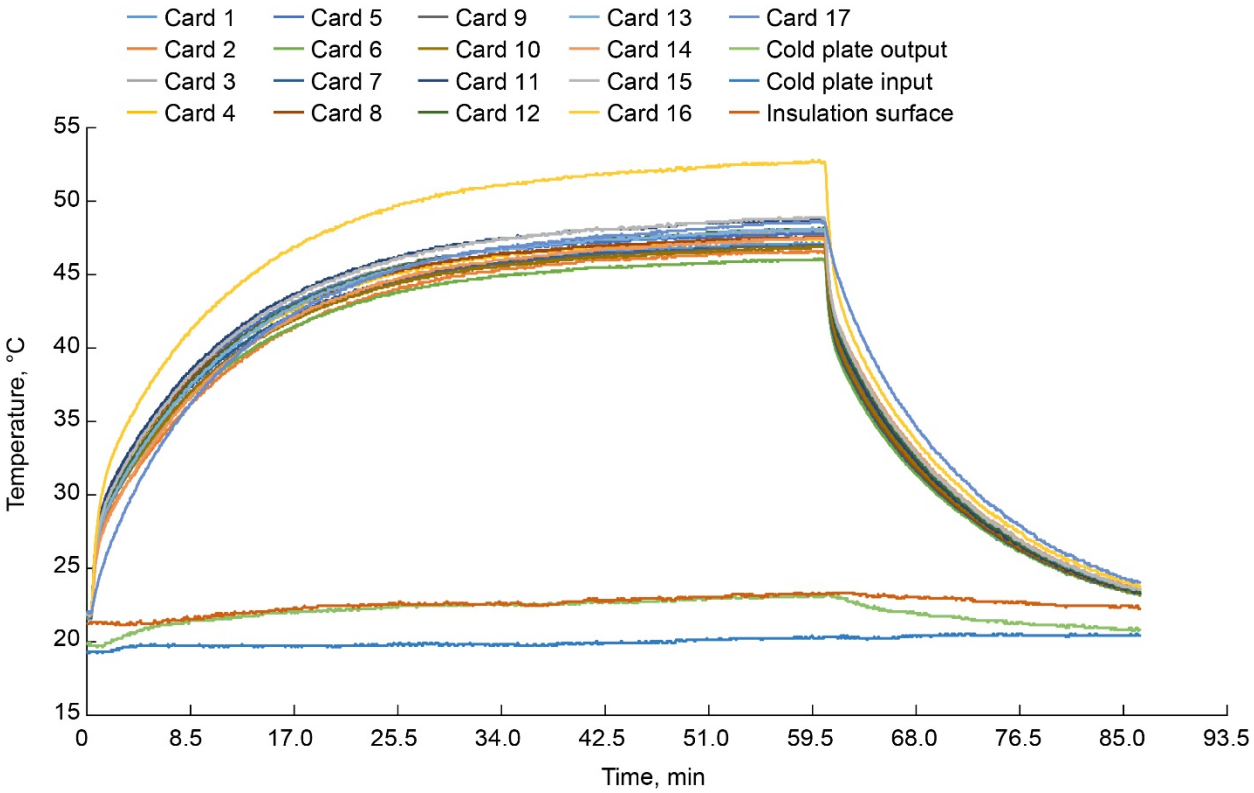

Figure 39.—Card temperature for 25.0 W heater power per card at 1.8 L/min cooling flow rate.

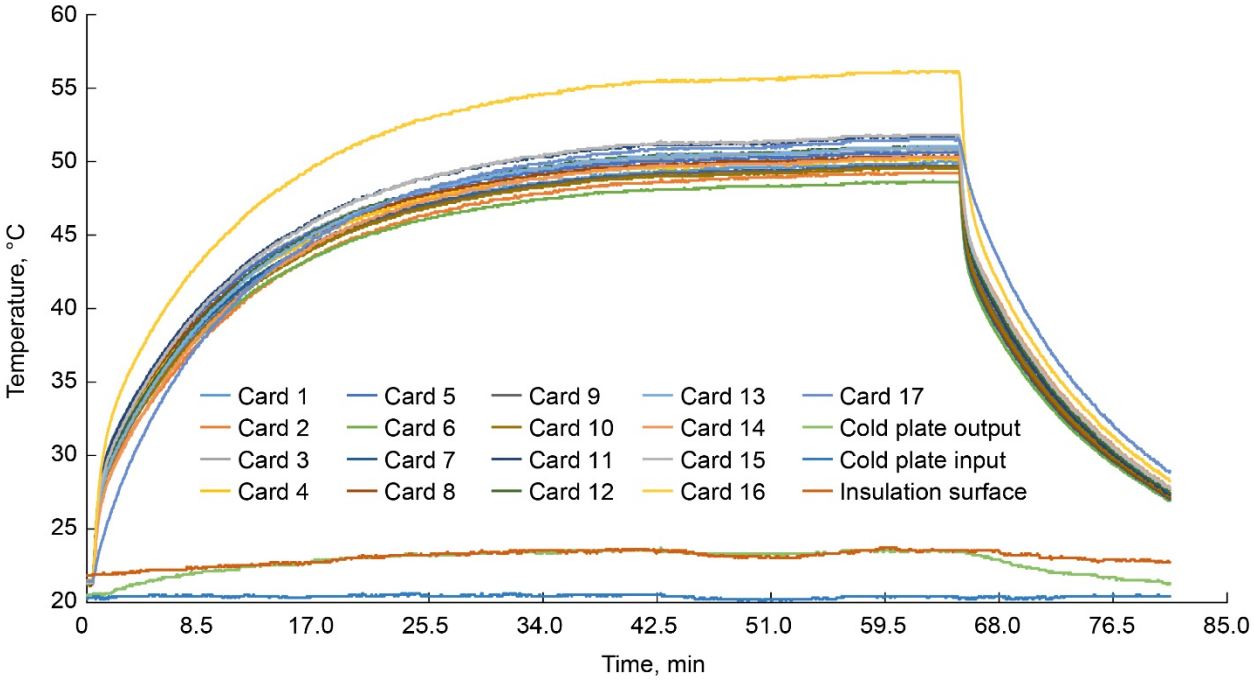

Figure 40.—Card temperature for 27.5 W heater power per card at 1.8 L/min cooling flow rate.

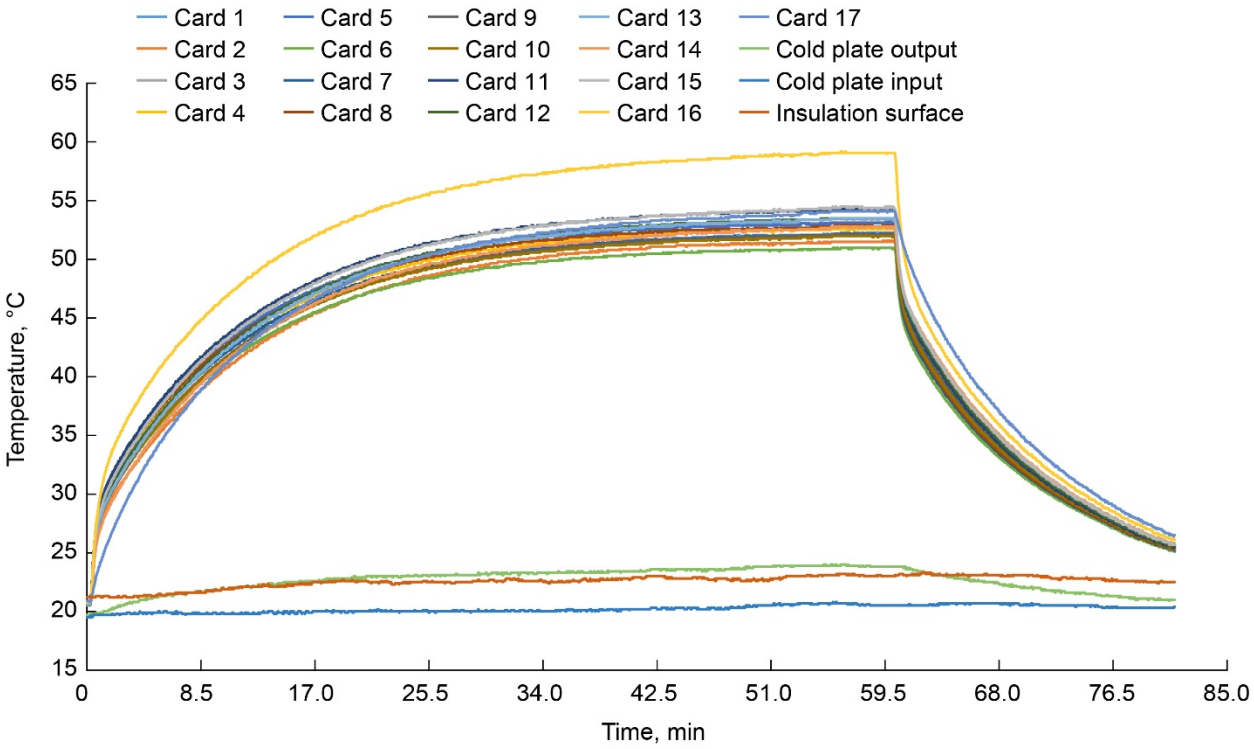

Figure 41.—Card temperature for 30.0 W heater power per card at 1.8 L/min cooling flow rate.

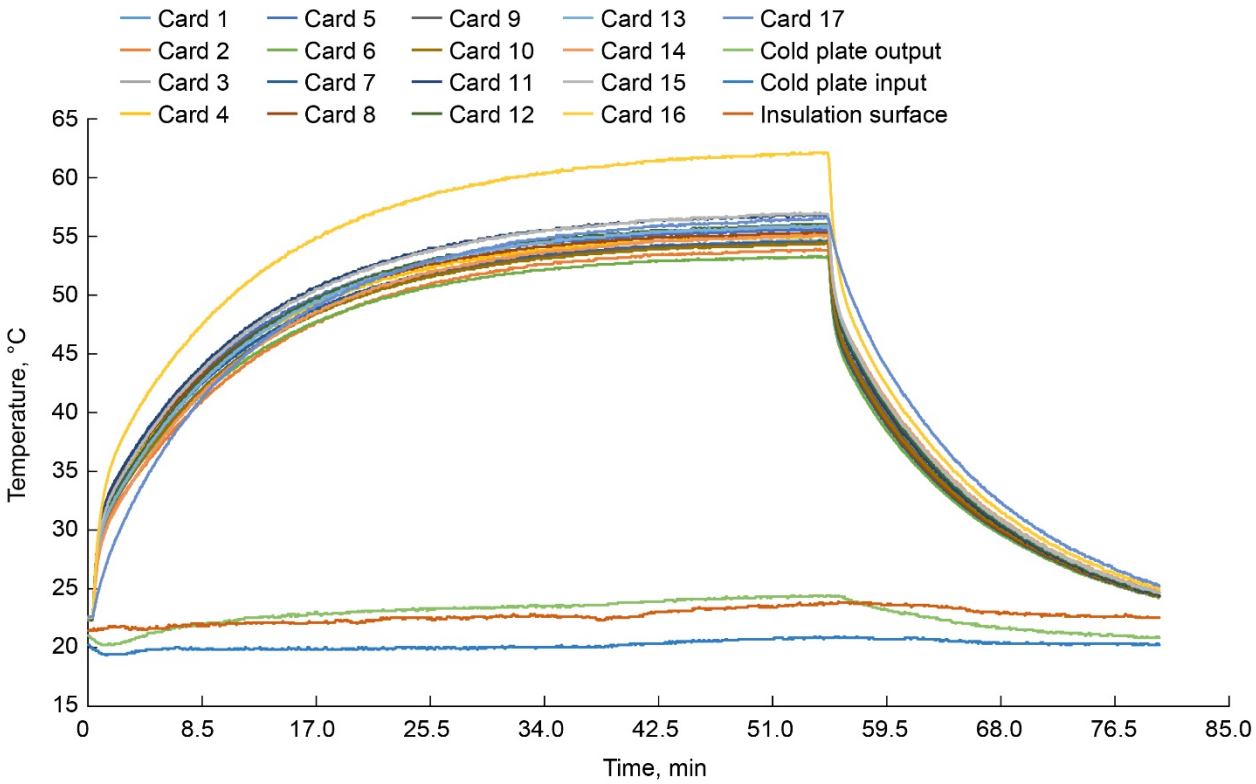

Figure 42.—Card temperature for 32.5 W heater power per card at 1.8 L/min cooling flow rate.

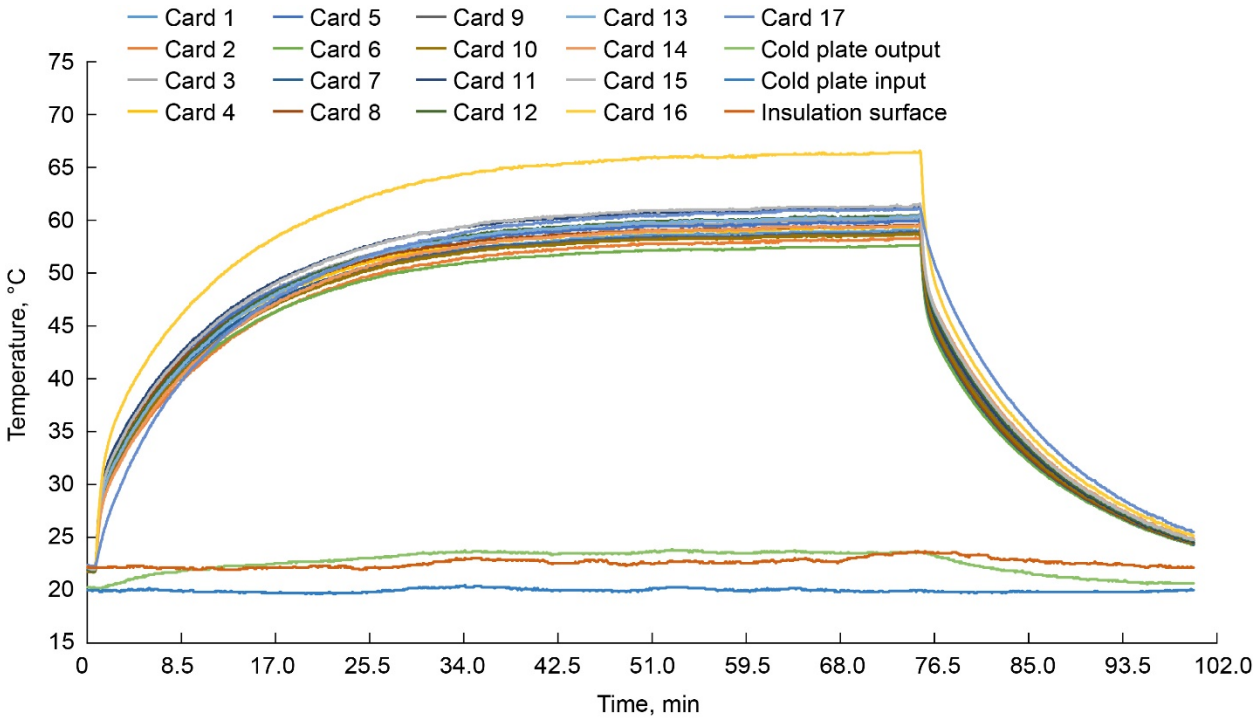

Figure 43.—Card temperature for 35.0 W heater power per card at 1.8 L/min cooling flow rate.

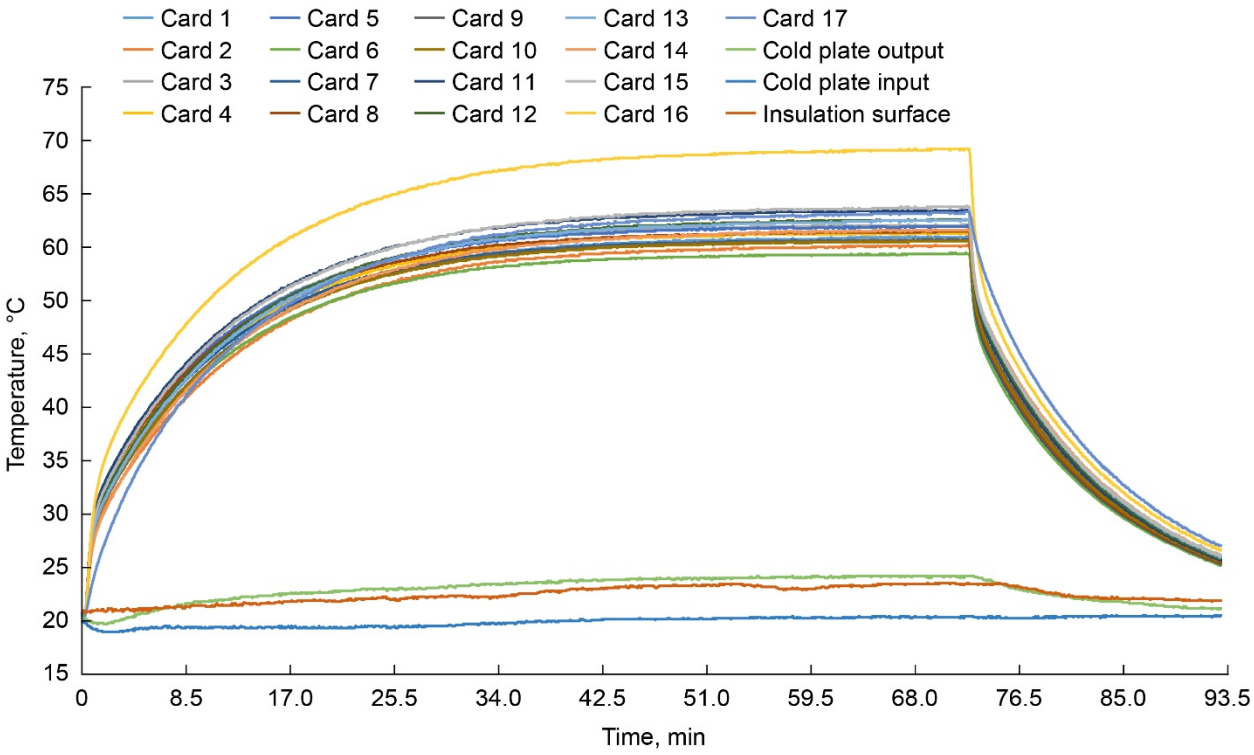

Figure 44.—Card temperature for 37.5 W heater power per card at 1.8 L/min cooling flow rate.

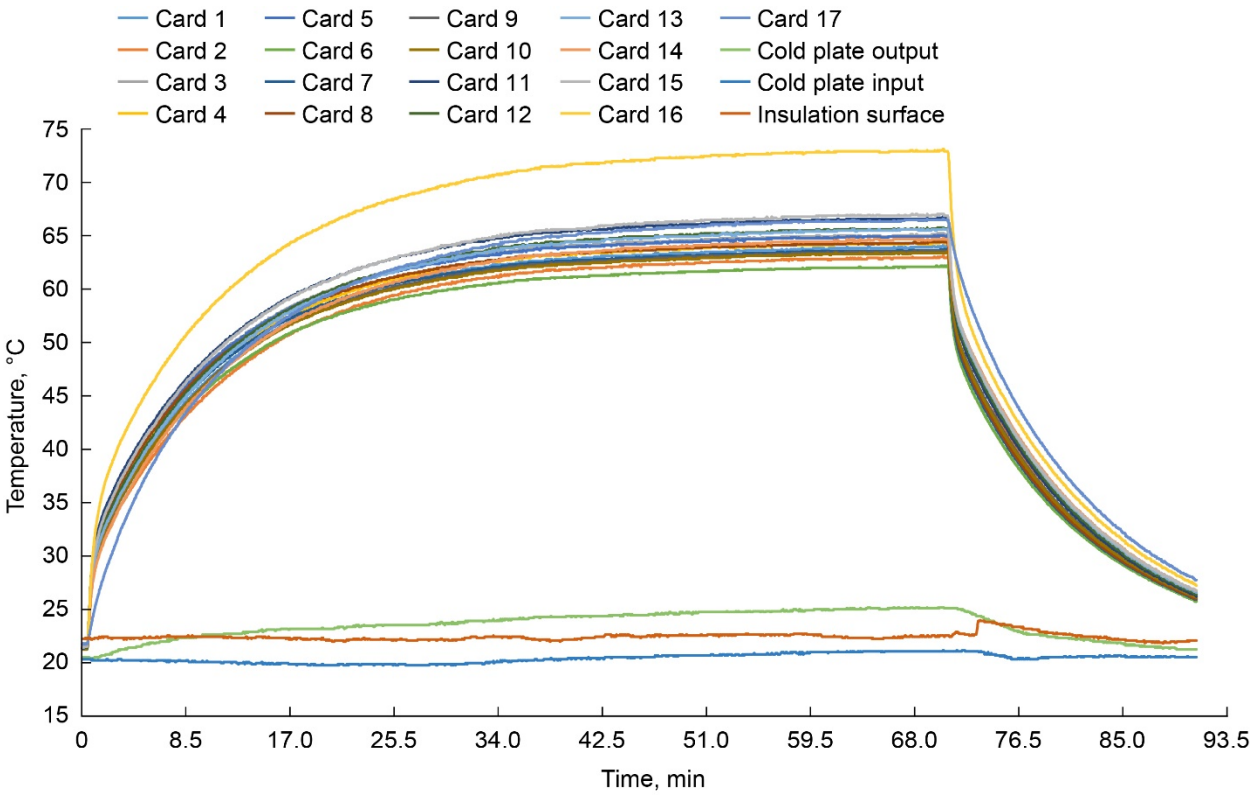

Figure 45.—Card temperature for 40.0 W heater power per card at 1.8 L/min cooling flow rate.

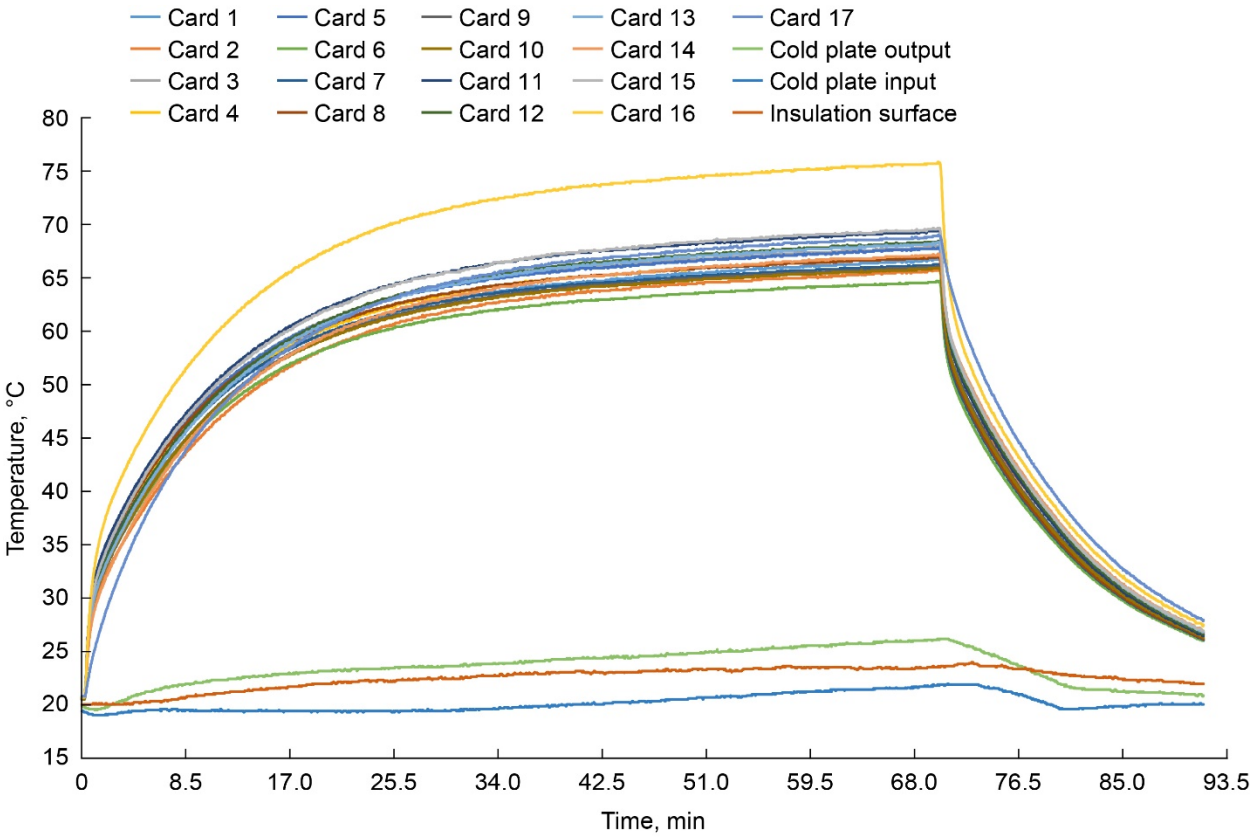

Figure 46.—Card temperature for 42.5 W heater power per card at 1.8 L/min cooling flow rate.

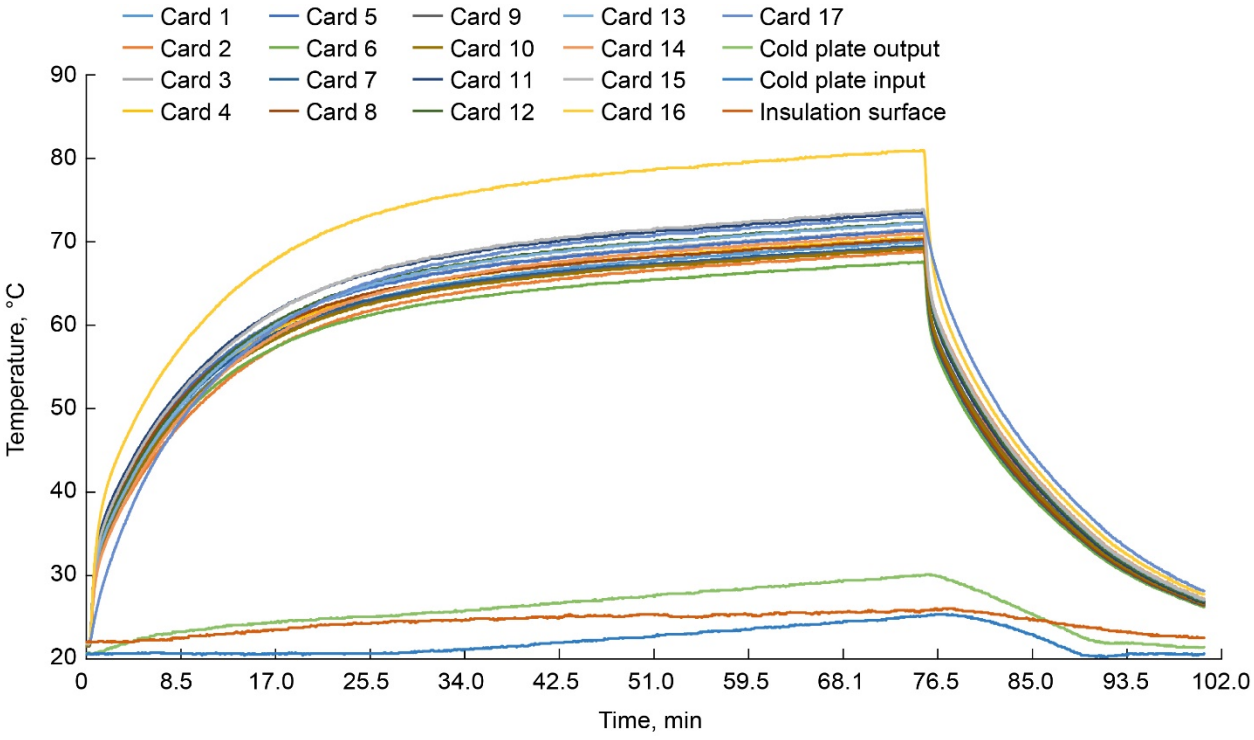

Figure 47.—Card temperature for 45 W heater power per card at 1.8 L/min cooling flow rate.

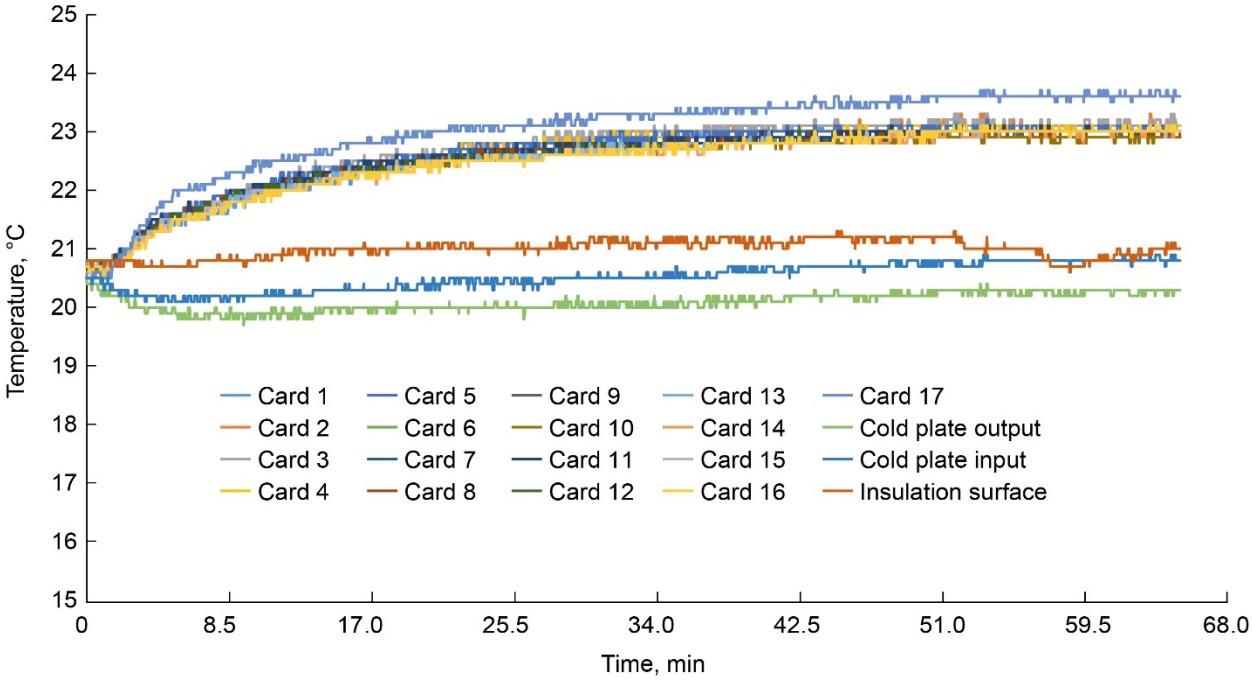

Figure 48.—Card temperature for 2.5 W heater power per card at 1.4 L/min cooling flow rate.

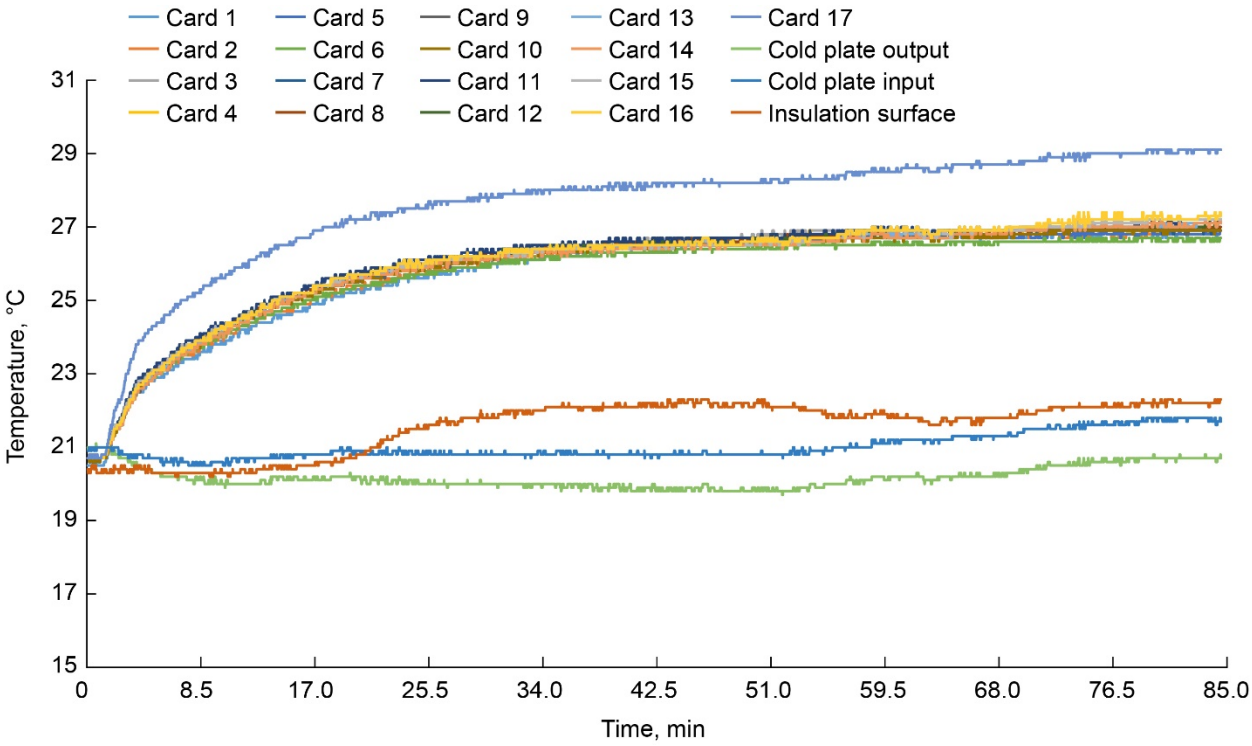

Figure 49.—Card temperature for 5.0 W heater power per card at 1.4 L/min cooling flow rate.

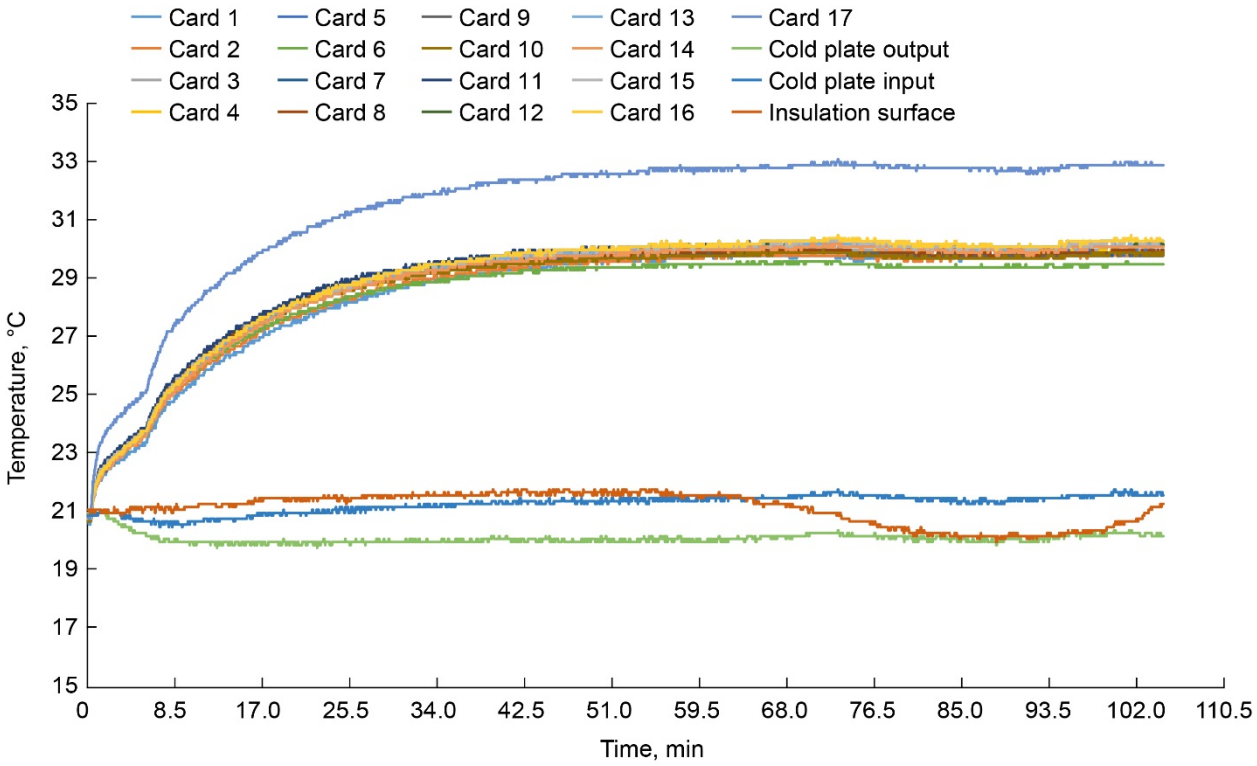

Figure 50.—Card temperature for 7.5 W heater power per card at 1.4 L/min cooling flow rate.

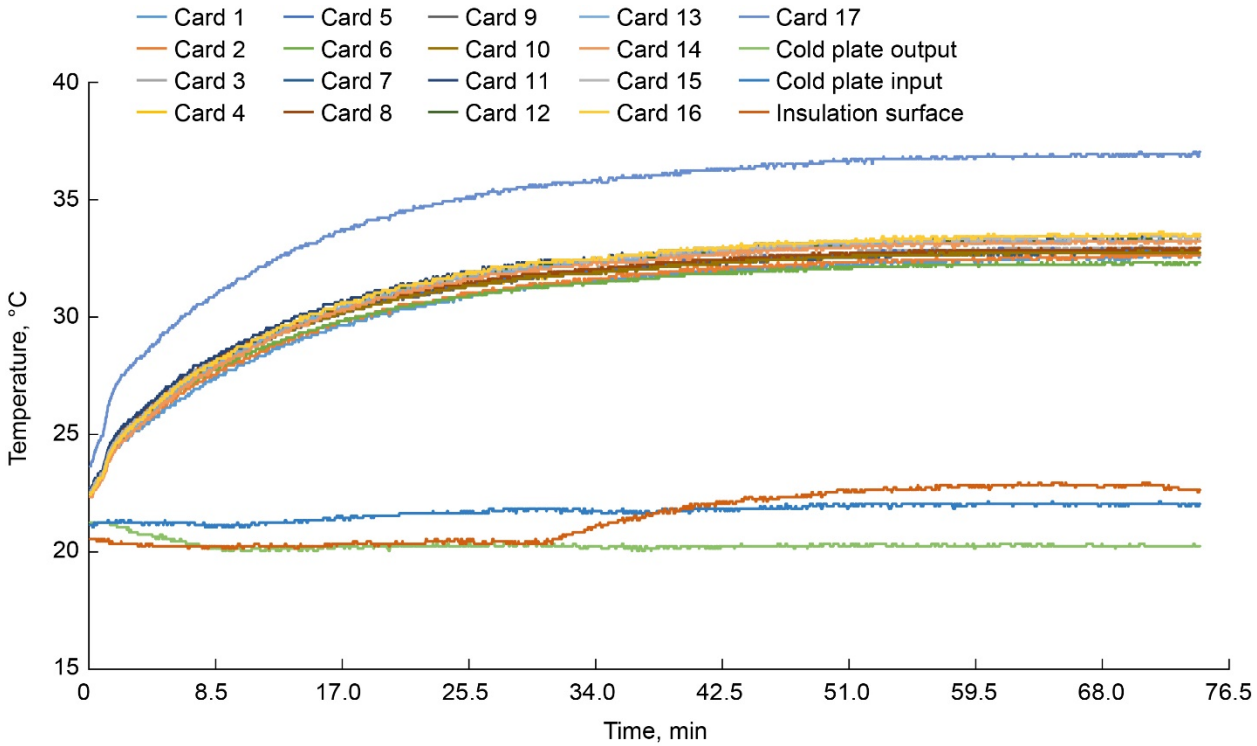

Figure 51.—Card temperature for 10.0 W heater power per card at 1.4 L/min cooling flow rate.

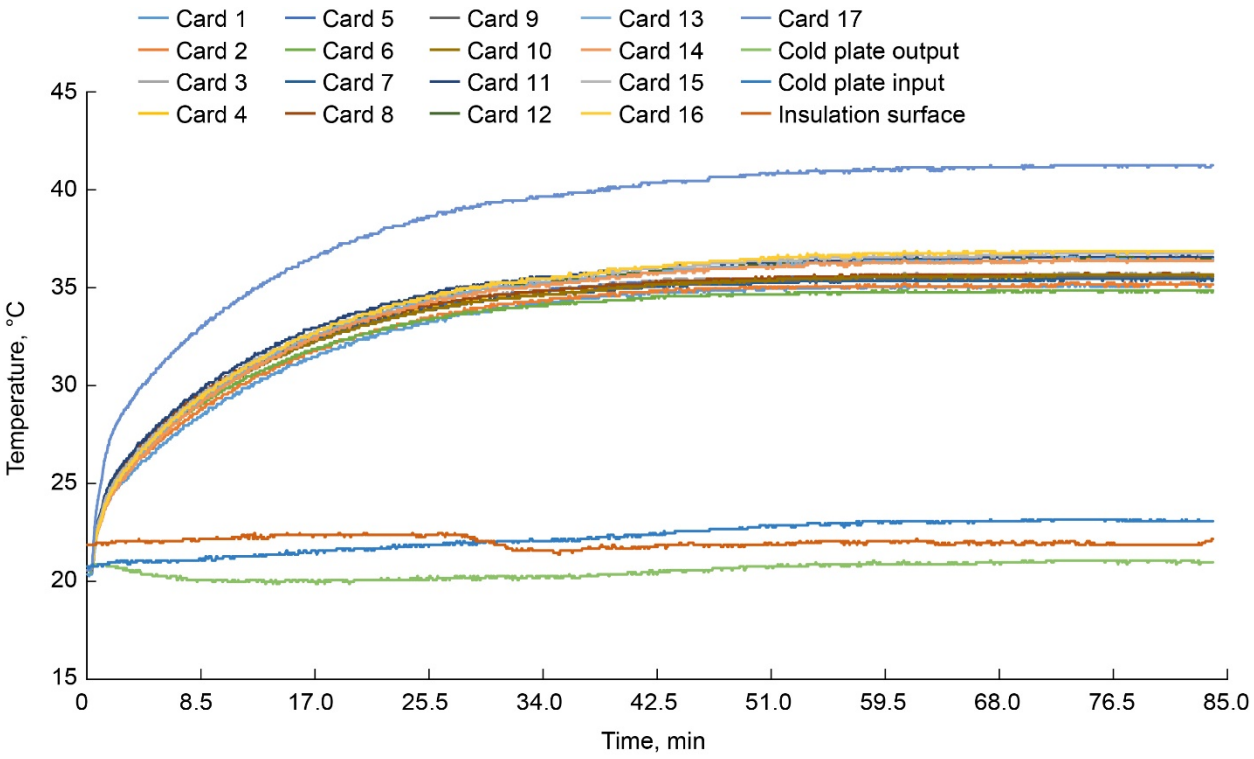

Figure 52.—Card temperature for 12.5 W heater power per card at 1.4 L/min cooling flow rate.

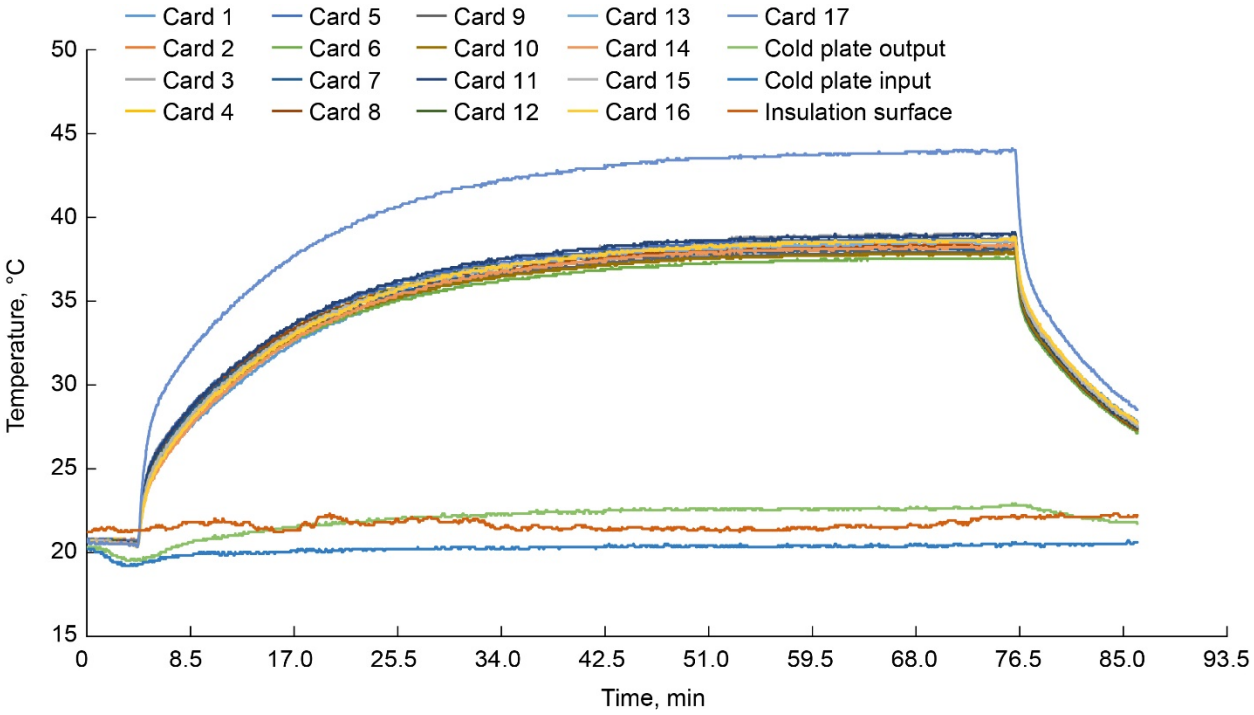

Figure 53.—Card temperature for 15.0 W heater power per card at 1.4 L/min cooling flow rate.

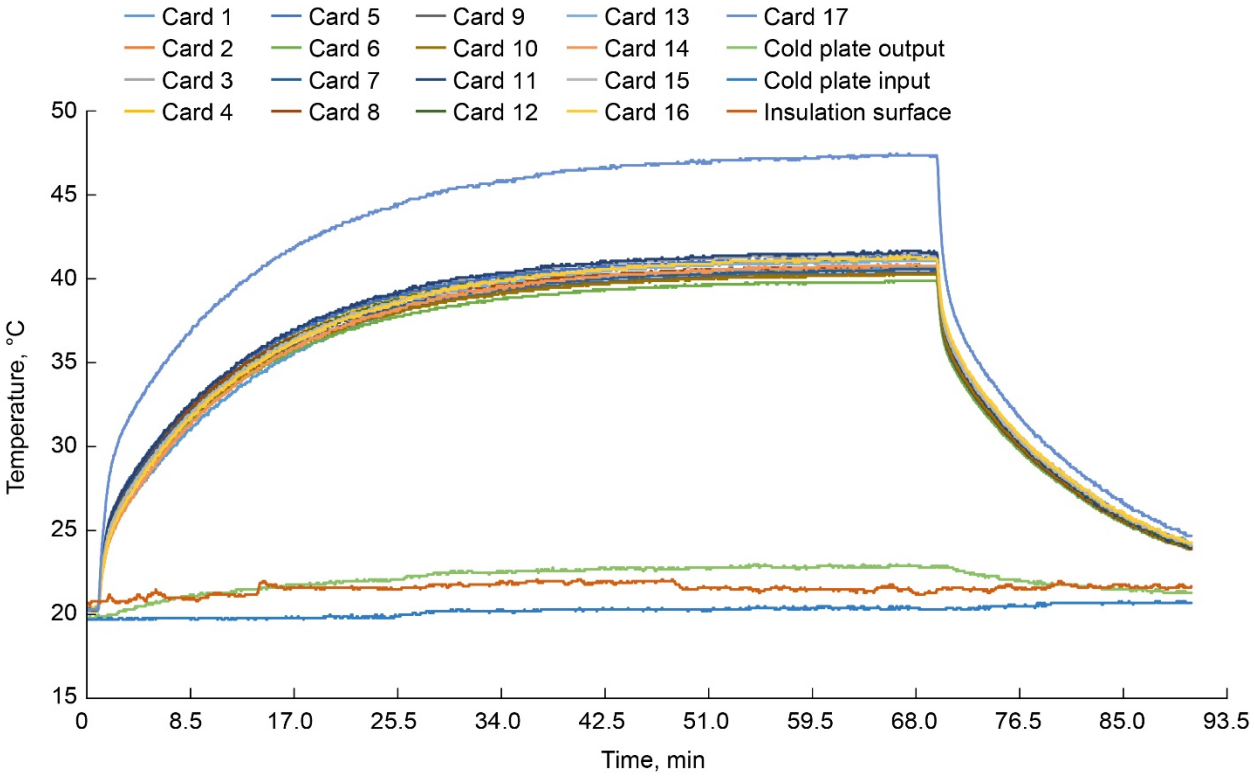

Figure 54.—Card temperature for 17.5 W heater power per card at 1.4 L/min cooling flow rate.

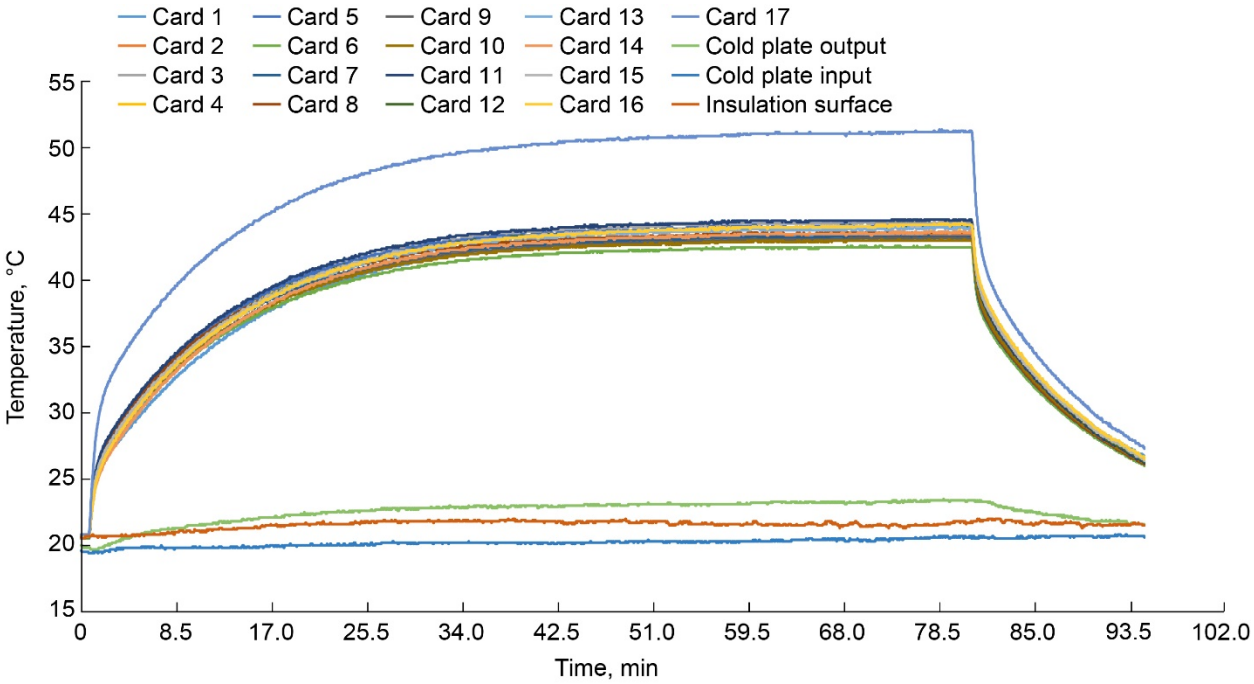

Figure 55.—Card temperature for 20.0 W heater power per card at 1.4 L/min cooling flow rate.

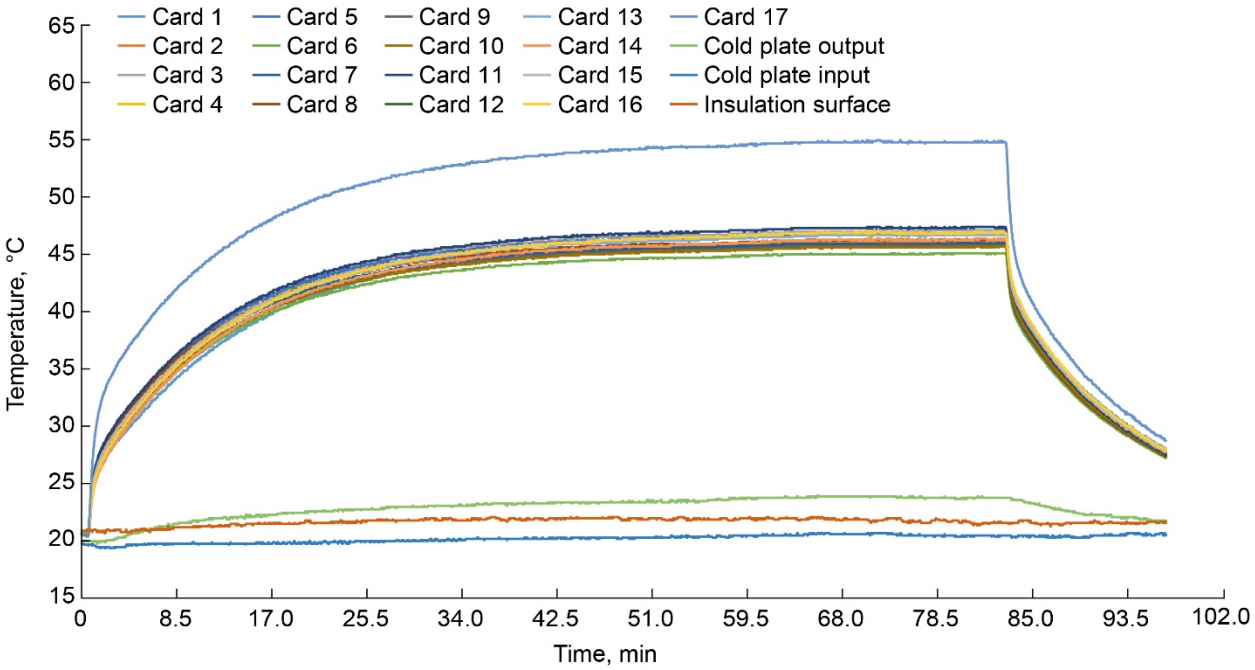

Figure 56.—Card temperature for 22.5 W heater power per card at 1.4 L/min cooling flow rate.

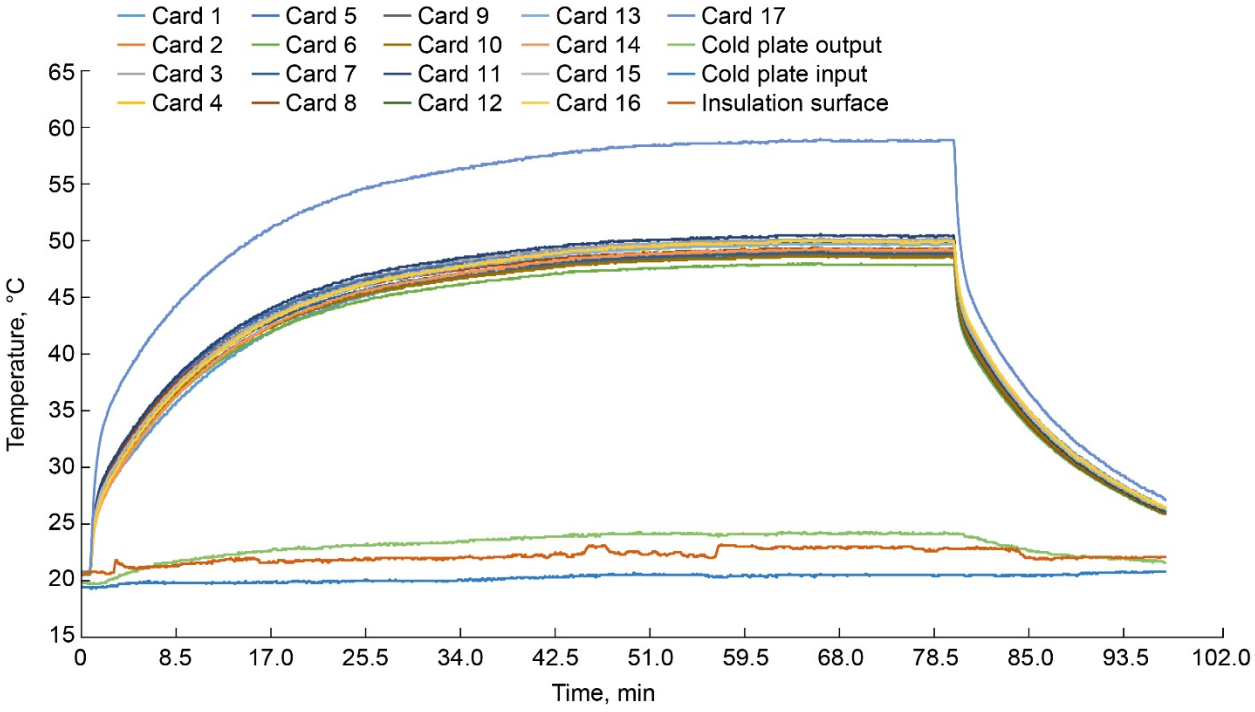

Figure 57.—Card temperature for 25.0 W heater power per card at 1.4 L/min cooling flow rate.

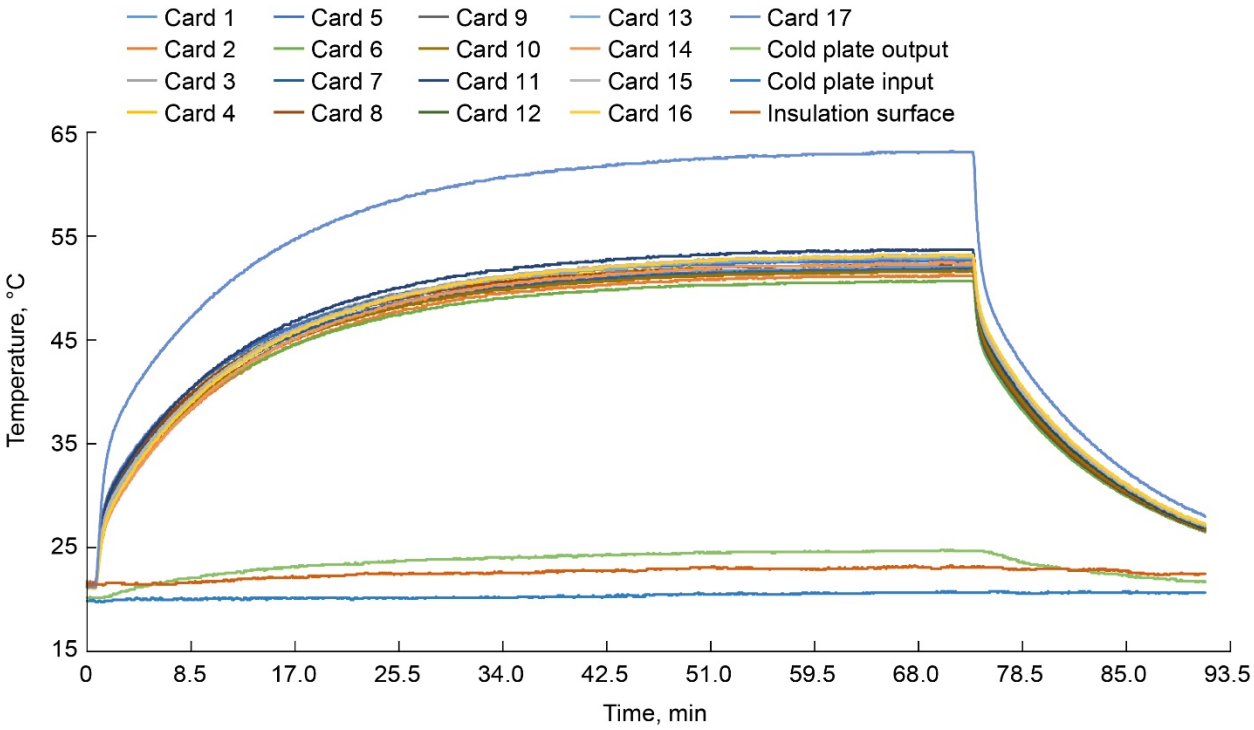

Figure 58.—Card temperature for 27.5 W heater power per card at 1.4 L/min cooling flow rate.

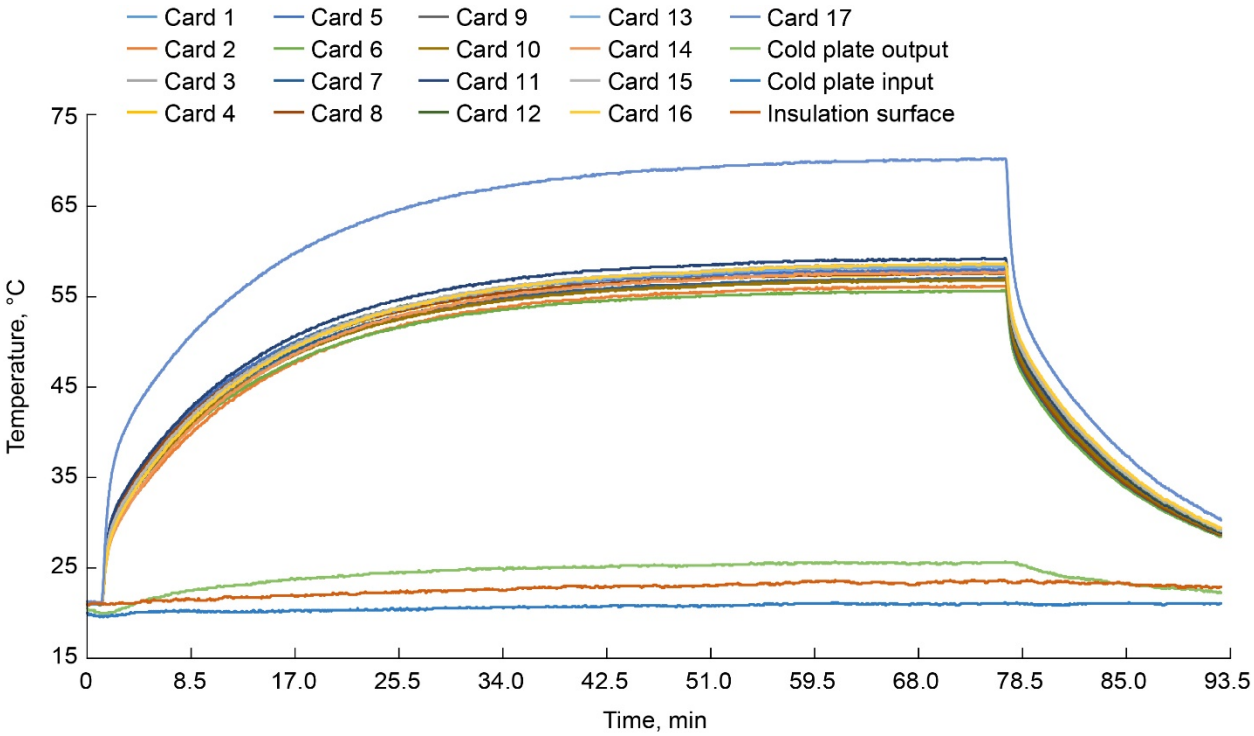

Figure 59.—Card temperature for 30.0 W heater power per card at 1.4 L/min cooling flow rate.

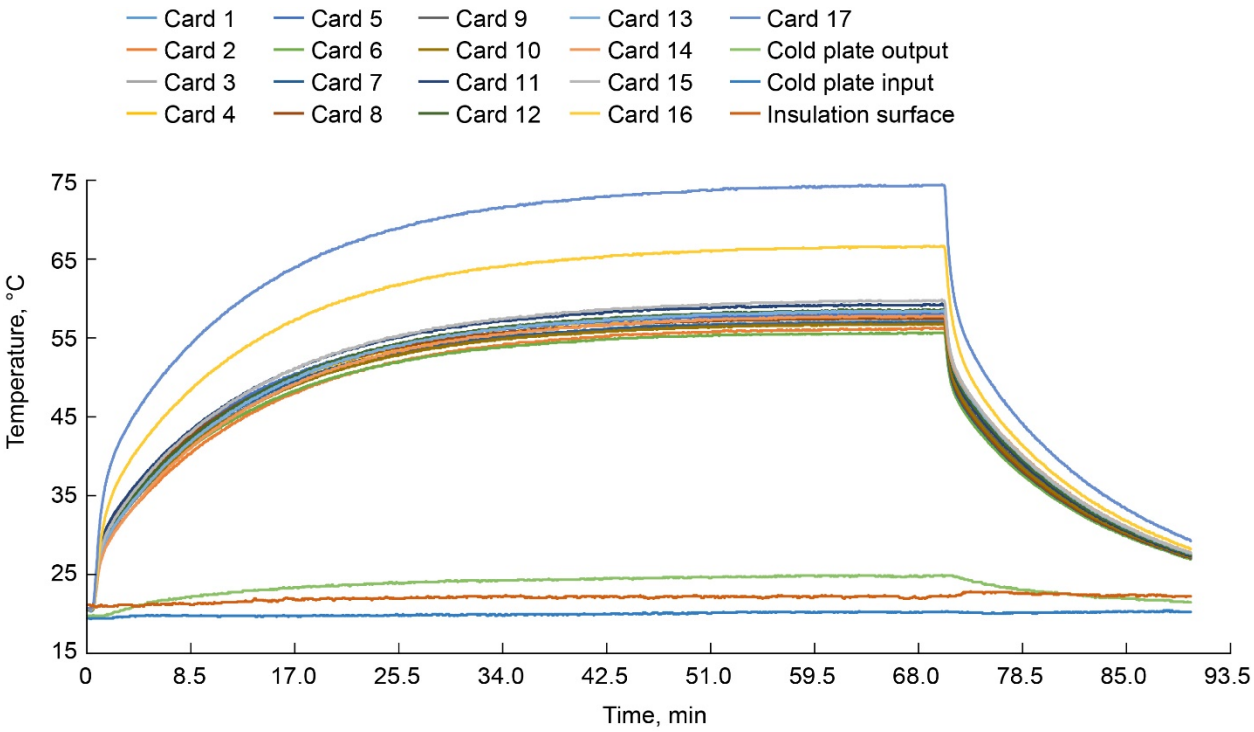

Figure 60.—Card temperature for 32.5 W heater power per card at 1.4 L/min cooling flow rate.

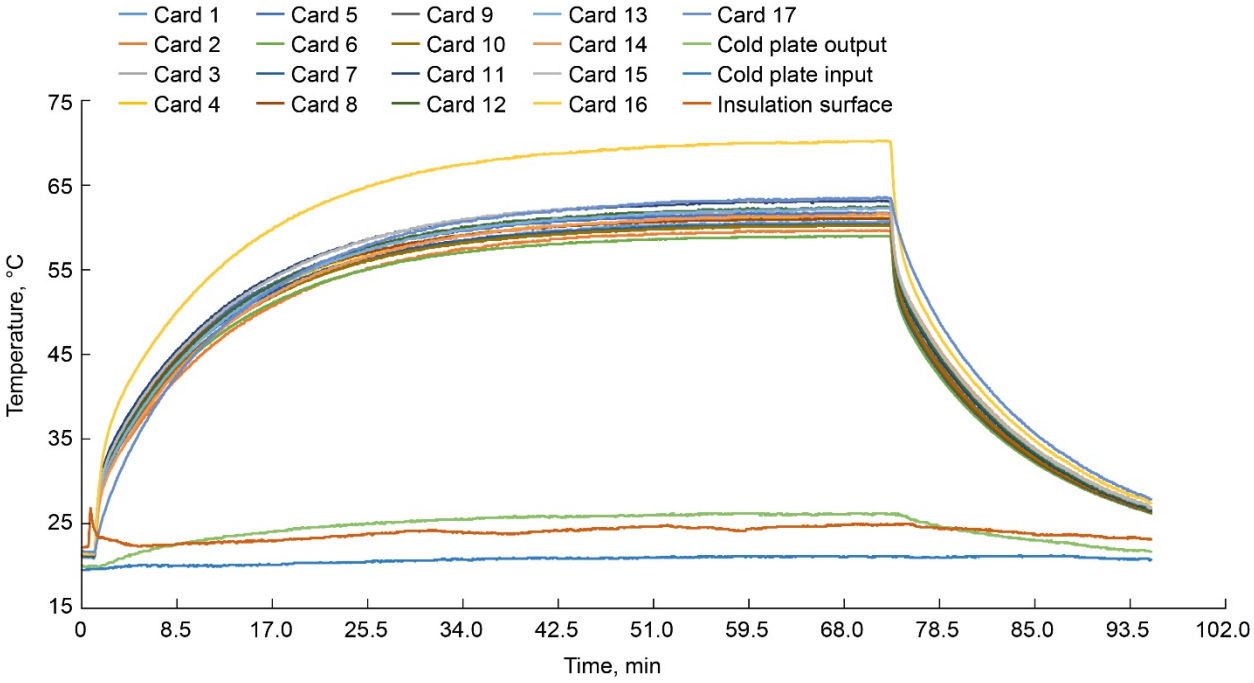

Figure 61.—Card temperature for 35.0 W heater power per card at 1.4 L/min cooling flow rate.

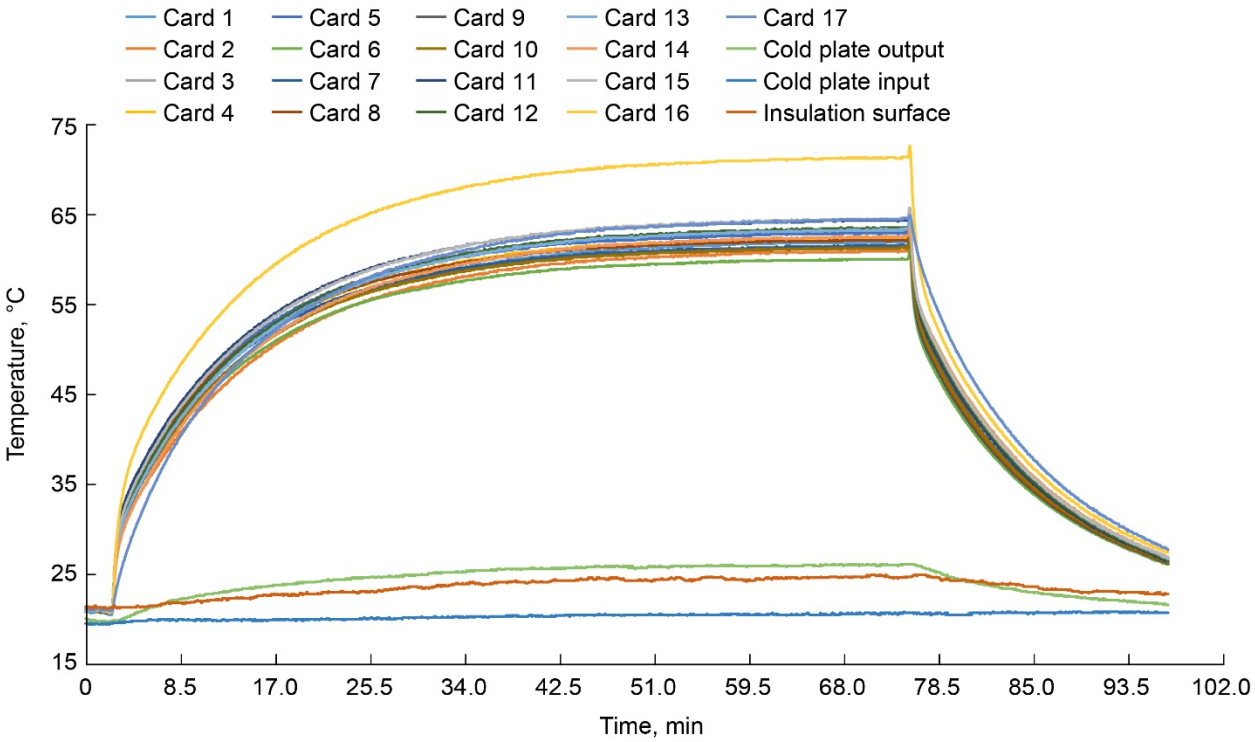

Figure 62.—Card temperature for 37.5 W heater power per card at 1.4 L/min cooling flow rate.

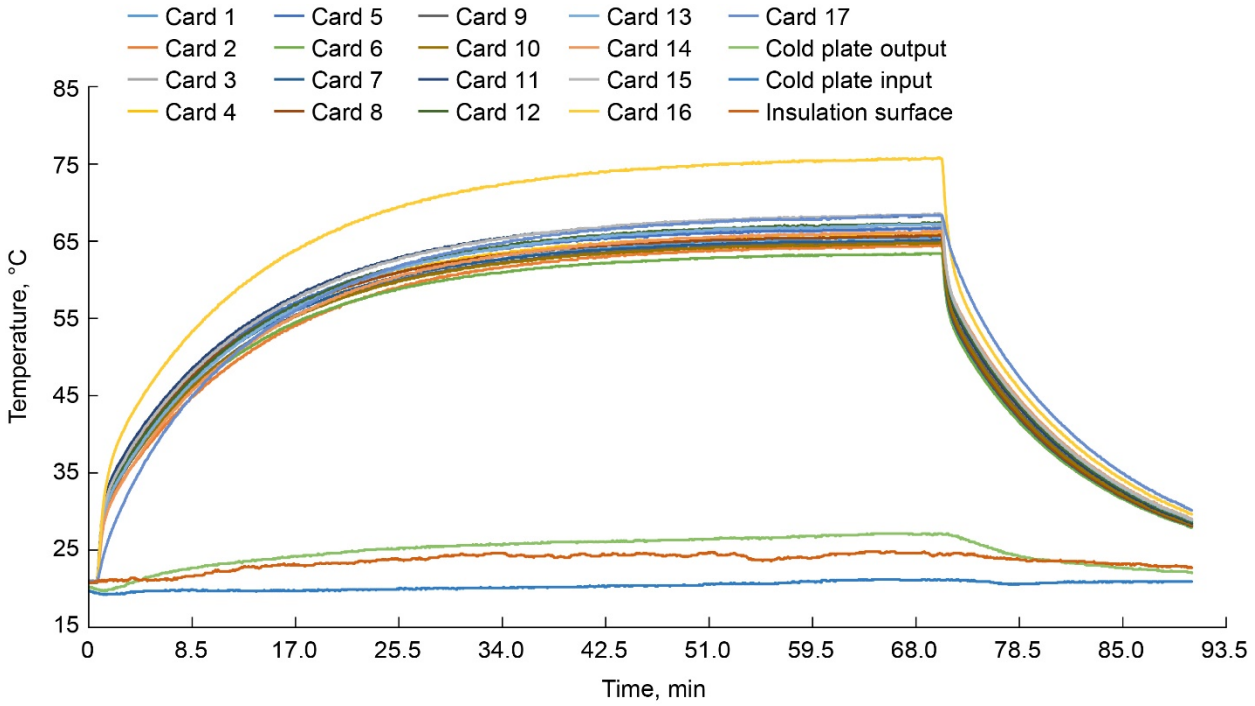

Figure 63.—Card temperature for 40.0 W heater power per card at 1.4 L/min cooling flow rate.

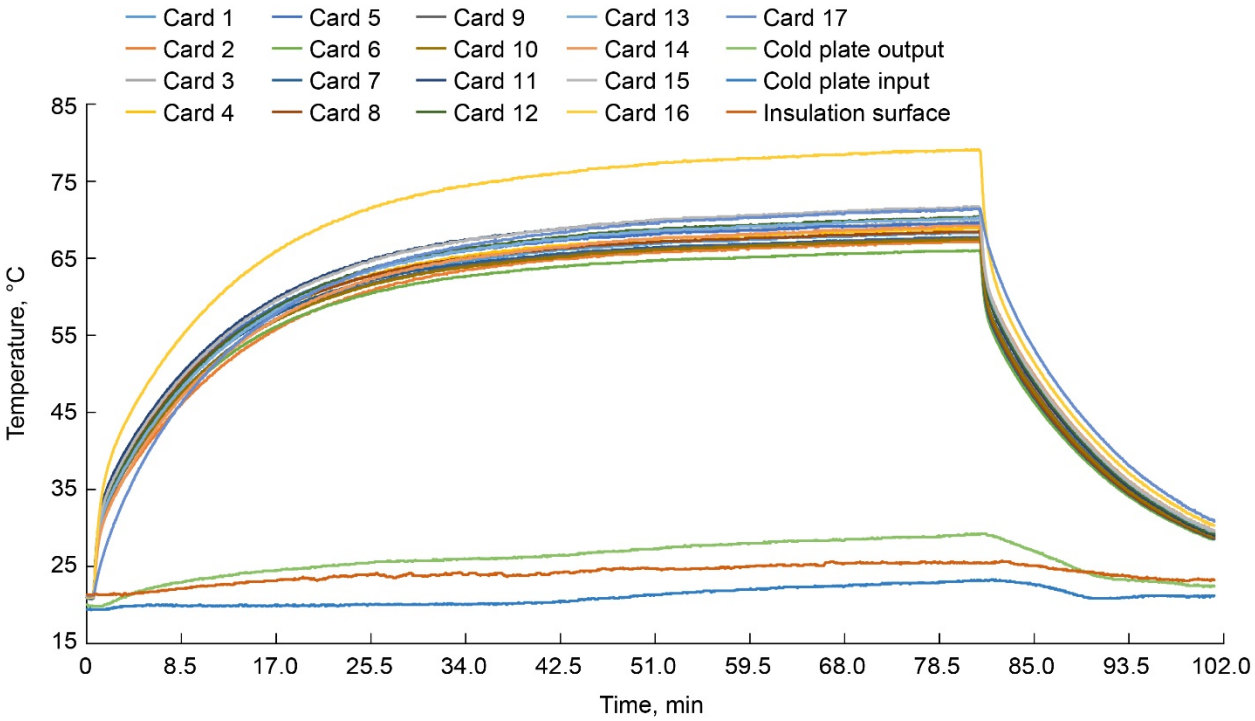

Figure 64.—Card temperature for 42.5 W heater power per card at 1.4 L/min cooling flow rate.

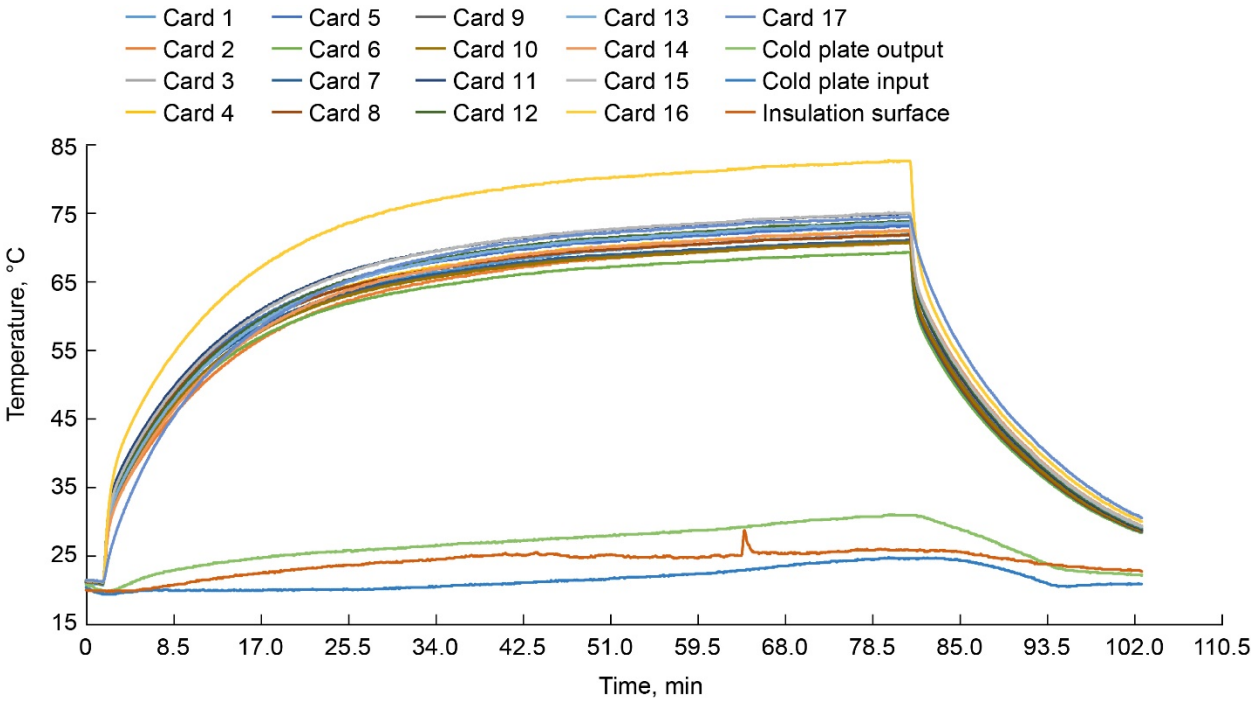

Figure 65.—Card temperature for 45.0 W heater power per card at 1.4 L/min cooling flow rate.

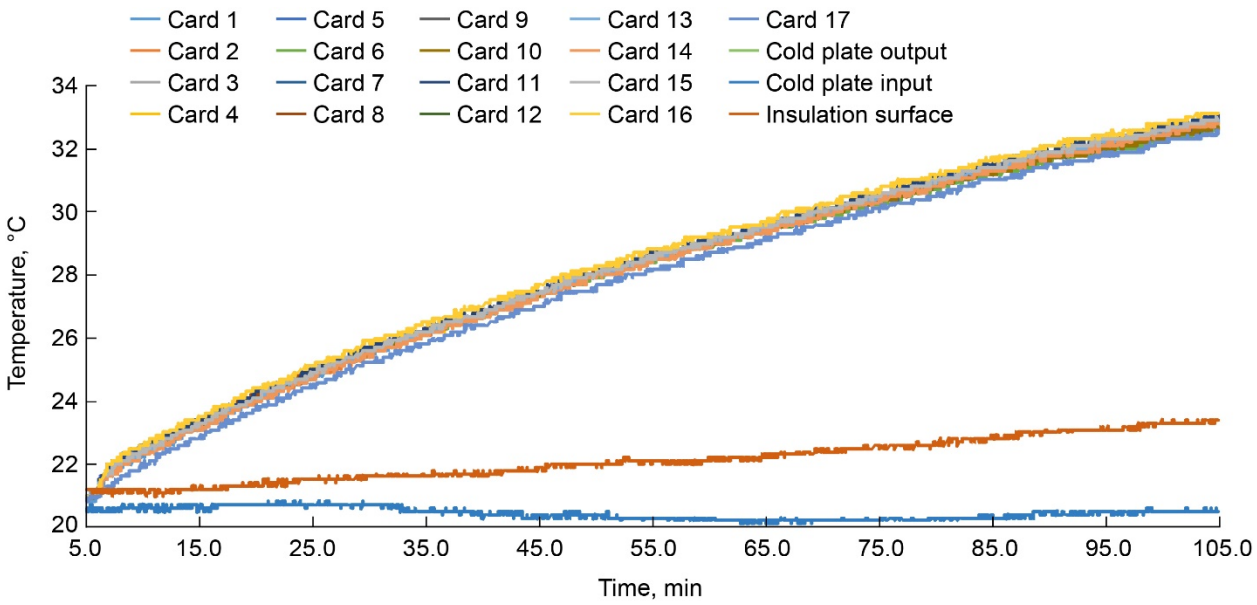

Figure 66.—Card temperature for 2.5 W heater power per card with 0.0 L/min cooling flow rate.

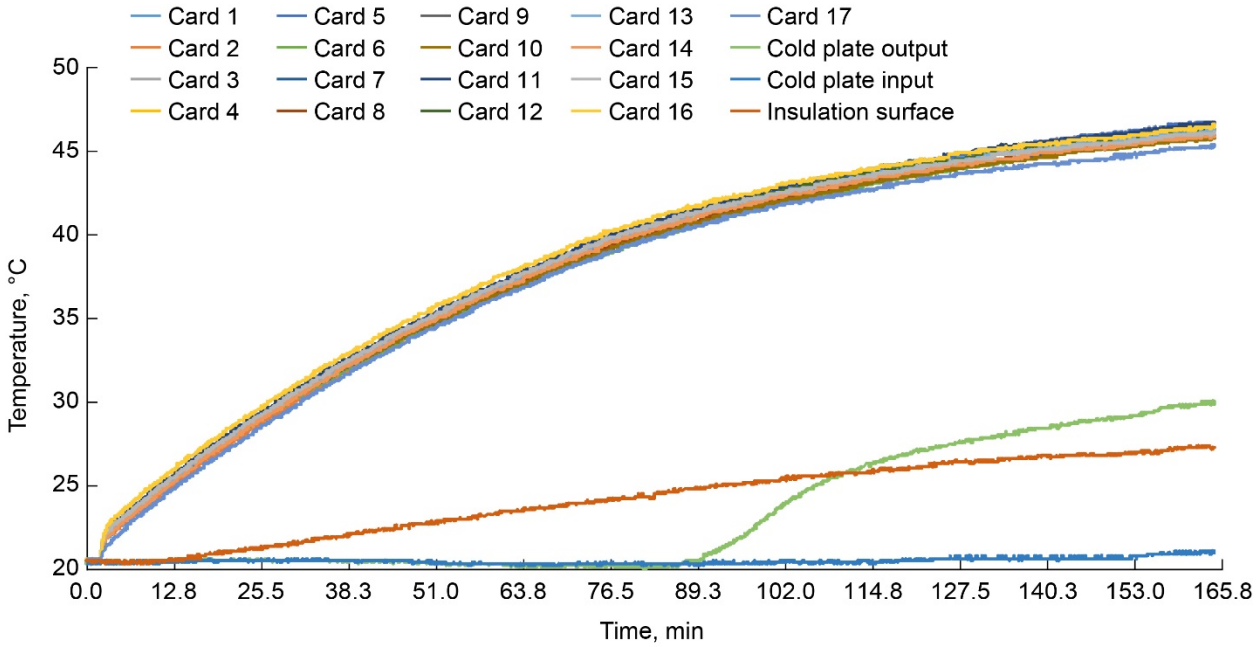

Figure 67.—Card temperature for 5.0 W heater power per card with 0.0 L/min cooling flow rate.

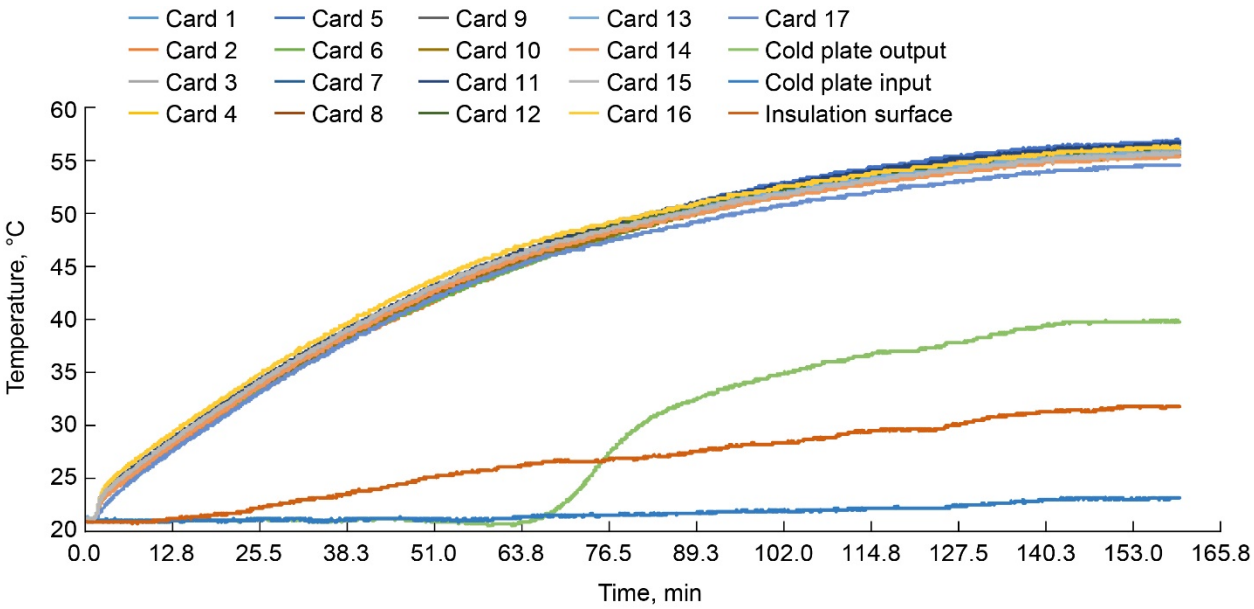

Figure 68.—Card temperature for 7.5 W heater power per card with 0.0 L/min cooling flow rate.

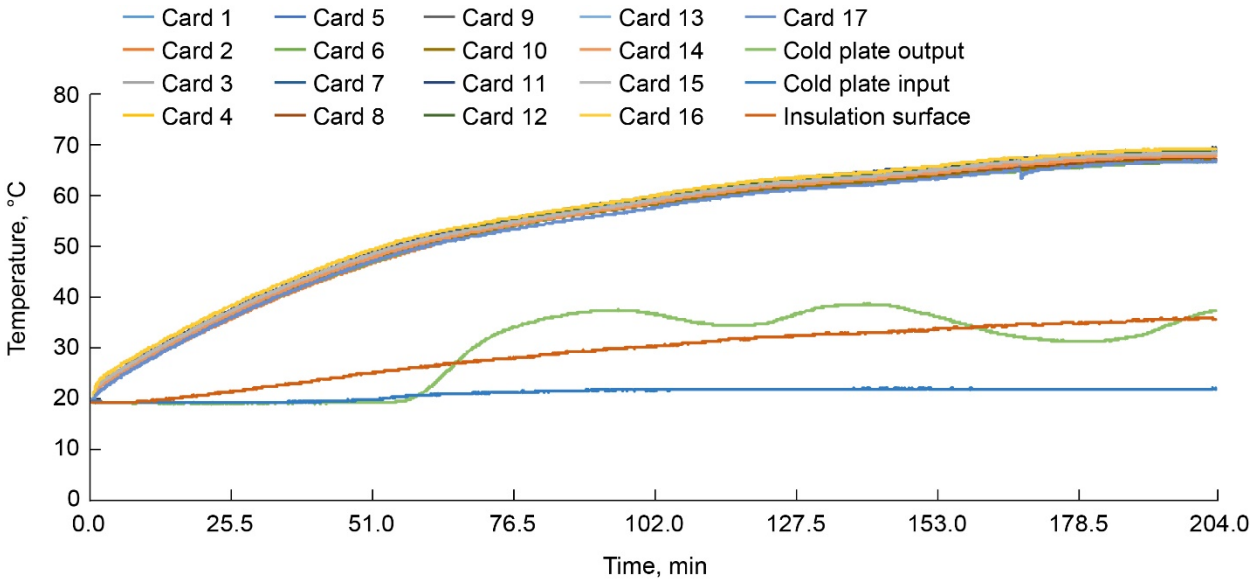

Figure 69.—Card temperature for 10.0 W heater power per card with 0.0 L/min cooling flow rate.

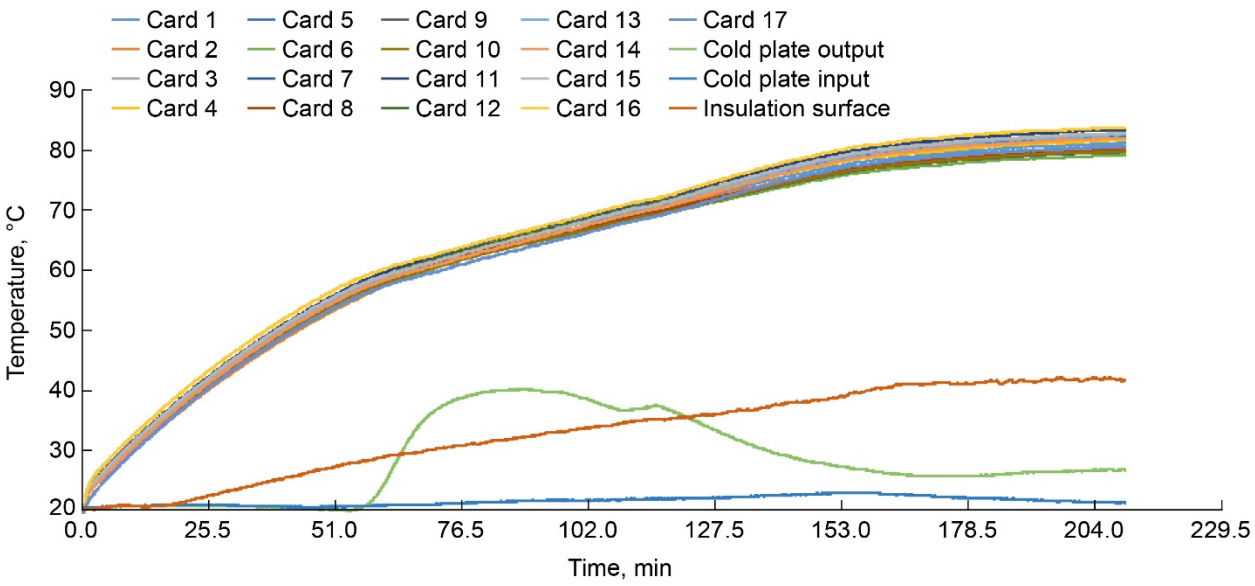

Figure 70.—Card temperature for 12.5 W heater power per card with 0.0 L/min cooling flow rate.

References

1. Colozza, Anthony J.; and Gardner, Brent G.: Advanced Modular Power System Electronics Enclosure Thermal Testing. NASA/TM—2019-220011, 2019. http://ntrs.nasa.gov
2. Incropera, Frank P.; and DeWitt, David P.: Fundamentals of Heat and Mass Transfer. Third ed., John Wiley & Sons, New York, NY, 1990.